Technische Universität München
TUM School of Computation, Information and Technology

Refraction based elevational angular compounding for ultrasound speckle reduction

Parastoo Afshari

Vollständiger Abdruck der von der TUM School of Computation, Information and Technology der Technischen Universität München zur Erlangung einer

Doktorin der Ingenieurwissenschaften (Dr. Ing.)

genehmigten Dissertation.

Vorsitz: Prof. Dr. Oliver Hayden

Prüfende der Dissertation:

1. Prof. Dr. Vasilis Ntziachristos
2. Prof. Dr. Peter E. Andersen

Die Dissertation wurde am 15.04.2024 bei der Technischen Universität München eingereicht und durch die TUM School of Computation, Information and Technology am 04.10.2024 angenommen.

Abstract

Speckle is an inherent property of ultrasound imaging, arising from the interference of backscattered acoustic waves caused by tissue heterogeneities. Although speckle can be advantageous for obtaining information, such as dynamic features like blood flow, it concurrently degrades the resolution and contrast of static structures, blurring the boundaries and therefore making it more challenging to differentiate between the various layers of tissues. This degradation impedes the interpretation of tissue morphology, more significantly, the fine structures, which adversely affecting the diagnostic procedures. While several methods have been proposed to mitigate speckle noise, compounding techniques emerge as a preferable solution due to their potential to enhance image quality by revealing obscured structures hidden beneath speckle noise, which is not possible in image processing techniques as they rely only on the data in one image. Compounding methods enhance image quality by acquiring and averaging sequential images from the same field of view (FOV) with varied spatial or frequency content, a process that often increases the size and complexity of the imaging setup and compromises spatial or temporal resolution. This limitation hinders the practical application of these techniques in clinical settings. The aim of this thesis is to present an attempt to overcome this challenge.

The first part provides an overview of existing despeckling methods and their associated challenges, which leads to identify elevational angular compounding (EAC) as a promising solution. EAC is a type of spatial compounding that can simultaneously offer high speckle noise reduction and good temporal resolution. However, current EAC implementations rely on

mechanically rotating a one-dimensional (1D) transducer array or electronically beam steering of two-dimensional (2D) arrays to provide different elevational imaging angles, which increases the size and cost of the systems. This lays the foundation for our focused exploration of EAC in this study.

In second part, a new refraction-based elevational angular compounding technique (REACT), using an acoustic refractive element is demonstrated. With REACT, clinical feasibility is increased by providing elevational angular compounding to low-cost 1D detector arrays without requiring bulky mechanical adjustments or expensive 2D arrays. The technique achieves up to a two-fold improvement in both signal- and contrast-to-noise ratios on phantoms and excised tissue samples, highlighting its efficacy in enhancing image quality. Additionally, the impact of elevational angular width on speckle reduction and image fidelity is also explored.

Lastly, the application of REACT is extended to radial Endoscopic Ultrasonography (EUS), a real-time diagnostic and therapeutic tool for gastrointestinal disorders. The proposed radial implementation of REACT in EUS introduces the first spatial compounding method in a radial endoscopy. Experimental results on cylindrical layered phantoms reveal a two-fold improvement in signal- and contrast-to-noise ratios, emphasizing the potential of REACT to enhance image quality in clinical EUS.

REACT offers a compact, low-cost solution for spatial compounding in both linear and radial ultrasound applications. Its ability to enhance speckle noise reduction while preserving image fidelity without compromising spatial and temporal resolution holds a promise for advancing current ultrasound imaging techniques using compounding methods, leading to more accurate diagnoses in medical field.

Zusammenfassung

Speckle ist eine inhärente Eigenschaft der Ultraschallbildgebung, die durch die Interferenz von rückgestreuten akustischen Wellen aufgrund von Gewebeheterogenitäten entsteht. Obwohl Speckle-Rauschen für die Gewinnung von Informationen, z. B. dynamischen Merkmalen wie dem Blutfluss, von Vorteil sein kann, verschlechtert es gleichzeitig die Auflösung und den Kontrast statischer Strukturen, verwischt die Grenzen und erschwert somit die Unterscheidung zwischen den verschiedenen Gewebeschichten. Diese Verschlechterung erschwert die Interpretation der Gewebemorphologie, insbesondere der feinen Strukturen, was sich nachteilig auf die Diagnoseverfahren auswirkt. Es wurden zwar mehrere Methoden zur Verringerung des Speckle-Rauschens vorgeschlagen, aber Compounding-Techniken sind aufgrund ihres Potenzials, die Bildqualität zu verbessern, indem sie unter dem Speckle-Rauschen verborgene Strukturen aufdecken, eine Lösung, die bei Bildverarbeitungstechniken nicht möglich ist, da sie nur auf den Daten eines Bildes basieren. Compounding-Methoden verbessern die Bildqualität, indem sie aufeinanderfolgende Bilder desselben Sichtfeldes (FOV) mit unterschiedlichem räumlichem oder frequenzmäßigem Inhalt aufnehmen und mitteln, ein Prozess, der häufig die Größe und Komplexität des Bildaufbaus erhöht und die räumliche oder zeitliche Auflösung beeinträchtigt. Diese Einschränkung behindert die praktische Anwendung dieser Techniken im klinischen Umfeld. Ziel dieser Arbeit ist es, einen Versuch zur Überwindung dieser Herausforderung zu präsentieren.

Der erste Teil bietet einen Überblick über die bestehenden Despeckling-Methoden und die damit verbundenen Herausforderungen, was dazu führt, dass Elevational Angular Compounding (EAC) als eine vielversprechende Lösung identifiziert wird. EAC ist eine Art von räumlichem

Compounding, das gleichzeitig eine hohe Reduzierung des Speckle-Rauschens und eine gute zeitliche Auflösung bietet. Derzeitige EAC-Implementierungen beruhen jedoch auf der mechanischen Drehung eines eindimensionalen (1D) Wandlerarrays oder der elektronischen Strahlsteuerung von zweidimensionalen (2D) Arrays, um verschiedene Elevationsabbildungswinkel zu erzielen, was die Größe und Kosten der Systeme erhöht. Dies bildet die Grundlage für unsere gezielte Erforschung der EAC in dieser Studie.

Im zweiten Teil wird eine neue, auf Refraktion basierende Elevational Angular Compounding Technik (REACT) vorgestellt, die ein akustisches refraktives Element verwendet. Mit REACT wird die klinische Durchführbarkeit erhöht, da die Elevationswinkelkompoundierung für kostengünstige 1D-Detektorarrays ohne sperrige mechanische Anpassungen oder teure 2D-Arrays möglich ist. Die Technik erzielt eine bis zu zweifacher Verbesserung des Signal- und Kontrast-Rausch-Verhältnisses an Phantomen und exzidierten Gewebeproben, was ihre Wirksamkeit bei der Verbesserung der Bildqualität unterstreicht. Darüber hinaus wird auch der Einfluss der Elevationswinkel auf die Speckle-Reduktion und die Bildtreue untersucht.

Schließlich wird die Anwendung von REACT auf die radiale endoskopische Ultraschalluntersuchung (EUS) ausgeweitet, ein Echtzeit-Diagnose- und Therapieinstrument für Magen-Darm-Erkrankungen. Die vorgeschlagene radiale Implementierung von REACT in EUS führt die erste räumliche Compounding-Methode in einer radialen Endoskopie ein. Experimentelle Ergebnisse an zylindrischen Schichtphantomen zeigen eine zweifache Verbesserung des Signal und Kontrast-Rausch-Verhältnisses und unterstreichen das Potenzial von REACT zur Verbesserung der Bildqualität in der klinischen EUS.

REACT bietet eine kompakte, kostengünstige Lösung für räumliches Compounding bei linearen und radialen Ultraschallanwendungen. Seine Fähigkeit, das Speckle-Rauschen zu reduzieren und gleichzeitig die Bildtreue zu erhalten, ohne die räumliche und zeitliche Auflösung zu beeinträchtigen, verspricht eine Verbesserung der derzeitigen Ultraschall-Bildgebungstechniken mit Compounding-Methoden, was zu genaueren Diagnosen im medizinischen Bereich führen wird.

Publications

This publication-based dissertation is based on the following, first-author publications which are reproduced in chapters 2 and 3 respectively:

1. **Afshari, P.,** Zakian, C. & Ntziachristos, V. *Improving ultrasound images with elevational angular compounding based on acoustic refraction*. Sci. Rep. 10, 18173 (2020).

   https://doi.org/10.1038/s41598-020-75092-8 (published)

2. **Afshari, P.,** Zakian, C., Bachmann, J. & Ntziachristos, V. *Speckle reduction in ultrasound endoscopy using refraction based elevational angular compounding*. Sci. Rep. 11, 18370 (2021).

   https://doi.org/10.1038/s41598-021-97717-2 (published)

Furthermore, the research performed for this dissertation project resulted in another peer-reviewed publication, which is not the core-publication of the presented work:

1. He, H., Stylogiannis, A., **Afshari, P.,** Wiedemann, T., Steiger, K., Buehler, A., Zakian, C & Ntziachristos, V. *Capsule optoacoustic endoscopy for esophageal imaging*. J. Biophotonics 12, (2019).

   https://doi.org/10.1002/jbio.201800439 (published)

International conference and proceeding

While being published in scientific journals is important for academic recognition, it's just as vital to share and discuss your research within the scientific community. This is best done by attending and presenting at scientific conferences:

1. **Parastoo Afshari**, Andrei Berezhnoi, Juan Aguirre, Christian Zakian, Vasilis Ntziachristos, "Development of optoacoustic microscopic and mesoscopic imaging handheld for skin imaging", 41st Annual International Conference of the IEEE Engineering in Medicine and Biology Society, Germany, Berlin, 2019. Poster presentation.

2. **Parastoo Afshari**, Christian Zakian and Vasilis Ntziachristos, "Development of hybrid optical resolution optoacoustic and fluorescent imaging for early detection and staging of the esophagus cancer", SPIE, Biophotonics summer school 2019, Sweden, Island of Ven. Poster Presentation.

Contents

Abbreviations

1D One Dimensional
2D Two Dimensional
3D Three Dimensional

CT Computed Tomography
CNR Contrast to Noise Ratio

EAC Elevational Angular Compounding

FOV Field of View

IBMI Institute of Biological and Medical Imaging
ITN Initial Training Network

ROI Region of Interest
REACT Refraction-based Elevational Angular Compounding Technique

SNR Signal to Noise Ratio

TUM Technical university of Munich

US Ultrasound

Chapter 1

1 Methods for speckle reduction in ultrasound imaging – An overview

1.1 Ultrasound imaging and speckle noise

Ultrasound (US) technology was first used in medical during World War II in various parts of the world. The first published research in medical ultrasonics was conducted in Austria in 1942 to investigate the use of US to study the brain. While researchers in the United States, Japan, and Europe were recognized in the mid-1950s for their significant contribution in making ultrasonography feasible [1-9]. This development paved the way for the widespread use of ultrasonography in medical practices in the next decades.

In the realm of the modern healthcare, biomedical imaging plays a crucial role, and US imaging due to its non-invasive nature and real-time capabilities standing out as an indispensable diagnostic and therapeutic tool [1-5]. However, the utility of US imaging is frequently hindered by the persistent issue of speckle noise, which substantially degrades image quality and impedes accurate medical diagnoses. This is an inherent problem arising from the random scattering effect, which is particularly prevalent when the dimensions of tissue structures are closely aligned with the employing US frequencies [6-9].

Speckle noise is characterized by the presence of bright and dark granular pattern on US images, which is due to the interference of backscattered ultrasonic waves. The speckle noise causes substantial degradation of image quality and spatial resolution and therefore poses a significant obstacle to achieving diagnostic clarity for medical practitioners by obscuring crucial image features essential for medical diagnosis [10-16]. Consequently, there is an imperative need to identify an effective denoising methodology tailored for medical US imaging.

1.1.1 Principles of ultrasound imaging

US imaging, commonly known as ultrasonography, is a non-invasive medical imaging technology that uses high-frequency sound waves to provide real-time images of the body's internal structures [3-9]. Unlike other imaging modalities, such as X-ray or computed tomography (CT), US is non-ionizing and non-invasive, making it safe for repeated use without exposing patients to harmful radiation. Aside from safety, adaptability, the ability to deliver real-time imaging and extensive anatomical insights also contribute to the prominence of US imaging in the field of modern medicine for diagnostic and therapeutic purposes [1-12].

US, characterized by a frequency surpassing 20 kHz, manifests as a propagating continuous pressure wave, serving as a carrier of energy. Defined by parameters such as pressure density, propagation direction, and particle displacement, ultrasound exhibits longitudinal characteristics, signifying a compression wave [6-9, 16]. The interaction of ultrasound waves with tissue adheres to the principles of geometrical optics, encompassing phenomena like reflection, refraction,

scattering, diffraction, interference, and absorption. Notably, all interactions, except for interference, contribute to the attenuation of ultrasound beam intensity [4-9, 16].

The core concept of US imaging is sound wave propagation. Its core physics principles involve the generation of high-frequency sound waves using piezoelectric crystals within a transducer, the transmission and interaction with tissues, and the subsequent reflecting echoes back to the same transducer [1-9, 16]. The echoes are subsequently converted by the transducer into electrical impulses, which are further processed to form visual images. The recorded signals can then be reconstructed as 2D or 3D images with the image contrast given by varying acoustic impedances in tissue.

US imaging is characterized by modest resolution, presenting limitations in applications such as visualizing tissue-bone interfaces [16]. Despite this constraint, ultrasound excels in imaging depths within the centimeter range, offering distinct advantages such as real-time imaging capabilities and non-invasive interactions with living tissue [5-9]. Another advantage of medical US imaging comes with the simplicity of US imaging systems, ultimately allowing high portability and low operating costs.

However, despite its numerous advantages, US imaging is not without its challenges. One of the primary limitations is the presence of speckle noise in US images, which can degrade image quality and spatial resolution and therefore hinder accurate diagnosis [9-16]. Traditional methods of addressing speckle noise are limited in their ability to enhance image quality without compromising other aspects of the imaging process. This work focuses on investigating the current methods for speckle reduction, their specific challenges, aiming to enhance the efficiency and reliability of US imaging in biomedical applications with proposing the new despekcling approach which can overcome the current challenges.

1.1.2 Physical properties and the pattern of the speckle noise

The existence of speckle noise in US images has been observed since the early 1970s, with researchers like Burckhardt, Wagner, and Goodman [11-16] delving into the fundamentals and statistical properties of speckle noise. It's worth noting that in some algorithms, speckle features

are intentionally utilized, and speckle is not considered merely as noise. The term "noise" in this context is used due to the visual observation that speckle might obscure the detection of edges and important object borders in both visual and automated analyses. As it can be seen in Figure 1. 1, the intricate relationship between constructive and destructive phasors in the context of speckle contributes to the variability of bright and dark spots observed in the images [9-16].

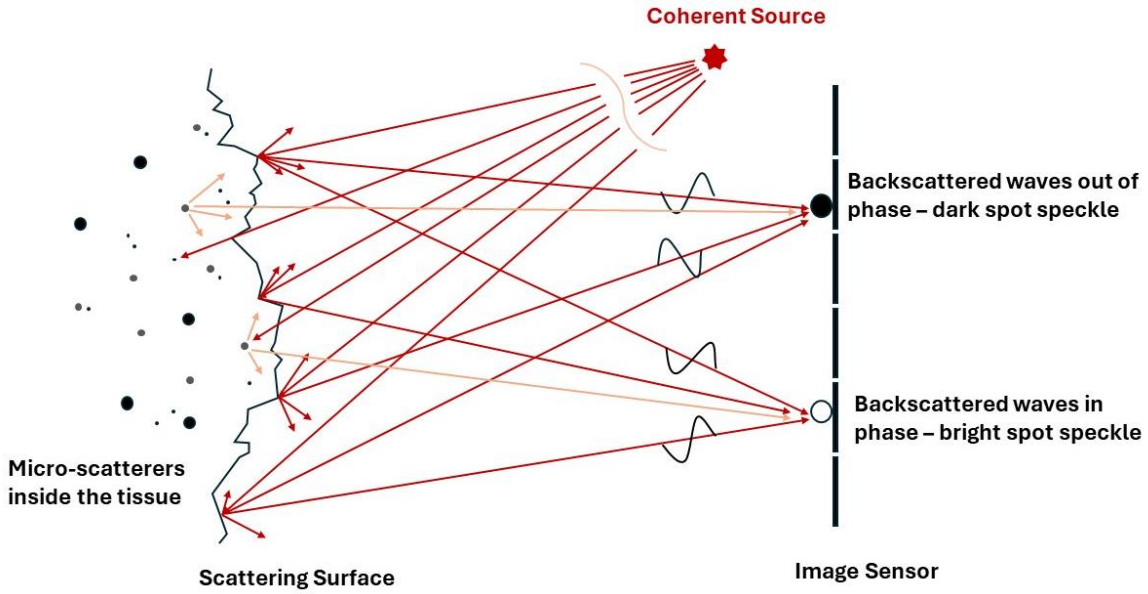

Figure 1. 1 Speckle formation. Speckle is distinguished by the presence of bright and dark granular patterns on acquired images, which result from the interference of backscattered in phase and out of phase of coherent waves from a coherence source. In medical imaging, the formation of speckle patterns originates from the intricate interaction of constructive and destructive interferences among backscattered echoes from scattering surface (laser speckle) or scatterers substantially smaller than the wavelength of the ultrasonic wave inside the tissue (US speckle).

In fact, its texture often holds valuable information about the viewed image, challenging the conventional notion of speckle as purely disruptive noise [12-17]. To illustrate, the utilization of speckle tracking in ultrasound imaging enables the evaluation of tissue motion and deformation by monitoring interference patterns across consecutive video frames [17]. This innovative technique has primarily been developed and implemented for assessing the mechanical properties of the myocardium. Additionally, there is a growing interest in speckle tracking for evaluating carotid arterial strain in recent years [16, 17].

However, speckle is a type of locally correlated multiplicative noise which poses a challenge in the context of medical US imaging [8-17]. The speckle pattern, that is visible as the typical light and dark spots the image is composed of results from destructive interference of US waves scattered from different sites. The nature of speckle has been a major subject of investigation. When a fixed, rigid object is scanned twice under the same conditions, one obtains identical speckle pattern [10-17]. Although of random appearance, speckle is not random in the same sense as electrical noise. However, if the same object is scanned under slightly different conditions, say with a different transducer aperture, pulse length or transducer angulation, the speckle pattern change [11-14, 17].

The most popular model adopted in the literature to explain the effect that occur when a tissue is isonated, a tissue may be modeled as a sound absorbing medium containing scatterers, which scatter the sound waves. These scatterers arise from inhomogeneities and structures approximately equal to or smaller in size that the wavelength of the US, such as parenchyma, where there are changes in acoustic impedance over a microscopic level within the tissue [10-17]. Tissue particles that area relatively small in relation to the wavelength, (blood cells), and particles with differing impedance that lie very close to one another, cause scattering or speckling. Absorption of the US tissue is an additional factor to scattering and refraction, responsible for pulse energy loss. The process of energy loss involving absorption, reflection, scattering is referred to as attenuation, which increases with depth and frequency. Because higher frequency of US, results into increased absorption, the consequence is a decrease of the depth of visualization [16-17].

In the realm of medical US imaging, the emergence of speckle patterns arises from the intricate interplay of constructive and destructive interferences among backscattered echoes from scatterers significantly smaller than the ultrasound wave's wavelength [6-20]. The occurrence of random scattering is rooted in the similarity between the scales of human tissue structures and ultrasonic wavelengths [10-17].

Speckle Noise Modeling

Goodman presents a theory for the origin of speckle [11], explaining the cause of speckle through a mathematical model. He describes speckle as a sum of many complex phasors, resembling a complex random walk [11, 16]. These phasors can either add up constructively or cancel each other out destructively. Consequently, we observe both bright and dark points closely packed together.

Notably, speckle exhibits a multiplicative nature [10-16]. The image encompassing speckle, denoted as $r(x,y)$, can be expressed as a combination of a noise-free image $h(x,y)$, multiplicative noise $n_m(x,y)$, and additive noise $n_a(x,y)$ according to [11, 16]:

$$r(x,y) = h(x,y) \cdot n_m(x,y) + n_a(x,y) \quad (1.\ 1)$$

Considering that the additive noise, such as thermal and electronic noises, is negligible in comparison to the multiplicative speckle noise, Equation (1. 1) can be simplified to [11, 16]:

$$r(x,y) = h(x,y) \cdot n_w(x,y) \quad (1.\ 2)$$

To facilitate further analysis, the multiplicative speckle noise is transformed into additive noise through the logarithm transform. Consequently, Equation (1. 2) can be reformulated as [16]:

$$\log r(x,y) = log\ h(x,y) + log\ n_m(x,y) \quad (1.\ 3)$$

Given the plethora of proposed techniques for reducing additive noise, representing speckle as additive noise, as in Equation (1. 3), provides a more effective avenue for its suppression. This mathematical framework forms the basis for the reported explorations in enhancing the quality of medical ultrasound images by mitigating the impact of speckle noise [11-16].

1.2 Despeckling in ultrasound imaging

Noise and artifacts in medical imaging lead to the degradation of signals or images, with distinct types of deterioration observed in different imaging modalities. Image degradation can have a significant impact on image quality and thus affect human interpretation and the accuracy of computer-assisted methods [2-16]. Poor image quality often makes feature extraction analysis, recognition, and quantitative measurements problematic and unreliable. Images formed with coherent energy, such as ultrasound, suffer from speckle noise [10-17]. Speckle is most often considered a dominant source of noise and limiting contrast resolution in diagnostic US imaging and should filtered out without affecting important features of the image. Speckle restricts the detectability of small, low contrast lesions and makes US images difficult for non-specialists to interpret. Numerous studies have demonstrated that the presence of speckle noise in the image reduces lesion detectability by around a factor of eight [16]. This drastic drop in contrast resolution is responsible for ultrasound's lower effective resolution when compared to X-ray and MRI [2-5, 16]. Therefore, despeckling is a very important procedure, which motivated a significant number of studies for speckle reduction in US medical imaging.

Here, a study is conducted on the two main despeckling techniques utilized in US imaging—image processing and compounding methods—with a specific emphasis on the underlying principles of each technique.

1.2.1 Image processing techniques

The efficacy of speckle reduction using image processing techniques is crucial for medical imaging because it must not only eliminate speckle noise but also should maintain the edges and critical features required for accurate diagnosis [16, 23-25]. The preservation of boundaries between large-scale organs, and the detailed structures such as small blood vessels or lesions with comparable dimensions to the average speckle size is essential for the accurate detection of abnormalities [6-25].

Speckle is interestingly characterized by a tendency to multiply or interact with the underlying structure of an image. This means that when we observe speckle in images, its impact isn't just additive but involves a multiplication effect [16, 18-22], making it distinct in how it influences the overall appearance. Therefore, the major of proposed image processing techniques for mitigating speckle in US images commonly employ multiplicative noise filtering [16, 18-22]. Nevertheless, the efficacy of these methods is somewhat limited, primarily due to the simplistic nature of the multiplicative noise model utilized to depict speckle [13-22].

Moreover, since image processing techniques rely on the information present in a single image, they face limitations in uncovering data concealed beneath speckle noise [16, 19-25]. While smoothing the image can be advantageous and would be easier with these methods, their inability to recover obscured data poses a challenge, particularly in the context of early and accurate diagnosis, especially for small lesions [20-25].

Considering the aforementioned challenges, image processing methods may not be the optimal speckle reduction method to retrieve the lost data due to speckle noise. To develop more effective speckle reduction techniques, it is crucial to fully understand speckle and consider its spatial correlation properties.

1.2.2 Compounding methods

Image processing methods have been suggested to mitigate speckle; however, their effectiveness is limited due to their suboptimal preserving edges and boundaries and retrieving the obscured data by speckle noise [16, 23-28].

However, compounding techniques, such as spatial and frequency compounding, offer effective solutions for mitigating speckle in imaging by acquiring multiple images with diverse speckle patterns by altering either the imaging frequency (frequency compounding) or the angle of incidence (angular compounding) [16, 26-28]. It is notable that image averaging is frequently referred to as compounding, and spatial compounding is used interchangeably with angular compounding [23-28]. These methods employ incoherent averaging approaches, introducing incoherence into the image generation process. The key advantage lies in reducing speckle

variations while retaining intrinsic intensity contrast. This technique results in smaller speckle fluctuations, enhancing contrast resolution. The reduction in speckle noise can be substantial, up to a factor of $\sqrt{N}$, where N represents the number of uncorrelated images captured at different frequencies or angles [16, 26-28]. It's essential to highlight that, despite these benefits, compounding techniques usually entail a trade-off, leading to a reduction in spatial resolution [16, 23-25].

Mathematically, if $I_i\ (x,y)$ represents the intensity of pixel (x,y) in the i-th acquired image, compounding involves forming the compounded image $C(x,y)$ as follows [16]:

$$C(x,y)= \frac{1}{N} \sum_{i=1}^{N} I_i(x, y) \tag{1. 4}$$

where N is the total number of sequentially acquired images. This averaging process capitalizes on the statistical independence of speckle patterns across different images, effectively attenuating the random noise component [16, 23-28]. In contrast, traditional image processing techniques often struggle to differentiate between noise and true structural information in a single image, leading to suboptimal results.

Moreover, compounding methods address the inherent variability of speckle patterns by providing a multisource perspective, enhancing the likelihood of capturing the real underlying structure. This is especially important when complex anatomical characteristics or fine details are present but obscured by speckle noise in individual frames.

1.2.3 Advantage of compounding methods over image processing techniques

The reduction of speckle noise in medical ultrasound imaging is a crucial pursuit for achieving optimal diagnostic clarity. In the context of this thesis, compounding approaches are preferred over typical image processing techniques as they offer a more robust and statistically validated approach to speckle elimination. Image processing algorithms, typically applied to individual frames, encounter challenges in distinguishing between true structural information and speckle noise due to their reliance on a single data source. In contrast, compounding methods excel by

exploiting the stochastic nature of speckle noise through the acquisition and averaging of multiple images [16, 18-28].

In conclusion, the compounding methods exploits the statistical independence of speckle patterns in different images, resulting in a more substantial reduction in speckle artifacts while preserving structural details. This not only elevates the interpretability of images but also contributes significantly to the precision of diagnoses in clinical contexts. That is why, in this thesis, we focused on compounding techniques rather than typical image processing. As we progress, we'll look into numerous proposed compounding methods to identify the most promising to focus and broaden its applicability in different medial contexts.

1.3 Different compounding methods for US despeckling

The compounding methods work by acquiring images of the same target volume in the same imaging plane, yet under various imaging conditions to create uncorrelated speckle patterns [26, 28]. Introducing decorrelation among acquired images can be achieved by imaging at distinct spatial locations, altering frequency ranges, or varying strain conditions [16, 23-28].

1.3.1 Frequency compounding

Frequency compounding aims to reduce speckle by compounding uncorrelated sub-images obtained by varying the center frequency during transmission or dividing the spectrum of radiofrequency (RF) signals into sub-bands during reception. Next, the sub-band images are added or averaged, with or without weighting variables used, to create the compounded image [29-40]. Speckle correlation across images is mostly dependent on center frequency variance, which is adjusted by a -6 dB pulse-envelope length of the sub-band signals [16]. Thus, when the sub-band bandwidths decrease, speckles show less correlation. But axial resolution must inevitably be compromised as a result of this narrowing.

Therefore, while this technique effectively reduces speckle, challenges like reduced temporal resolution and potential axial resolution deterioration persist.

1.3.2 Strain compounding

Strain compounding utilizes the inherent decorrelation between signals corresponding to different strain states. The external forces, utilized in techniques like sonoelastography, introduce three-dimensional tissue motion, enabling the creation of diverse strain states [41]. Noteworthy is the emphasis on selectively correcting in-plane motion (axial and lateral), leading to images with similar characteristics, aside from variations in speckle appearance attributed to uncorrected out-of-plane (elevational) motion [41]. Furthermore, an additional layer of speckle decorrelation is introduced through the correction of tissue motion, arising from dynamic changes in effective in-plane sample volume geometry.

Strain compounding differs fundamentally from previous proposed compounding methods in that signal decorrelation is predominantly caused by scatterer redistribution and changes in sample volume shape in the context of introducing external forces [41]. In contrast, in other compounding approaches the scatterer distribution is constant, and signal decorrelation results from phase shifts caused by changes in aperture position, elevational imaging plane, or imaging frequency [23-28]. Moreover, the drop in spatial resolution observed in other compounding approaches is due to underutilization of the whole aperture and/or bandwidth. In contrast, for strain compounding, spatial resolution deterioration is predominantly caused by tissue motion and subsequent motion correction [41]. However, due to the need for employing different strain condition needed for various image acquisition, temporal resolution degradation is unavoidable.

Strain compounding raises different challenges, such as the necessity for higher strain levels. This may limit therapeutic applications to deep-seated tissues that require significant compression for providing uncorrelated speckle patterns in different taken images [41]. Besides, tissue motion can lead a small object in the original image to move out of the image plane after compression. Consequently, maintaining contrast resolution poses an additional challenge in this compounding method compared to alternative techniques [41].

1.3.3 Spatial compounding

Spatial compounding, an alternative approach, reduces speckle by compounding sub-images acquired at different beam orientations or positions [42-49]. While this method results in a compromise on lateral and temporal resolutions, by given an identified loss of lateral resolution, the spatial compounding approach has a greater speckle reduction rate than the frequency compounding approach, making it more advantageous when considering spatial resolution [16, 42-49].

Despite the advantage in spatial resolution, spatial compounding suffers from a significant drawback: a loss of temporal resolution. This limitation makes it less suitable for imaging moving tissues, such as in cardiac imaging [16, 45-49]. The challenge is particularly pronounced in high-frequency US imaging, where the majority of scanners utilize single-element transducers. This is attributed to the fact that spatial compounding necessitates mechanical translation of the transducer multiple times to acquire uncorrelated speckle patterns for different ultrasound propagation directions [16, 42-49].

Despite its challenge, spatial compounding remains valuable, particularly in scenarios requiring a cleaner ultrasound image with well-defined boundaries. Spatial compounding methods exhibit versatility based on the viewing angle, manifesting as either azimuthal angular compounding or elevational angular compounding. The distinction lies in how the compounding is applied concerning the angular orientation during image acquisition.

1.3.3.1 Azimuthal angular compounding

Azimuthal angular compounding involves compounding images obtained from different azimuthal angles, typically achieved by steering the ultrasound beam laterally. By combining information acquired from various azimuthal perspectives, this approach enhances lateral resolution and reduces artifacts in the azimuthal direction [50, 51].

Azimuthal angular compounding, while beneficial in certain aspects, is not without its limitations. One notable drawback is the constrained spatial overlap of images acquired from

multiple transmission angles [16, 45-51]. This limitation arises from the lateral steering of the ultrasound beam, leading to areas in the imaged anatomy that may not be covered by all acquired perspectives. Consequently, the spatial continuity and comprehensive coverage of the imaged region may be compromised [49-54].

Additionally, the implementation of azimuthal angular compounding often necessitates extensive pre-processing for image alignment. Aligning images from different azimuthal angles requires careful registration to ensure accurate spatial correlation [50-52]. This pre-processing step not only introduces computational complexity but can also result in reduced frame rates during real-time imaging. The additional processing time required for alignment may impact the ability to achieve optimal temporal resolution, particularly in dynamic imaging scenarios.

1.3.3.2 Elevational angular compounding

Elevational angular compounding (EAC) captures partially correlated images by incrementally steering the elevational imaging plane through small angular steps [52-55]. Unlike azimuthal angular compounding, where scatterer distribution remains fixed, EAC leverages changes in sample volume geometry and scatterer redistribution during different elevational steps. This results in a dynamic acquisition of images that collectively contribute to a compounded representation with enhanced image quality. To elaborate, EAC's effectiveness arises from its ability to exploit the inherent decorrelation between signals acquired from slightly varied elevational perspectives.

The distinctive feature of EAC lies in its capacity to combine two key factors in medical imaging: mitigating speckle noise, which is inherent in ultrasound imaging, and preserving temporal resolution [6-16, 50-55]. By steering the elevational imaging plane with precision, EAC strikes a balance between noise reduction and temporal fidelity, making it a desirable choice for applications in medical diagnostics where both aspects are crucial for accurate interpretation and diagnosis.

However, the implementation of elevational angular compounding becomes feasible when either a two-dimensional array is available or laterally rotating a one-dimensional array is possible [52-55]. This method allows for the collection and incoherently averaging of partially correlated measurements taken from various elevational viewing angles. EAC involves acquiring partially correlated measurements by steering the image plane elevationally with slight inclinations. The result is an effective increase in elevational slice thickness, without directly impacting the in-plane (i.e., lateral and axial) resolution [52, 53]. This technique offers a practical means of optimizing spatial compounding, utilizing the array's two-dimensional capabilities to enhance elevational information without compromising lateral and axial clarity [52-55].

In EAC contrast resolution is improved only at the price of a slightly wide elevational beam. Simulations have been performed to show both the change in spatial resolution and the improvement in contrast resolution [52]. Results indicated minimal increase in the correlation length both laterally and axially. It was also shown that detectability can be significantly enhanced by increasing the number of measurements or increasing the differential inclination between measurements. This technique is therefore effective for reducing speckle noise while maintaining in-plane spatial resolution.

In the realm of medical imaging, despite the anticipated integration of this speckle reduction approach due to its potential to offer both high spatial and temporal resolution—which are the key factors in medical imaging and diagnostics—its application in clinical settings has not yet realized the expected traction [50-55]. In the following chapters, we will delve into this speckle reduction method in US imaging, shedding light on its advantages compared to other compounding techniques. Our research aims to reveal new insights and address the challenges associated with the implementation of this approach in medical context. The goal is to pave the way for its widespread use in medical imaging, ensuring that its benefits can be fully harnessed for improved diagnostic outcomes.

1.4 Thesis objectives

The motivation to preform research on new approaches for ultrasound despeckling came from the studies in section 1.3, where the limitations of present compounding methods for ultrasonic applications became apparent. Following these insights, the aim of the research presented in this thesis was to investigate both the theoretical and experimental applicability of a new implementation approach for elevational angular compounding for speckle reduction. The aim is to simultaneously maintain high speckle reduction efficiency and spatial resolution in real-time ultrasound imaging. The primary objective is to improve the utility of ultrasound, extending its applicability for diverse early diagnostic purposes. In other words, the ongoing efforts for the techniques and methods in speckle reduction for ultrasound imaging, contributing to maximize the potential of this promising imaging modality in the field of biomedical imaging.

The main objectives of this thesis are as follows:

1. Analysis and comprehensive review of the current research and the state of the art regarding techniques employed for speckle reduction in US imaging
2. Develop a new approach for implementation of the elevational angular compounding method to enhance its efficacy and feasibility in despeckling of US imaging in clinical context
3. Extend the application of the proposed despeckling method to radial US endoscopy, marking the first implementation of spatial compounding in this imaging setting.

1.5 Thesis outline

Aligned with the research objectives and motivation for this study, the dissertation is structured into four chapters in the following manner:

Chapter 1 have already covered the theoretical foundations of compounding methods, in particular the underlying concept which highlight it as a preferred approach compared to image processing techniques in retrieving the data obscured by the speckle noise. Following an in-depth review of the existing compounding methods, we were inspired to delve deeper into the elevational angular compounding. This technique shows great promise for clinical applications, offering effective speckle reduction while maintaining temporal and spatial resolution. However, there are challenges behind its adoption in clinical settings, despite its possibly greater overall efficiency over to other compounding methods. The aim of this research is to propose a new implementation approach that could broaden applicability of the elevational angular compounding in clinical context by addressing the current challenges.

Chapter 2 introduces a novel implementation approach utilizing acoustic refraction for the elevational angular compounding method using the existing 1D transducer arrays. Experimental validation on phantoms and excised tissue samples assesses the proposed method's efficacy in speckle reduction compared to conventional techniques. The chapter also includes a detailed analysis of the efficiency and impact of elevational angular deflection on speckle reduction and image fidelity.

Chapter 3 extends the application of the proposed method to radial ultrasound endoscopy, marking the first implementation of spatial compounding in this context. The chapter presents an in-depth analysis of speckle reduction efficiency and introduces optimized elevational angular deflection for lymph nodes, aiming to achieve the highest speckle reduction efficiency with minimal image fidelity loss.

Chapter 4 summarizes the key findings of the research and provides insights for future development and research directions. The conclusion reflects on the contributions of the study and outlines recommendations for overcoming existing challenges.

References

[1] N. B. Smith and A. Webb, Introduction to Medical Imaging: Physics, Engineering and Clinical Applications. Cambridge University Press, 2011.

[2] P. Morris, Biomedical Imaging: Application, and advances, Elsevier, 2014.

[3] A. Maier, S. Steidl, V. Christelyn, and J. Hornegger, Medical Imaging systems, Springer, 2018.

[4] P. Sprawls, Physical principles of Medical Imaging, 2nd Ed, Medical Physics Pub. Corp., 1995.

[5] W.R. Hendee, and E. R. Ritenour, Medical Imaging Physics, 4th Ed., John Wiley & Sons, Inc., 2002.

[6] P. Hoskins, A. Thrush, K. Martin, and T. A. Whittingham, Diagnostic Ultrasound: Physics and Equipment. Cambridge University Press, 2003.

[7] Th. L. Szabo, Diagnostic Ultrasound Imaging: Inside Out, 2nd Ed., Elsevier, 2014.

[8] V. Gibbs, D. Cole, and A. Sassano, Ultrasound Physics and Technology, How, Why and When, Churchill Livingstone Elsevier, 2009

[9] J. L. Cura, P.Segui, and C. Nicolau, Learning Ultrasound Imaging, Springer, 2012.

[10] J. G. Abbott and F. L. Thurstone, Acoustic speckle: Theory and experimental analysis, Ultrason. Imaging, vol. 1, pp. 303–324, 1979.

[11] J. W. Goodman, Statistical properties of laser speckle patterns, in Laser Speckle and Related Phenomena, J. C. Dainty, Ed. Berlin, Germany: Springer-Verlag, 1984, pp. 9–75.

[12] R. F. Wagner, S. W. Smith, J. M. Sandrik, and H. Lopez, Statistics of speckle in ultrasound B-scans, IEEE Trans. Sonics Ultrason., vol. SU–30, no. 3, pp. 156–163, May 1983.

[13] C. B. Burckhardt, Speckle in ultrasound B-mode scans, IEEE Trans. Sonics Ultrason., vol. 25, no. 1, pp. 1–6, 1978.

[14] R. F. Wagner, M. F. Insana, and S. W. Smith, Fundamental correlation lengths of coherent speckle in medical ultrasonic images, IEEE Trans. Ultrason., Ferroelectr., Freq. Control, vol. 35, no. 1, pp. 34–44, Jan. 1988.

[15] J. Zhang, Y. Cheng, Despeckling Methods for Medical Ultrasound Images, Springer Nature Singapore, 2019.

[16] Ch. Loizou, C. Pattichis, Despeckle filtering for Ultrasound imaging and videos, Second Edition, 2015.

[17] L. N. Bohs, B. J. Geiman, M. E. Anderson, S. C. Gebhart, G. E. Trahey, Speckle tracking for multi-dimensional flow estimation, V. 38, pp. 369-375, 2000.

[18] Ch. P. Loizou, C. S. Pattichis, Despeckle filtering algorithms and software for ultrasound imaging, Springer, 2022.

[19] Sh. Wu, Q. Zhu, and Y. Xie, Evaluation of various speckle reduction filters on medical ultrasound images, Annu. Int. Conf. IEEE Eng. Med. Biol. Soc., 2013.

[20] Sh. K. Pal, A. Bhardwaj, and A.P. Shukla, A review on despeckling filters in ultrasound images for speckle noise reduction, IEEE, 2021.

[21] T. Loupas, W. N. McDicken, & P. L. Allan, An adaptive weighted median filter for speckle suppression in medical ultrasonic images. IEEE Trans. Circuits Syst. 36, 129–135, 1989.

[22] M. A. Karaman, Kutay, & G. Bozdagi, An adaptive speckle suppression filter for medical ultrasonic imaging. IEEE Trans. Med. Imag. 14, 283–292, 1995.

[23] J. Zhang, & Y. Cheng, Despeckling Methods for Medical Ultrasound Images, Springer, Singapore, 2020.

[24] O. V. Michailovich, & A. Tannenbaum, Despeckling of medical ultrasound images. IEEE Trans. Ultrason. Ferroelectr. Freq. Control. 53, 64–78, 2006.

[25] P. C. Tay, Ch. D. Garson, S. T. Acton, & J. A. Hossack, Ultrasound despeckling for contrast enhancement. IEEE Trans. Image Process. 19, 1847–1860, 2010.

[26] M. Berson, A. Roncin, and L. Pourcelot, Compound scanning with an electrically steered beam, Ultrason. Imaging, vol. 3, no. 3, pp. 303–308, 1981.

[27] D. P. Shattuck and O. T. von Ramm, Compound scanning with a phased array, Ultrason. Imaging, vol. 4, no. 2, pp. 93–107, 1982.

[28] S. K. Jespersen, J. E. Wilhjelm, and H. Sillesen, Multi-Angle Compound Imaging, Ultrason. Imaging, vol. 20, no. 2, pp. 81–102, Apr. 1998.

[29] P. A. Magnin, O. T. on Ramm, and F. L. Thurstone, Frequency compounding for speckle contrast reduction in phased array images, Ultrason. Imaging, vol. 4, no. 3, pp. 267–281, 1982.

[30] H. E. Melton and P. A. Magnin, A-mode speckle reduction with compound frequencies and compound bandwidths, Ultrason. Imaging, vol. 6, no. 2, pp. 159–173, 1984.

[31] I. S. Song, C. H. Yoon, G. D. Kim, Y. Yoo, and J. H. Chang, Adaptive frequency compounding for speckle reduction, in IEEE International Ultrasonics Symposium, IUS, 2011.

[32] J. Lee and J. H. Chang, Dual-Element Intravascular Ultrasound Transducer for Tissue Harmonic Imaging and Frequency Compounding: Development and Imaging Performance Assessment, IEEE Trans. Biomed. Eng., 2019.

[33] M. W. Urban, A. Alizad, and M. Fatemi, Vibro-acoustography and multifrequency image compounding, Ultrasonics, 2011.

[34] J. S. Ullom, M. Oelze, and J. R. Sanchez, Ultrasound speckle reduction using coded excitation, frequency compounding, and postprocessing despeckling filters, in Proceedings IEEE Ultrasonics Symposium, 2010.

[35] C. Yoon, G. D. Kim, Y. Yoo, T. K. Song, and J. H. Chang, Frequency equalized compounding for effective speckle reduction in medical ultrasound imaging, Biomed. Signal Process. Control, 2013.

[36] G. E. Trahey, J. W. Allison, S. W.Smith, and O. T. von Ramm, A quantitative approach to speckle reduction via frequency compounding, Ultrason. Imaging, vol. 8, no. 3, pp. 151–164, 1986.

[37] S. M. Gehlbach and F. G. Sommer, Frequency Diversity Speckle Processing, Ultrason. Imaging, vol. 9, no. 2, pp. 92–105, Apr. 1987.

[38] G. E. Trahey, J. W. Allison, S. W. Smith, and O. T. von Ramm, Speckle Pattern Changes with Varying Acoustic Frequency: Experimental Measurement and Implications for Frequency Compounding, in IEEE 1986 Ultrasonics Symposium, pp. 815–818, 1986.

[39] Y. Li, Y. Winetraub, O. Liba, A. De La Zerda, and S. Chu, Optimization of the trade-off between speckle reduction and axial resolution in frequency compounding, IEEE Trans. Med. Imaging, vol. 38, no. 1, 2019.

[40] G. Cincotti, G. Loi, and M. Pappalardo, Frequency decomposition and compounding of ultrasound medical images with wavelet packets, IEEE Trans. Med. Imaging, 2001.

[41] P. Li, M. Ch. Chen, Strain compounding: a new approach for speckle reduction, IEEE Trans Ultrason Ferroelectr Freq Control, 49(1):39-46, 2002.

[42] G. E. Trahey, S. W. Smith, and O. T. von Ramm, Speckle Pattern Correlation with Lateral Aperture Translation: Experimental Results and Implications for Spatial Compounding, IEEE Trans. Ultrason. Ferroelectr. Freq. Control, vol. 33, no. 3, pp. 257–264, 1986.

[43] J. J. Dahl, D. A. Guenther, and G. E. Trahey, Adaptive imaging and spatial compounding in the presence of aberration, IEEE Trans. Ultrason. Ferroelectr. Freq. Control, 2005.

[44] H. Tu, J. A. Zagzebski, A. L. Gerig, Q. Chen, E. L. Madsen, and T. J. Hall, Optimization of angular and frequency compounding in ultrasonic attenuation estimations, J. Acoust. Soc. Am., 2005.

[45] Z. Zhang, L. Li, and H. Liu, Ultrasonic elastography optimization algorithm based on coded excitation and spatial compounding, Autom. Control Comput. Sci., 2017.

[46] J. F. Krücker, C. R. Meyer, G. L. Le Carpentier, J. B. Fowlkes, and P. L. Carson, 3D spatial compounding of ultrasound images using image-based nonrigid registration, Ultrasound Med. Biol., 2000.

[47] A. R. Groves and R. N. Rohling, Two-dimensional spatial compounding with warping, Ultrasound Med. Biol., 2004.

[48] M. O'Donnell and S. D. Silverstein, Optimum Displacement for Compound Image Generation in Medical Ultrasound, IEEE Trans. Ultrason. Ferroelectr. Freq. Control, 1988.

[49] G. E. Trahey, J. W. Allison, S. W. Smith, and O. T. von Ramm, Speckle Reduction Achievable by Spatial Compounding and Frequency Compounding: Experimental Results and Implications For Target Detectability, vol.768, no., p.768, 1987.

[50] Y. Li, N. Toyonaga, J.s Jiang, Al. Cable, S. Chu, Multiplicative frequency and angular speckle reduction in ultrasound imaging, 2023.

[51] D. P. Shattuck, & O. T. von Ramm, Compound scanning with a phased array. Ultrason. Imaging 4, 93–107, 1982.

[52] Li, P. C. & O'Donnell, M. Elevational spatial compounding. Ultrason. Imaging 16, 176–189 ,1994.

[53] Perperidis, A., McDicken, N., MacGillivary, T. & Anderson, T. Elevational spatial compounding for enhancing image quality in echocardiography. Ultrasound 24, 74–85 (2016). 9 Vol.:(0123456789) Scientifc Reports, 2020, 10:18173.

[54] P. Afshari, Ch. Zakian, J. Bachmann, and V. Ntziachristos, Speckle reduction in ultrasound endoscopy using refraction based elevational angular compounding, Scientific Reports, 2021.

[55] P. Afshari, Ch. Zakian, J. Bachmann, and V. Ntziachristos, Improving ultrasound images with elevational angular compounding based on acoustic refraction, Scientific Reports, 2020.

Chapter 2

2 Improving Ultrasound Images with Elevational Angular Compounding Based on Acoustic Refraction

Parastoo Afshari, Christian Zakian & Vasilis Ntziachristos, Improving ultrasound images with elevational angular compounding based on acoustic refraction. Scientific Reports 10, 18173, 2020.
https://doi.org/10.1038/s41598-020-75092-8

Summary and Author Contribution

The study explores an approach to enhance the quality of ultrasound (US) images through Elevational Angular Compounding (EAC). EAC aims to mitigate speckle noise, a common limitation in ultrasound imaging that hinders diagnostic accuracy. Existing EAC methods involve mechanically rotating 1D transducer arrays or employing costly 2D arrays, which complicates and increases the expense of US systems.

In this research, the authors introduce Refraction-Based Elevational Angular Compounding (REACT), a novel technique that overcomes these challenges. REACT utilizes a translating cylindrical acoustic lens to steer the ultrasound beam along the elevational direction, eliminating the need for complex mechanical components or expensive arrays. The authors demonstrate the superior speckle noise reduction and improving image quality capabilities of REACT compared to traditional EAC methods. This innovation eliminates the need for complex and costly mechanical components and offers a more practical solution for medical ultrasound devices. By improving image quality and reducing speckle noise, REACT has the potential to enhance the diagnostic precision of ultrasound examinations, making it a promising technology for future medical ultrasound devices.

My contribution to the presented manuscript where the following:

Methodology The study was designed by me and Christian Zakian. I developed the experimental hardware set-up required for the measurement, which included the electronics, mounting of the ultrasound transducer, preparation of the phantom, and ex vivo samples, and mechanical stages. I also developed the programming code needed to automate the acquiring the images, i.e., to control the stages and the data acquisition system. I also conducted the experiment and collected all the data.

Analysis I generated the code required to process and analyze the collected data using MATLAB. I and Christian Zakian worked together to interpretate the collected data and signals.

Writing and Revisions I drafted the initial manuscript with significant contributions from all authors. I created all figures using MATLAB and Microsoft word with valuable inputs from all authors. In response to the reviewer's requests, I carried out further experiments, and with help of Christian Zakian made changes to the article and adjusted the figures.

Abstract

Ultrasound imaging is affected by coherent noise or speckle, which reduces contrast and overall image quality and degrades the diagnostic precision of the collected images. Elevational angular compounding (EAC) is an attractive means of addressing this limitation since it reduces speckle noise while operating in real-time. However, current EAC implementations rely on mechanically rotating a one-dimensional (1D) transducer array or electronically beam steering of two-dimensional (2D) arrays to provide different elevational imaging angles, which increases the size and cost of the systems. Here we present a novel EAC implementation based on a 1D array, which does not necessitate mechanically rotating the transducer. The proposed refraction-based elevational angular compounding technique (REACT) instead utilizes a translating cylindrical acoustic lens that steers the ultrasound beam along the elevational direction. Applying REACT to investigate phantoms and excised tissue samples demonstrated superior suppression of ultrasound speckle noise compared to previous EAC methods, with up to a two-fold improvement in signal- and contrast-to-noise ratios. The effects of elevational angular width on speckle reduction were further investigated to determine the appropriate conditions for applying EAC. This study introduces acoustic refractive elements as potential low-cost solutions to noise reduction, which could be integrated into current medical ultrasound devices.

2.1 Introduction

Speckle noise is an inherent property of ultrasound (US) imaging that results from constructive and destructive interference of backscattered acoustic waves caused by heterogeneities in tissue [1–4]. While speckle can be exploited to obtain dynamic information (e.g., on blood flow) [5], it can also degrade both the resolution and contrast of static structures and blur the boundaries of layered tissues, which can hinder the interpretation of tissue morphology and fine structure and adversely affect diagnostic procedures [6–10]. Image post-processing or compounding methods are commonly used to reduce speckle in US imaging [11–20]. Post-processing is based on image filter algorithms that use information extracted from the images [11–13], which limits realistic enhancement of structures obscured by speckle noise. Compounding methods average sequential images from the same field of view (FOV) with varied spatial or frequency content [7–10], enhancing correlated features while removing uncorrelated speckle noise, which can reveal structures obscured by speckle in individual images. Frequency compounding methods either vary the emitted frequency or decompose the spectrum of the echo signal to obtain images with uncorrelated speckle patterns, while spatial compounding methods acquire images at different US beam orientations [14–20]. However, both compounding methods typically result in a loss of spatial or temporal resolution, as capturing multiple images reduces acquisition speeds and collecting signals from adjacent fields of view reduces the lateral resolution [18]. Elevational angular compounding (EAC) is a type of spatial compounding that can simultaneously offer high speckle noise reduction and good temporal resolution, making it desirable for medical applications [19]. EAC obtains partially correlated images by steering the elevational imaging plane with small angular steps [19, 20]. EAC methods typically employ either one-dimensional (1D) arrays that can only control the US beam in the azimuthal direction (i.e., parallel to the imaging plane) or two-dimensional (2D) arrays that can control the US beam in both the azimuthal and elevational directions (the latter being perpendicular to the imaging plane) [21–23]. US systems with 1D arrays are simple and inexpensive. However, implementing EAC in such systems necessitates bulky mechanical stages to physically move or rotate the 1D array in order to steer the beam in the

elevational direction [19], which is impractical in clinical applications. In contrast, US systems integrating 2D arrays can electronically steer the beam along the elevational direction without changing the detector's position [21–23]. However, EAC has only been preliminarily validated in systems integrating 2D detector arrays on simulated data and, although this implementation was reported in patents [24, 25], it has not thus far been experimentally validated. Furthermore, the use of 2D array detectors increases the size and cost of the US system. Thus, there is a need for a means of incorporating EAC into US systems that are both economical and have a small form factor. In this work, we aimed to develop a method of implementing EAC, which could be integrated into simple and low-cost US system without sacrificing the image enhancement capabilities. We hypothesized that an acoustic refractive lens could steer a US beam from a 1D transducer array, imparting it with the elevational steering ability of a stationary 2D array while retaining the advantages in size, cost, and simplicity of a 1D array. Furthermore, linear micro-translation of a refractive element should impart precision control of elevational angular steering in a 1D transducer array while minimizing motion artifacts compared to rotating the entire transducer. We describe herein this refraction based EAC technique (REACT) and assess its qualitative and quantitative enhancements of US images in experiments on phantoms and tissues ex vivo. Moreover, we examine the effect of experimental parameters that can cause image deformation due to compounding different elevational angular views.

2.2 Methods

2.2.1 Image acquisition. The implementation scheme of REACT using an acoustic refractive element is shown in Figure 2. 1a, c. In short, linear translation of the acoustic cylindrical lens (ACL) across the stationary 1D transducer array steers the acoustic beam along the elevation direction and can be adjusted by changing the ACL's position and radius of curvature (Figure 2. 1b). A linear transducer array with 128 unfocused elements and a central frequency of 7.5 MHz (12L5V, Terason, USA) connected to a portable acquisition console (Terason 2000+, USA) was employed for US imaging. A motorized translation stage (MTS50-Z8, Thorlabs) was used to shift the ACL at

predetermined linear steps (δ) in front of the 1D array transducer to obtain different elevational angular views by virtue of acoustic refraction. Each step has an approximate error of 0.7% of the step size. Because the lens translation was not automated, the acquisition was limited to an average of 20 frames per minute. However, implementing REACT with automated lens translation would allow for frame rates that are only limited by the acquisition speed of the US imaging system. Moreover, to provide two different effective elevational angular widths (Δ) needed for image fidelity exploration, samples were imaged at two different imaging depths (d). Figure 2. 1d depicts the elevational steering angle of the acoustic beam at different positions of the ACL.

2.2.2. Refractive element fabrication. Customized ACLs designed to cover the full sensor area were manufactured from Polymethyl methacrylate (PMMA), which has a sound speed of 2750 m/s and low acoustic attenuation of 1.4 dB/cm/MHz [26, 27]. The lenses were fabricated from 2.5 mm ± 4 µm thick PMMA blocks. Figure 2. 1b shows a schematic of the three manufactured lenses, ACL1, ACL2, and ACL3, with infinite (flat), 88 mm, and 24 mm curvature radii, respectively. The acoustic beam was steered in the elevational direction by refraction caused by the difference in acoustic impedance (Z) between the PMMA lens ($Z = 3.23 \times 10^6$ kg/m^{2}s) and water (the imaging medium, $Z = 1.49 \times 10^6$ kg/m^{2}s) [26, 27]. The distance between the transducer and ACL was held to <1 mm (while avoiding contact) to minimize the effect of multiple refection artefacts on the image due to the impedance mismatch between the PMMA and water. Each ACL can produce a characteristic maximum elevational angular defection, which is 0° for ACL1, 2.5° for ACL2, and 5° for ACL3. Given the radius of curvature, the usable scanning length (w) is geometrically constrained, and the translation step is defined to acquire a fixed number of images (N = 100). ACL1 and ACL2 were scanned with steps of $\delta_1 = \delta_2 = 150$ µm, whereas ACL3 was scanned in steps of $\delta_3 = 100$ µm. The total defection angle was theoretically calculated using Snell's law as $c_1 \sin\theta_2 = c_2 \sin\theta_1$ (where c_1 and c_2 are the longitudinal wave velocities, and θ_1 and θ_2 are incidence and exit angles in materials 1 and 2, respectively) [28, 29] and confirmed experimentally as follows.

2.2.3. Effective field of view and elevation angle characterization. The transducer's inherent elevational angular FOV (θ_i), without ACLs, was first determined by measuring the distance between two opposing needle tips, which were inserted into opposite sides of an agar

phantom until they just appeared on each side of the image. By recording their imaging depth, an inherent elevation angular FOV of 29.5° was calculated for the employed linear transducer. Similarly, the extended elevational angular FOVs (θ_E) when employing ACL2 and ACL3 were calculated as 32° and 34.5°, respectively. The effective compounding angles of 0° (ACL1, serving as a non-angular compounding reference), 2.5° (ACL2), and 5° (ACL3) were computed by subtracting the inherent transducer angular elevation FOV from the extended ones obtained for each ACL. Imaging samples. Custom acoustic phantoms (50 mm × 20 mm × 15 mm) comprising 2% agar and 4% TiO_2 in 100 ml water were manufactured to assess speckle reduction efficiency and image fidelity. Phantom A embedded three 7 mm-diameter cylindrical holes and was used to evaluate REACT's speckle reduction efficiency. Phantom B contained three different holes in the shape of a cylinder (no diameter gradient), frustum (intermediate diameter gradient), and cone (high diameter gradient) and was used to explore the effect of elevational angular width and the target's cross-sectional variation on EAC image fidelity. An excised chicken heart and swine kidney were utilized as biological phantoms to further explore the importance of the cross-sectional appearance of the sample on image fidelity for a given elevational angular width using REACT. The chicken heart was chosen due to its conical shape to represent a sample with high cross-sectional variation. The swine kidney, which is larger than a chicken heart, was selected because of its low cross-sectional variation. For comparability, US images of the biological phantoms were captured and despeckled under the same imaging condition utilizing ACL3. The phantoms were stabilized during imaging by pinning them to polystyrene foam. No live specimens were used in the experiments.

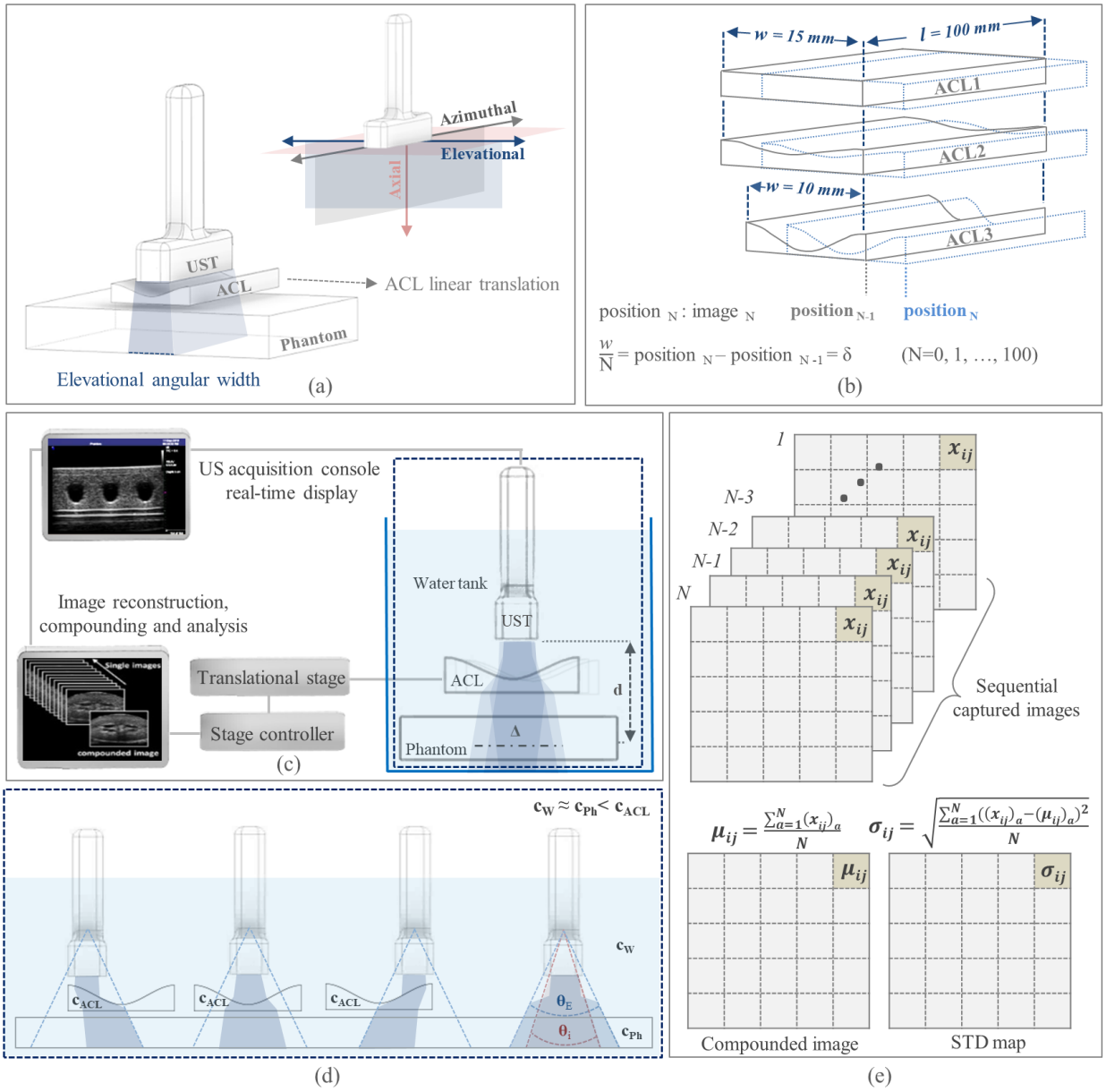

Figure 2. 1 REACT elevational angular steering concept and implementation. **(a)** Linear translation of the ACL along the elevational direction in front of the stationary 1D transducer controls the elevational angular FOV. UST, ultrasound transducer, ACL, acoustic cylindrical lens, Δ, elevational angular width. **(b)** Renderings of ACL1, ACL2, and ACL3, which produce 0°, 2.5° and 5° angular defections, respectively. The width and length of the ACLs are indicated by w and l, respectively. The ACLs are moved in consistent step sizes (δ), which are equal to the width of the ACL (w) divided by number of images (N) needed for compounding. **(c)** REACT imaging acquisition configuration. d, imaging depth. **(d)** Elevational angular steering in different positions of the ACL. Sound waves propagate through the water, phantom, and ACLs at speeds of c_w, c_{Ph}, and c_{ACL}, respectively, where $c_w \approx c_{Ph} < c_{ACL}$ Imaging at different positions of the ACL extends the elevational angular FOV (θ_E) of the transducer compared to its inherent elevational angular FOV (θ_i). **(e)** Matrix operators used to compute the compounded image

and standard deviation (STD) decorrelation map at the pixel level using the sequentially captured images.

2.3.4 Analysis method. Sequential images were captured in different positions of the ACL and compounded using a mean compound operator30 (Figure 2. 1e). The intensity and standard deviation (STD) were mapped at the pixel-level to investigate the efficiency of REACT to generate correlated structures and uncorrelated speckle patterns across acquired images (Figure 2. 1e). Single and compounded images were compared for each elevational angular defection case to assess the despeckling efficiency. Rectangular regions of interest (ROIs = 28 × 140 pixels) within solid and empty (holes) regions in the phantom were selected to derive the intensity average and standard deviation to compute SNR and CNR. These indices were used as quantitative indicators of image improvement. The speckle and electrical noise suppression was also evaluated by inspecting the A-line intensity profiles of the single and compounded images.

2.3 Results

Figure 2. 2 shows the speckle reduction efficiency achieved using REACT. Figure 2. 2a–h depicts uncompounded (single), averaged and compounded US images of a phantom with cylindrical holes (phantom A) at direct view and elevational angular defections of 0°, 2.5°, and 5°. Visual inspection of the US image pairs in Figure 2. 2a–h reveals noticeable speckle noise reduction with wider elevational angular defection, with the greatest despeckling effect observed for the 5° case. Despite this wide defection angle (5°), the edges of the holes in the phantom are preserved upon compounding, as highlighted by the arrows in Figure 2. 2h. Figure 2. 2i shows the A-line intensity profiles obtained for a single image (Figure 2. 2c) compared to profiles of the images that were compounded at elevational defections of 0° (Figure 2. 2d) and 5° (Figure 2. 2h). Inspecting the A-line intensity profile of the single image across the solid phantom sections (blue rectangles in Figure 2. 2i) shows high intensity variations related to the granular nature of speckle noise. These variations are strongly suppressed by REACT at an elevational angular defection of 5°. In contrast, compounding with a 0° elevational angular defection, which acts as a comparative reference to normal averaging, only moderately suppresses the intensity variations. The noise reduction upon

compounding at 0° is primarily due to electrical noise averaging, which is apparent in the A-line intensity profile variation across the water-filled regions (gray rectangles in Figure 2. 2i), where no scatterers are expected to produce speckle. Still, even in the absence of speckle, compounding at a 5° elevational angle results in greater noise reduction than at 0°, demonstrating that REACT reduces both speckle noise and overall US electrical noise more efficiently than normal averaging. To quantify this observation, Figure 2. 2j shows the effect of increasing the number of images used for averaging and compounding on the SNR, as calculated within the ROI (red rectangle) in the solid region of the phantom in Figure 2. 2b. As expected, SNR increases for all cases, yet at a greater rate for the 5° EAC case, owing to a reduction in both speckle and electrical noise. Note that, for all EAC cases (with the ACL), initial SNR is lower compared to the normal averaging case (without the ACL), as seen in the inset of Figure 2. 2j. This is due to the signal loss caused by the acoustic attenuation and refection. However, owing to the high despeckling efficiency of REACT, the final SNR in the 5° EAC case is two times higher than for normal averaging (Figure 2. 2j).

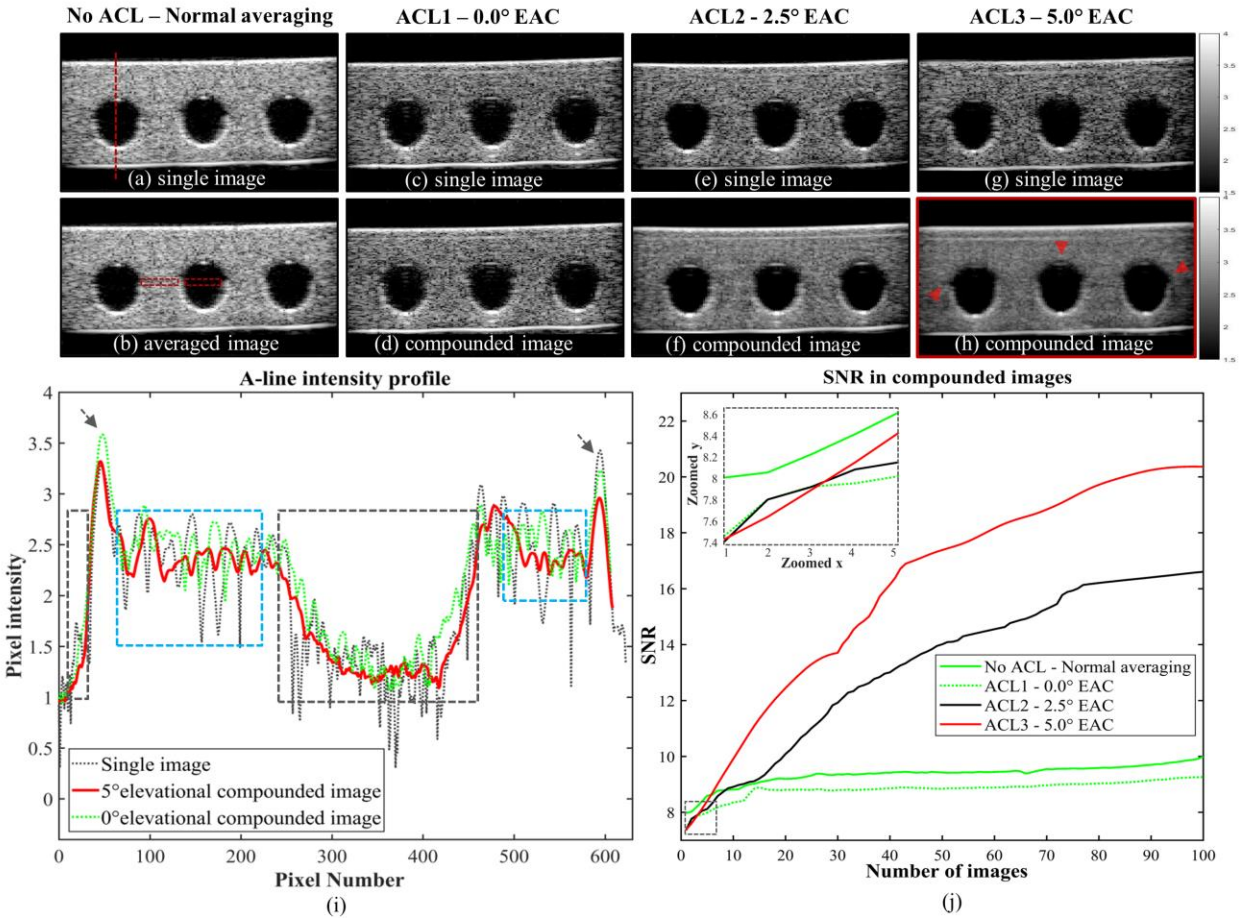

Figure 2. 2 Speckle reduction achieved with REACT. **(a)-(h)** Single and compounded US images of a phantom with embedded cylindrical holes (phantom A) using three different ACLs. Images captured through no ACL in (a) and (b), ACL1 (0° deflection angle) in (c) and (d), ACL2 (2.5° deflection angle) in (e) and (f), and ACL3 (5° deflection angle) in (g) and (h). Arrows in (h) show despeckled features and preserved edges obtained with the 5° elevational compounding. **(i)** A-line intensity profiles along the vertical dashed line in (a) applied through the single and compounded images with 0° and 5° elevation angle deflection; arrows indicate the phantom's surfaces. Gray rectangles indicate water-filled regions above the top surface and inside the hole, blue rectangles indicate the regions inside the solid phantom. **(j)** Effect of increasing the number of images on SNR, for the cases of normal averaging using no ACL and compounding using ACL1, ACL2 and ACL3. Rectangular ROIs in (b) show regions used for deriving the SNR and CNR in (j) and Table 1.

Table 2. 1 shows SNR and CNR improvements obtained using REACT. Quantitative indices extracted from the two ROIs (28×140 pixels) specified in Figure 2. 2b were used to compare the despeckling efficiency of normal averaging and REACT at different elevational angular defections. The higher SNR and CNR in the wider elevational angular acquisition are consistent with the observations in Figure 2. 2

Table 2. 1 SNR and CNR improvement using REACT. SNR: signal to noise ratio = μ/σ, CNR: contrast to noise ratio = $|\mu_{Hole} - \mu_{Phantom}|/\sigma_{Hole}$.

ACL Type	Phantom ($SNR_{compounded}/SNR_{single} - 1$)	Phantom and Hole ($CNR_{compounded}/CNR_{single} - 1$)
No ACL (normal averaging)	0.24	0.27
ACL1 (0.0° deflection angle)	0.23	0.28
ACL2 (2.5° deflection angle)	1.22	1.84
ACL3 (5.0° deflection angle)	1.72	2.18

Figure 2. 3 demonstrates the effect of elevational angular width (Δ) and the target's cross-sectional variation on image fidelity after elevational angular compounding. The schematic in Figure 2. 3a illustrates the configuration of phantom B, which contains three holes with shapes approximating a cylinder, frustum, and cone. These holes have different diameter gradients along the entire angular imaging width, enabling the investigation of the correlation between Δ and image fidelity. Phantom B was imaged using ACL3 at two different imaging depth (d_1=1.5 cm and d_2 = 5.5 cm), i.e., two effective Δ values. A single image and two compounded images using 5°

elevational angular defection are shown in Figure 2. 3b–d. As expected, image fidelity upon compounding suffered most for the conical hole (Figure 2. 3c, d, cone), which has the highest diameter gradient along elevational direction, even for the shallow imaging depth (d_1, smaller Δ). The cone with an intermediate diameter gradient (Figure 2. 3c, d, frustum) displays acceptable image fidelity for the smaller Δ at d_1 but is more impacted at d_2. However, the cylindrical hole (no diameter gradient, labeled cylinder) shows image fidelity for both Δ cases, without blurry edges. The impacts of these findings were further explored using a biological phantom of an excised chicken heart (Figure 2 .3e). Figures 2. 3f, g show the single (Figure 2. 3f) and compounded (Figure 2. 3g) images obtained from the organ with the ACL3 at d_2. Visual examination of these US images reveals edge blurring and structure distortion in the compounded image (arrows in Figure 2. 3g) due to the high diameter gradient of the organ in the elevational direction, similar to the cone case in Phantom B (as depicted by the blue dotted triangle in Figure 2. 3e).

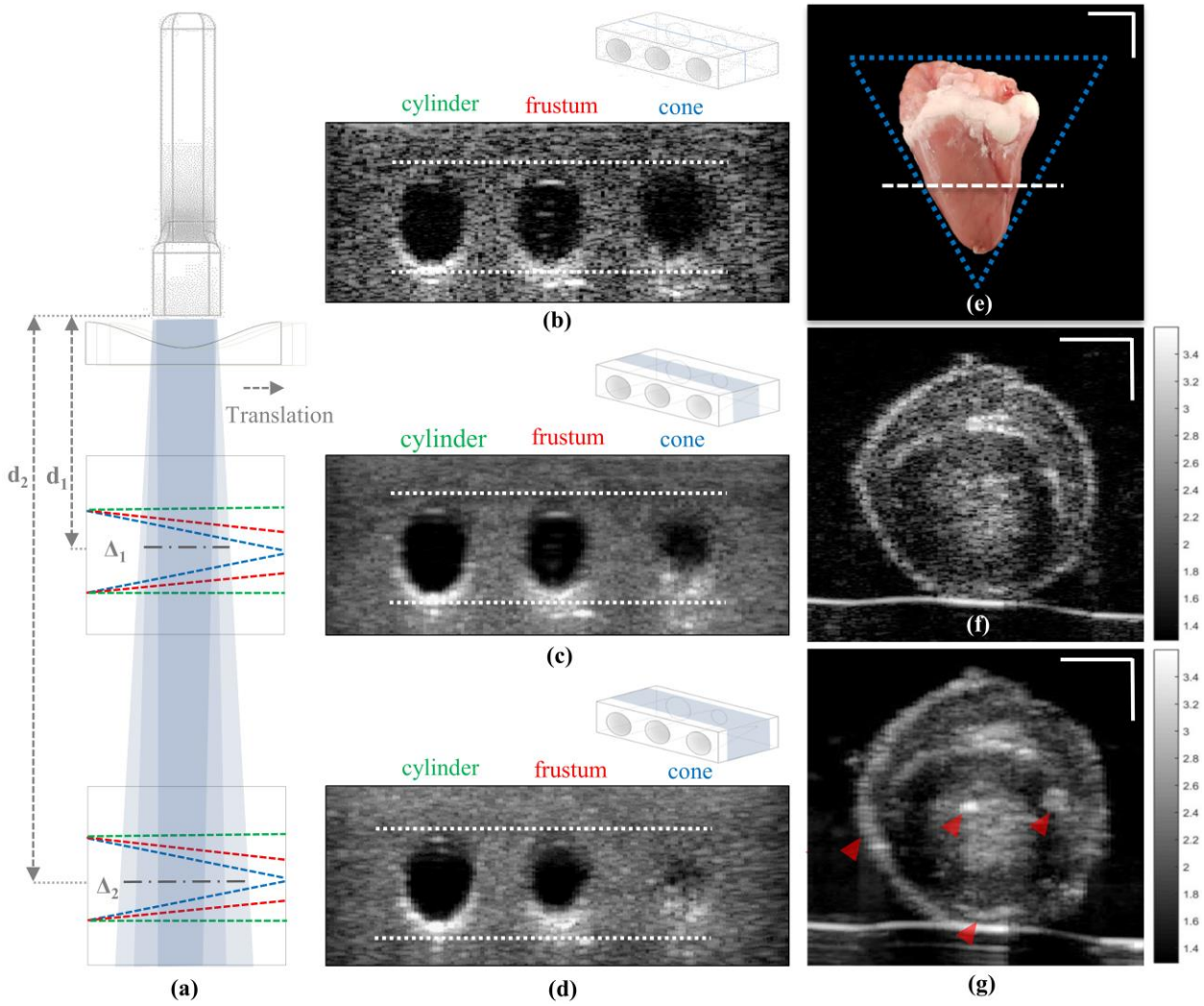

Figure 2. 3 Elevational angular width affects elevational angular compounded image fidelity. **(a)** Schematic of the imaging acquisition configuration depicting the elevation angular width ($\Delta_1 \simeq 1.3$ mm and $\Delta_2 \simeq 4.8$ mm) at different phantom distance positions (d_1=1.5 cm and d_2=5.5 cm). Green, red, and blue dashed lines show the cross-section of the cylinder, frustum, and conical hole shapes in the phantom, respectively (phantom B). **(b)** Single US image of the phantom at depth d_2. White dashed lines show the holes' boundaries. **(c), (d)** 5° elevational compounded images at depths d_1 and d_2, respectively. **(e)** Excised chicken heart; white dashed line shows the image cross section location in (f) and (g). Blue dashed lines indicate the conical shape of the chicken heart. **(f), (g)** Single and 5° elevational compounded US images of chicken heart at depth d_2. Red arrows highlight the effect of compounding and loss of fidelity compared to the single image in (f). Scale bars: 1 mm in e, 0.5 mm in (f) and (g).

Figure 2. 4 demonstrates speckle reduction upon applying REACT to image a swine kidney (Figure 2. 4a), which has a cylindrical shape and thus a low diameter gradient. Figure 2. 4b, c show

single and compounded US images of the swine kidney, with the latter produced using ACL3 at a depth of $d_2 = 5.5$ cm. Visual inspection of the US images in Figure 2. 4 reveals marked speckle noise reduction using REACT without blurriness or structure distortion, despite the use of the same imaging conditions as for the chicken heart (Figure 2. 4g). The difference in image fidelity between the two organs is attributable to the lower variation of the swine kidney's cross-sectional appearance (low diameter gradient) across the angular imaging width compared to that of the chicken heart. Figure 2. 4e, f display the variation in pixel intensity for images compounded at elevational angles of 0° and 5°, which was mapped to investigate the speckle pattern decorrelation between individual captured images (Figure 2. 4d). As expected, higher speckle pattern decorrelation is obtained for images captured within the 5° elevational angle, which therefore resulted in higher speckle reduction as demonstrated in Figure 2. 4c. Figure 2. 4g shows A-line intensity profiles from a single image of the swine kidney (corresponding to the red dotted line in Figure 2. 4c) compared to images compounded at elevational angle of 0° and 5°. As in the case of phantom A (Figure 2. 4g), the high variation of the A-line intensity profile of the single image across solid tissue sections (blue rectangles in Figure 2. 4g) is strongly suppressed upon compounding at a 5° elevational angle, but much less so at 0°. It can be seen that electrical noise is largely suppressed using compounding at both 0° and 5° elevational angles, observable in the A-line intensity profile across the hypoechoic regions where minimal speckle source is expected (gray rectangles in Figure 2. 4g). It is noteworthy that using REACT with 5° elevational compounding shows better efficiency not only in speckle reduction but also in US electrical noise suppression, similar to the results in Figure 2. 2g. To quantify this observation, Figure 2. 4h, i show the effect of increasing the number of images used for compounding on SNR, standard deviation (STD), and CNR for 0° and 5° EAC, calculated within the specified ROIs in Figure 2. 4b. In both cases, SNR and CNR trend upward while STD trends downward, yet with greater rates for the 5° case due to reduction in both speckle and electrical noise.

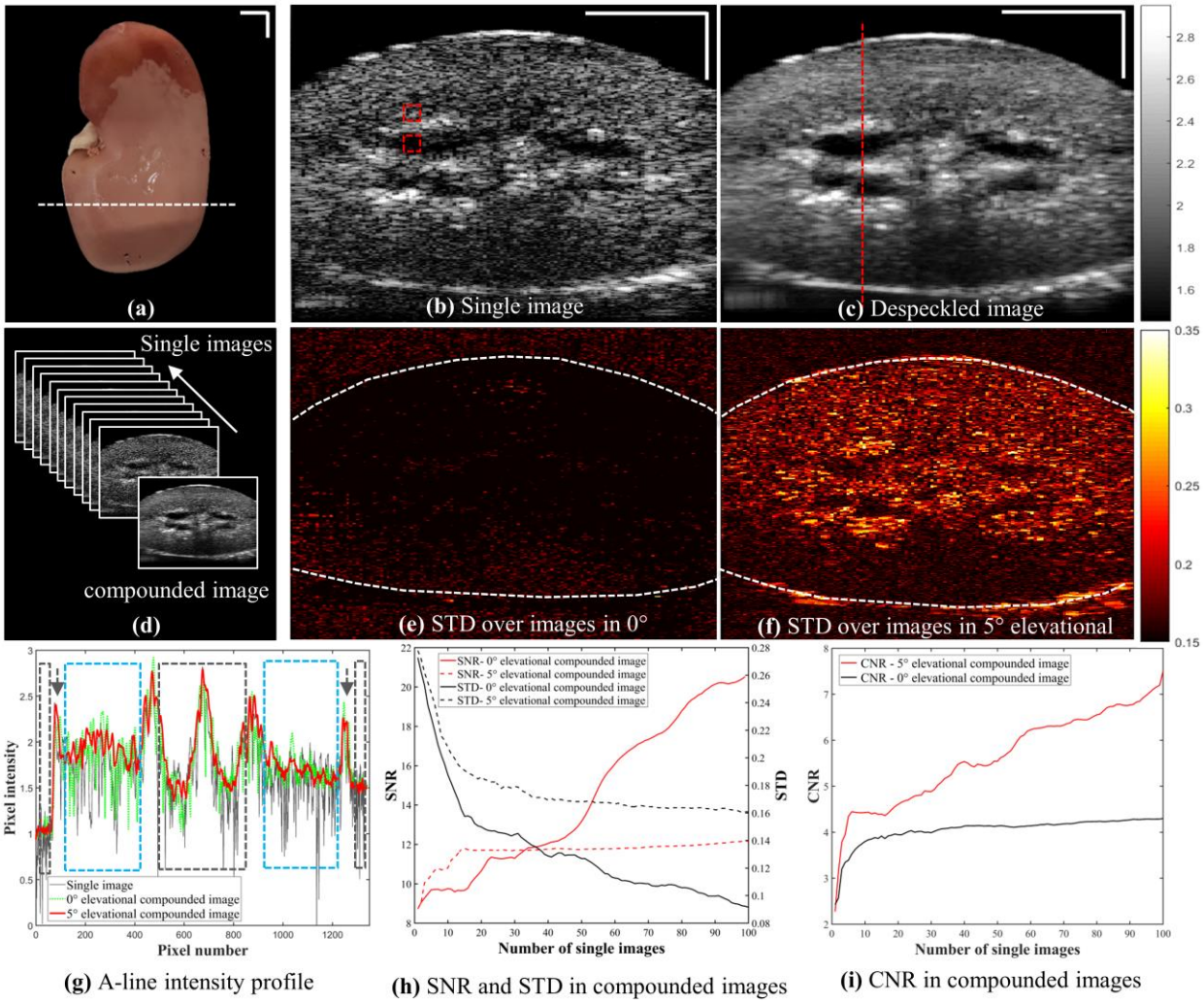

(g) A-line intensity profile **(h)** SNR and STD in compounded images **(i)** CNR in compounded images

Figure 2. 4 REACT demonstrates efficient US speckle reduction in a swine kidney. **(a)** Excised swine kidney; white dashed line shows the image cross-section location in (b) and (c). **(b), (c)** Single and compounded US images of a swine kidney at a depth of 5.5 cm using ACL3. Rectangular ROIs in (b) show regions used for deriving the SNR, STD and CNR indices plotted in (h) and (i). **(d)** Representation of the compounding of a series of images by REACT. **(e), (f)** Intensity of STD maps at pixel-level along all captured images, using ACL1 and ACL3, respectively; dashed lines delineate the tissue surface contour. **(g)** A-line intensity profiles along the vertical dashed line in (c) applied through the single and elevational compounded images within 0° and 5° elevation angle deflection. Arrows demonstrate the tissue's surfaces. Grey rectangles indicate hypoechoic regions above the top surface and inside the holes. Blue rectangles indicate regions within the tissue. Scale bars: 1 mm. **(h)** Effect of increasing the number of images used for compounding on SNR and STD within tissue and inside the hole for the cases of 0° and 5° EAC. **(i)** Effect of increasing the number of images used for compounding on CNR for the cases of 0° and 5° EAC.

2.4 Discussion

Speckle noise in US imaging adversely affects its diagnostic accuracy. Among proposed despeckling methods, compounding techniques are preferable because they can improve image quality and reveal real structures obscured by speckle noise, which are otherwise irretrievable using image processing techniques. This functionality requires the acquisition of multiple images with uncorrelated speckle patterns, which often comes at the cost of increased size and complexity of the imaging setup, limiting its applicability for clinical translation. Here, we have demonstrated a new refraction-based elevational angular compounding technique (REACT), which efficiently despeckles US images using an acoustic refractive element. This method enables EAC in a US system comprising a low-cost 1D detector array without moving or tilting the entire transducer head, eliminating the need for bulky mechanical stages or costly 2D arrays and easing implementation in current US imaging systems equipped with 1D arrays.

In contrast to previous EAC implementations, REACT uses a fixed 1D transducer array with a translating acoustic cylindrical lens. Visual and quantitative inspection of US images depicted in Figure 2. 2 and Figure 2. 4 illustrates the capability of REACT to reduce speckle noise. Compounded images acquired with elevational angular defections of 0°, 2.5°, and 5° improved the CNR by 0.28×, 1.84×, and 2.18×and SNR by 0.23×, 1.22×, and 1.72×compared to single images, respectively. Note that CNR and SNR improvement in the 0° elevational compounded image is due to electrical noise suppression, whereas the corresponding improvement for the 2.5° and 5° cases is due to the both electrical and speckle noise reduction achieved by averaging uncorrelated speckle image patterns from different elevational angular views. As expected, the wider the elevational angular acquisition, the greater the speckle suppression in the compounded image [13, 14]. While the widest angle employed in our study was 5°, the selection of the optimal compounding angle should take into account the trade-of between speckle reduction efficiency and image distortion (discussed below). Our results in Table 1 suggest that REACT offers at least twice the enhancement in SNR and CNR compared to previous reported implementations of EAC14. This superior enhancement could be attributed to a reduction in motion artifacts because of the fixed transducer. Note that imaging through the PMMA refractive lenses caused a 7.5% signal loss due

to acoustic attenuation and refection (inset in Figure 2. 2j). REACT's SNR could be further improved by minimizing this signal loss using materials with lower acoustic impedance and attenuation compared to PMMA (e.g., TPX [27]) and utilizing diffraction lenses with lower effective thicknesses [31].

Although EAC is recognized as an efficient way to suppress speckle noise in US images, it suffers from anatomic structure deformation and edge blurriness in compounded images captured within wide elevational angular views [13,14]. Our results demonstrate that image deformation can also occur in EAC with narrow elevational angles, particularly from deeper imaging positions, due to the associated increase in elevational angular width (Δ). Image fidelity in EAC, or in other words, accurate representation of structural features from the despeckled plane, is affected by interference from structures in adjacent elevational planes. We explored the trade-of between imaging depth and elevational angular width when employing EAC methods on targets with shapes that have no (cylinder), low (frustum), and high (cone) diameter gradient along the elevational direction (Figure 2. 3). We found that higher image fidelity is obtained with targets that preserve their cross-sectional appearance along the elevational angular width (cylinder), while image fidelity increasingly suffers for targets with intermediate and high diameter gradients (frustum and cone). The effect of cross-sectional variation on image fidelity was further validated by imaging an ex vivo chicken heart and swine kidney with REACT, which demonstrated the importance of accounting for the morphology of the sample for a given elevational angular width in EAC. The spatial resolution along elevational direction is the main limiting factor in all EAC implementation and depends on the total elevational beam width. Hence, out of plane signals can degrade compounding quality, particularly when imaging small organs. This was confirmed in our experiments, where the high variation of the cross sectional appearance of the chicken heart resulted in distortions in the compounded image (Figure 2. 3f, g), whereas the low variation in the cross-sectional appearance of the excised swine kidney led to speckle reduction with no loss in image fidelity (Figure 2. 3b, c). Despeckling of smaller organs using EAC could be performed by reducing the angular compounding width at the cost of a lower despeckling efficiency. We found through experiment that 5° EAC afforded high despeckling efficiency with minimal image fidelity loss in large organs, such as the kidney. However, determination of the optimal elevational angle

width for different organs or applications is required to ensure the highest despeckling efficiency without significant loss of image fidelity. Future studies will be conducted on optimization algorithms using quantitative image analysis to investigate the optimal compounding angle for specific targets. REACT could be attractive in targets with lower expected elevational variations such as peripheral vascular, muscle, or bone imaging. In summary, we utilized acoustic refraction to introduce elevational angular steering into existing 1D transducer arrays and demonstrated its application in a novel implementation of EAC called REACT. Such a low-cost and simple compounding despeckling method can be of great benefit in clinics to improve current US visualization and interpretation during disease diagnosis. Further work aims at miniaturizing ACL embodiments and allowing real-time despeckling by automating the position of the lens and synchronizing frames to evaluate REACT in a clinical context.

Data availability

The datasets generated during and/or analyzed during the current study are available from the corresponding author on reasonable request.

Received: 11 August 2020; Accepted: 12 October 2020

Published online: 23 October 2020

References

[1] Rumack, C. M., Wilson, S. R. & Charboneau, J. W. Diagnostic Ultrasound, 1–28 (Elsevier Mosby, London, 2005).

[2] Szabo, T. L. Diagnostic Ultrasound Imaging: Inside Out, 1–37 (Academic press, 2013).

[3] Goodman, J. W. Some fundamental properties of speckle. J. Opt. Soc. Am. 66, 1145–1150 (1976).

[4] Burckhardt, Ch. B. Speckle in ultrasound B-mode scans. IEEE Trans. Sonics Ultrason. 25, 1–6 (1978).

[5] Nyrnes, S. A., Fadnes, S., Wigen, M. S., Mertens, L. & Lovstakken, L. Blood speckle-tracking based on high-frame rate ultrasound imaging in pediatric cardiology. J. Am. Soc. Echocardiogr. 33, 493–503 (2020).

[6] Tay, P. C., Garson, Ch. D., Acton, S. T. & Hossack, J. A. Ultrasound despeckling for contrast enhancement. IEEE Trans. Image Process. 19, 1847–1860 (2010).

[7] Zhang, J. & Cheng, Y. Despeckling Methods for Medical Ultrasound Images (Springer, Singapore, 2020).

[8] Park, J., Kang, J. B., Chang, J. H. & Yoo, Y. Speckle reduction techniques in medical ultrasound imaging. Biomed. Eng. Lett. 4, 32–40 (2014).

[9] Narayanan, S. K. & Wahidabanu, R. S. D. A view on despeckling in ultrasound imaging. Int. J. Signal Process. Image Process. Pattern Recognit. 2, 85–98 (2009).

[10] Michailovich, O. V. & Tannenbaum, A. Despeckling of medical ultrasound images. IEEE Trans. Ultrason. Ferroelectr. Freq. Control. 53, 64–78 (2006).

[11] Joel, T. & Sivakumar, R. An extensive review on despeckling of medical ultrasound images using various transformation techniques. Appl. Acoust. 138, 18–27 (2018).

[12] Loupas, T., McDicken, W. N. & Allan, P. L. An adaptive weighted median filter for speckle suppression in medical ultrasonic images. IEEE Trans. Circuits Syst. 36, 129–135 (1989).

[13] Karaman, M. A., Kutay, M. A. & Bozdagi, G. An adaptive speckle suppression filter for medical ultrasonic imaging. IEEE Trans. Med. Imag. 14, 283–292 (1995).

[14] Shattuck, D. P. & von Ramm, O. T. Compound scanning with a phased array. Ultrason. Imaging 4, 93–107 (1982).

[15] Magnin, P. A., von Ramm, O. T. & Turstone, F. L. Frequency compounding for speckle contrast reduction in phased array images. Ultrason. Imaging 4, 267–281 (1982).

[16] Trahey, G. E., Allison, J. W., Smith, S. W. & von Ramm, O. T. A quantitative approach to speckle reduction via frequency compounding. Ultrason. Imaging 8, 151–164 (1986).

[17] Trahey, G. E., Smith, S. W. & von Ramm, O. T. Speckle pattern correlation with lateral aperture translation: experimental results and implications for spatial compounding. IEEE Trans. Ultrason. Ferroelectr. Freq. Control 33, 257–264 (1986).

[18] Chang, J. H., Kim, H. H., Lee, J. & Shung, K. K. Frequency compounded imaging with a high-frequency dual element transducer. Ultrasonics 50, 453–457 (2010).

[19] Perperidis, A., McDicken, N., MacGillivary, T. & Anderson, T. Elevational spatial compounding for enhancing image quality in echocardiography. Ultrasound 24, 74–85 (2016). 9 Vol.:(0123456789) Scientifc Reports | (2020) 10:18173 | https://doi.org/10.1038/s41598-020-75092-8 www.nature.com/scientificreports/

[20] Li, P. C. & O'Donnell, M. Elevational spatial compounding. Ultrason. Imaging 16, 176–189 (1994).

[21] Hooi, F. M., Tomenius, K. E., Fisher, R. & Carson, P. L. Hybrid beamforming and steering with reconfgurable arrays. IEEE Trans. Ultrason. Ferroelectr. Freq. Control. 57, 1311–1319 (2010).

[22] Shung, K. K. Te principle of multidimensional arrays. Eur. J. Echocardiogr. 3, 149–153 (2002)

[23] Wildes, D. G. et al. Elevation performance of 125D and 15D Transducer arrays. IEEE Trans. Ultrason. Ferroelectr. Freq. Control. 44, 1027–1037 (1997).

[24] Haugen, G. U., Kristofersen, K. & Sornes A. R. Method and apparatus for performing ultrasound elevation compounding. U.S. Patent 9 204 862. (2015).

[25] Adams, D. P. & Tiele, K. E. Ultrasound imaging system and method for spatial compounding. U.S. Patent 6 464 638. (2002).

[26] Xia, W., Piras, D., van Hespen, J. C. G., Steenbergen, W. & Manohar, S. A new acoustic lens material for large area detectors in photoacoustic breast tomography. Photoacoustics 1, 9–18 (2013).

[27] Bloomfeld, P. E., Lo, W. J. & Lewin, P. A. Experimental study of the acoustical properties of polymers utilized to construct PVDF ultrasonic transducers and the acousto-electric

properties of PVDF and P(VDF/TrFE) flms. IEEE Trans. Ultrason. Ferroelectr. Freq. Control. 47, 1397–1405 (2000).

[28] Hohenwarter, D. & Jelinek, F. Snell's law of refraction and sound rays for a moving medium. J. Acoust. Soc. Am. 105, 1387–1388 (1999).

[29] Finn, S., Glavin, M. & Jones, E. Speckle Reduction in Echocardiography: Trends and Perceptions. In Echocardiography—New Techniques, G. Bajraktari, 41–68 (InTech, 2012).

[30] Wilhjelm, J. E., Jensen, M. S., Jespersen, S. K., Sahl, B. & Falk, E. Visual and quantitative evaluation of selected image combination schemes in ultrasound spatial compound scanning. IEEE Trans. Med. Imaging 23, 181–190 (2004).

[31] Chen, J., Xiao, J., Lisevych, D., Shakouri, A. & Fan, Zh. Deep-subwavelength control of acoustic waves in an ultra-compact metasurface lens. Nat. Commun. 9, 4920 (2018).

Acknowledgments

This project has received funding from the European Union's Horizon 2020 research and innovation program under grant agreement 732720 (ESOTRAC) as well as from European Union's Horizon 2020 research and innovation program under the Marie-Sklodowska-Curie grant agreement No 721766 (FBI). The authors also thank Dr. Robert J. Wilson for proofreading the manuscript. Author contributions P.A. and C.Z. designed the study. P.A. produced phantoms, prepared ex vivo samples and carried out the experiments. P.A. collected and analyzed the data and prepared all figures in the manuscript. P.A. and C.Z. interpreted the data and wrote the manuscript. V.N. reviewed and approved the final manuscript.

Funding: Open Access funding enabled and organized by Project DEAL.

Competing interests: The authors declare no competing interests.

Additional information: Correspondence and requests for materials should be addressed to V.N

Chapter 3

3 Speckle reduction in ultrasound endoscopy using refraction based elevational angular compounding

Parastoo Afshari, Christian Zakian, Jeannine Bachmann & Vasilis Ntziachristos. Speckle reduction in ultrasound endoscopy using refraction based elevational angular compounding. Scientific Reports. 11, 18370, 2021.

https://doi.org/10.1038/s41598-021-97717-2

Summary and Author Contribution

This study introduces Refraction-Based Elevational Angular Compounding (REACT) as a first spatial compounding speckle reduction method in radial endoscopic ultrasonography (EUS). The method, specifically tailored for radial EUS, tested on cylindrical phantoms, showcasing its superiority in speckle reduction over standard image processing techniques and averaging. The results reveal up to a two-fold improvement in signal- and contrast-ratios, demonstrating a notable improvement in image quality and diagnostic precision.

The research also delves into the impact of elevational angular deflection on image fidelity, particularly in the context of lymph node-like structures. Through experimentation, the authors find that a 5° elevational angular deflection offers an optimal balance between speckle reduction efficiency and image fidelity, which is crucial insight for achieving high-quality imaging and therefore accurate staging of gastrointestinal tract cancers. The findings open avenues for future integration of REACT into clinical settings, promising real-time spatial compounding despeckling method and improved diagnostic capabilities in radial EUS applications.

My contribution to the presented manuscript where the following:

Methodology The study was designed by me and Christian Zakian. Jeannine Bachmann provided expert clinical advice and insightful discussion on validation of. I developed the experimental hardware set-up required for the measurement, which included the electronics, mounting of the ultrasound transducer, preparation of the phantom, and ex vivo samples, and mechanical stages. I also developed the programming code needed to automate the acquiring the images, i.e., to control the stages and the data acquisition system. I also conducted the experiment and collected all the data.

Analysis I generated the code required to process and analyze the collected data using MATLAB. I and Christian Zakian worked together to interpretate the collected data and signals.

Writing and Revisions I drafted the initial manuscript with significant contributions from all authors. I created all figures using MATLAB and Microsoft word with valuable inputs from all authors. In response to the reviewer's requests, I with help of Christian Zakian carried out further experiments, made changes to the article, and adjusted the figures.

Abstract

Endoscopic ultrasonography (EUS) is a safe, real-time diagnostic and therapeutic tool. Speckle noise, inherent to ultrasonography, degrades the diagnostic precision of EUS. Elevational angular compounding (EAC) can provide real-time speckle noise reduction; however, EAC has never been applied to EUS because current implementations require costly and bulky arrays and are incompatible with the tight spatial constraints of hollow organs. Here we apply refraction-based elevational angular compounding technique (REACT) in radial EUS and demonstrate for the first time the spatial compounding in a radial endoscopy. The proposed implementation utilizes a translating cylindrical acoustic lens that steers the ultrasound beam along the elevational direction. The radial implementation of REACT was investigated in phantoms and demonstrated superior suppression of ultrasound speckle noise compared to standard image processing techniques and normal averaging. We observe up to a 2-fold improvement in signal- and contrast-to-noise ratios over uncompounded images using REACT in layered cylindrical phantom. The effects of elevational angular deflection on image fidelity were further investigated in a phantom with lymph node-like structures to determine the optimum elevational angular width to achieve the both high speckle reduction efficiency while maintaining image fidelity. This study introduces REACT as a potential compact and low-cost solution to impart current radial echo-endoscopes with spatial compounding. This could enable accurate identification and precise sizing of lymph nodes in staging of gastrointestinal tract cancers.

3.1 Introduction

Endoscopic ultrasonography (EUS) is a real-time, minimally invasive diagnostic imaging modality with therapeutic applications in the gastrointestinal (GI) tract region [1-7], as well as neighboring organs within [4-5] cm of the GI tract, such as the pancreas, liver, and lymph nodes [8-10]. Because of the high spatial resolution and the proximity to the organs, EUS is superior to spiral computed tomography (CT) and magnetic resonance imaging (MRI) for detecting the small lesions [11-13]. Thus, EUS is an ideal modality to detect lymph node tumor metastasis, which is a crucial for staging of GI tract cancers [8-13].

Despite these advantages, EUS suffers from poor contrast in the mucosal layers of the GI tract wall [8, 9] due to speckle noise, which is inherent in coherent imaging and arises from the interference of the back scattered waves from tissue microstructures. Speckle noise hinders the identification of tissue-layer boundaries within the GI tract where differences in acoustic impedance are low [10]. Therefore, speckle degrades image quality and contrast, which impedes accurate identification of pathological tissues.

Post-processing techniques to remove speckle from ultrasound images often fail to reveal structures that were obscured by speckle in the original image [14, 15]. In contrast, compounding methods can overcome missing information in individual frames by acquiring and averaging a sequence of images containing both correlated features and uncorrelated speckle patterns, with spatial compounding being preferred due to its higher speckle reduction efficiency [14]. To our knowledge, spatial compounding has only been implemented in linear EUS using azimuthal angular compounding [4, 10]. Azimuthal angular compounding requires laborious spatial alignment of sequential frames to extract the common region of interest and to avoid blurring. Despite its use in linear ultrasound endoscopy, azimuthal compounding is not applicable for radial EUS, as the radial geometry captures the image over a full 360-degree angle in the azimuthal plane, which negates the option of acquiring multiple decorrelated speckle patterns. In contrast, elevational angular compounding (EAC), which relies on capturing partially correlated images by steering the imaging plane with small angular steps in the elevational direction (perpendicular to the imaging plane) [16], is ideal for radial EUS because its geometry is suitable for capturing

sequential frames in a radial configuration. In addition, EAC allows imaging of the same region of interest in all sequential frames, therefore eliminating the need for spatial alignment, which is desirable for real time imaging 16-18. However, no EAC implementations for EUS have yet been introduced, likely due to spatial and cost constraints. Previous implementations of EAC for traditional ultrasound imaging used either a two-dimensional (2D) array [16] or a mechanical rotating one dimensional (1D) array [17] to provide the elevational angular imaging; however, 2D arrays are costly and mechanical rotating 1D arrays cause motion artifacts. Moreover, the need for multiple piezoelectric elements in 2D arrays and mechanical stage in rotating 1D arrays make these implementations of EAC bulky and cumbersome, which increases the risk of damage to the GI tract during examination. These factors prevent the translation of EAC to clinical EUS applications.

Our group recently introduced a refraction-based elevational angular compounding technique (REACT), wherein a customized refractive element imparts a fixed linear array with elevational angular steering capabilities [18]. REACT demonstrated more efficient ultrasound despeckling compared to the previous EAC implementations, primarily because the fixed transducer array minimized motion artifacts. However, the refractive element of the REACT prototype was designed for linear arrays and was therefore not suitable for use in radial ultrasound endoscopy [18].

In this work, we developed a radial implementation of REACT by using an engraved acoustic cylindrical refractive lens on an annular PMMA substrate to steer ultrasound waves along the elevational angle in cylindrical coordinates. This development represents the first application of spatial compounding in radial EUS. Our radial implementation of REACT achieves elevational angular steering using a stationary 1D-array transducer, making it compact to avoid potential damage to the GI tract during examination process. By integrating radial REACT into a commercially available radial ultrasound endoscope, we image cylindrical layered phantom and demonstrate a 2-fold improvement in contrast- and signal- to noise ratios over uncompounded US images. Moreover, we characterize the optimal elevation angle of deflection for the lymph node like structures to yield both high speckle reduction efficiency and image fidelity.

3.2 Methods

3.2.1 Image acquisition. The implementation scheme of REACT in EUS is shown in Figure 3. 1a. The employed ultrasound imaging system (HI VISION Avius®, Hitachi) utilized a convex radial 360-degree transducer array with central frequency of 7.5 MHz (EUP-R54AW-19, Hitachi). An annular-shaped acoustic cylindrical lens (see below) was attached to a linear translation stage to provide the fixed radial transducer with the elevational angular steering capability. A motorized linear translation stage (MTS50-Z8, Thorlabs) was used to shift the acoustic lens at predetermined linear steps, δ, along the longitudinal axis of the fixed transducer to obtain different elevational angular views by virtue of acoustic refraction (Figure 3. 1b). Each longitudinal step has an approximate error of 0.7% of the step size. Compounded images were attained by capturing (N = 100) sequential images from the same region of interest, yet at different elevational angular views with a rate of 20 frames per minute. The elevational angular field-of-view (FOV) of the transducer were adjusted by changing the acoustic lens's position and radius of curvature.

3.2.2 Refractive element fabrication. Figure 3. 1c shows a schematic of the annular-shaped acoustic cylindrical lens. Customized acoustic cylindrical lenses were manufactured from Polymethyl methacrylate (PMMA), which has a speed of sound of 2750 m/s and a low acoustic attenuation of 1.4 dB/cm/MHz [19, 20]. The lenses were machined from PMMA rods with diameters of 15 mm ± 4 µm. The acoustic beam refracts in the elevational direction due to the acoustic impedance (Z) difference between the PMMA lens ($Z = 3.23 \times 10^6$ kg/m^{2}s) and water (the imaging medium, $Z = 1.49 \times 10^6$ kg/m^{2}s)19, 20. The distance between the transducer and cylindrical acoustic lenses was held to <1 mm (while avoiding contact) to minimize the effect of multiple reflection artifacts on the image due to the impedance mismatch between the PMMA and water. Five cylindrical acoustic lenses were manufactured to provide different elevational angular deflections of 0°, 2.5°, 5°, 15°, and 30°. To acquire a fixed number of images, the translation steps (δ) for each acoustic lens were specified by dividing the length of each lens (l) by number of acquired images (N = 100) for compounding. The effective deflection angle was calculated using Snell's law as $c_1 \sin\emptyset_2 = c_2 \sin\emptyset_1$ (where c_1 and c_2 are the longitudinal wave

velocities, and $Ø_1$ and $Ø_2$ are incidence and exit angles in materials 1 and 2, respectively) [21, 22] and confirmed experimentally in a similar manner to that reported in our previous study [18].

3.2.3 Imaging samples. Two custom tube-shaped phantoms were manufactured to assess speckle reduction efficiency and image fidelity. They comprised 2% agar and different concentrations of TiO2 (0.25% – 4%) and had outer diameters of 80 mm and inner diameters of 20 mm. Phantom A consisted of five agar layers with TiO2 concentrations of 0.25%, 0.5%, 1%, 2%, and 4%, from the outer to the innermost layer, respectively. The phantom contained rod-shaped holes with a 1 mm-diameter to test REACT's ability to reveal fine structures obscured by speckle noise. Phantom B consisted of a single agar layer with 4% TiO2 concentration with embedded spherical water beads with diameters ranging between 10 mm to 12 mm to mimic lymph nodes-like structures in the GI tract [23]. Phantom B was used to determine the optimum elevational angular width needed for imaging lymph nodes to achieve both high speckle reduction efficiency and image fidelity.

3.2.4 Analysis method. To attain each compounded image, 100 sequential images were captured in different positions of the annular-shaped acoustic cylindrical lens and compounded using a mean compound operator [24]. To preform image post-processing for despeckling of the US images, Matlab was used to perform Frost filtering, which is a common speckle noise filtering technique based on an adaptive filter [25]. Processed and compounded images were compared to their respect single images to assess the despeckling efficiency. Circular regions of interest (ROIs = 1950 pixels) within a water sphere and solid regions in the phantom were selected to derive the average and standard deviation of the pixel intensities in order to compute SNR and CNR. These indices were used as quantitative indicators of image improvement to evaluate the despeckling efficiency and preserving the image fidelity. The despeckling efficiency was also evaluated by inspecting the A-line intensity profiles of the single, processed, and compounded images.

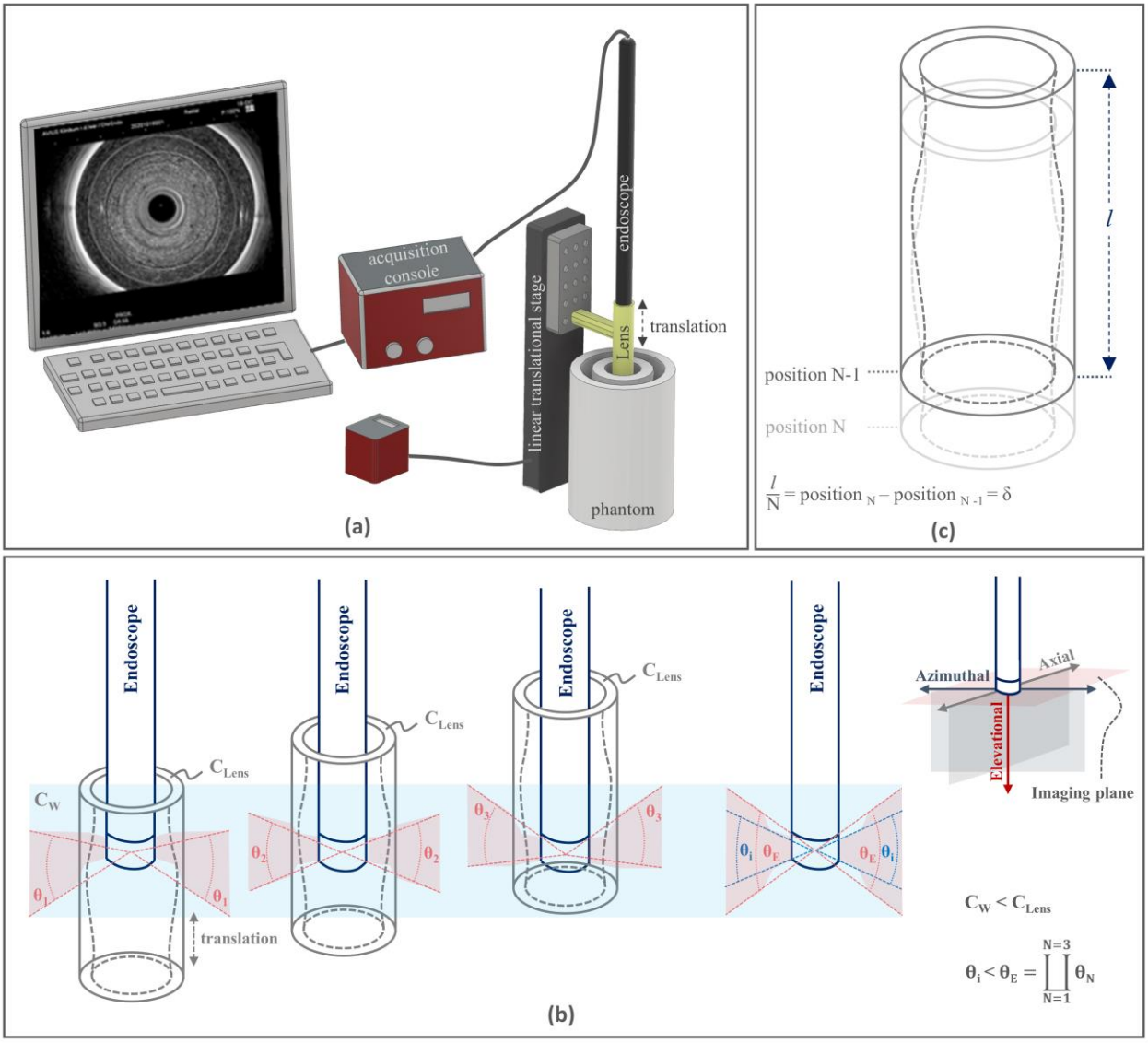

Figure 3. 1 REACT implementation in EUS. **(a)** REACT imaging acquisition configuration using radial transducer array. Linear translation of the annular-shaped acoustic cylindrical lens along the elevational direction in front of the stationary radial transducer array controls the elevational angular FOV. **(b)** Elevational angular steering in different positions of the acoustic cylindrical lens. Sound waves propagate through the water and lens substrate at speeds of c_w and c_{Lens}, respectively, where $c_w < c_{Lens}$. Imaging at different positions of the acoustic lens extends the elevational angular FOV (θ_E) of the transducer compared to its inherent elevational angular FOV (θ_i). **(c)** Schematic of annular-shaped acoustic cylindrical lens. The annular-shaped acoustic cylindrical lens is moved in consistent step sizes (δ), which are equal to the length of the acoustic lens (*l*) divided by the number of recorded images (N) for compounding.

3.3 Results

In order to evaluate the speckle reduction efficiency of REACT in a radial geometry and verify its advantage over image post-processing, ultrasound images of a five-layered cylindrical phantom containing seven 1 mm-diameter holes (Phantom A, Figure 3. 2a) using a radial ultrasound endoscope were recorded and analysed. Figure 3. 2b-g show single images recorded without (Figure 3. 2b) and with (Figure 3. 2c) an acoustic lens, a normal averaged image of 100 single images recorded with a stationary acoustic lens (Figure 3. 2d), a processed image by Frost filtering (Fig. 2f), and compounded images of 100 single images using a translating acoustic lenses providing 0˚ (as a control, Figure 3. 2e) and 5˚ elevational angular deflections (Figure 3. 2g). Visual inspection of the ultrasound images in Figure 3. 2b–g reveals noticeable speckle noise reduction with 5° EAC compared to the single images. Furthermore, the boundaries of the layers and edges of the holes in the phantom are clearer upon 5° EAC compared to normal averaging and Frost filtering, as highlighted by the red arrows in Figure 3. 2g.

To quantify the speckle reduction performance, we calculated SNR values (Figure 3. 2b-g, lower right corner) for each image. To access a higher number of pixels within the same radius for the SNR calculation, a ring-shaped region within the outer layers of the phantom was selected (enclosed by the dashed white circles in Figure 3. 2c). The single image recorded with the acoustic lens (Figure 3. 2c) exhibits a slightly lower SNR than recorded without a lens (Figure 3. 2b) due to the acoustic attenuation and reflection induced by the cylindrical lens substrate. Compounding of 100 single images recorded using both a stationary (Figure 3. 2d) and translating acoustic lens with a 0˚ elevational angular deflection (Figure 3. 2e), improved the SNR by 0.27×. However, the SNR obtained using 5° EAC (Figure 3. 2g) is 1.69× greater than the corresponding single image (Figure 3. 2c) and 0.71× greater than the Frost filtered image (Figure 3. 2f).

Figure 3. 2h shows the A-line intensity profiles (dashed line in Figure 3. 2b) for a single image recorded with lens (dotted black line), Frost filtered image (solid green line), and the compounded image using 5° EAC (solid red line). The blue, green, red, and gray rectangles in Figure 3. 2h indicate layers 1 – 4 of Phantom A, respectively. Inspecting the A-line intensity profile of the single image shows high intensity variations due to presence of scatterers producing speckle noise. Frost

filtering affords a slight dampening of the high intensity variations (solid green line), yet it follows the noise pattern of the main signal since it operates only on the available data in a single image. In contrast, these variations are strongly suppressed by 5° EAC (solid red line), regardless of the noise pattern of the original signal. The higher speckle noise suppression in 5° EAC is due to compounding of different speckle patterns acquired at different elevational angular views. The high speckle reduction afforded by REACT is exemplified by a hole that is only reveal upon 5° EAC (blue arrow in Figure 3. 2g and Figure 3. 2h).

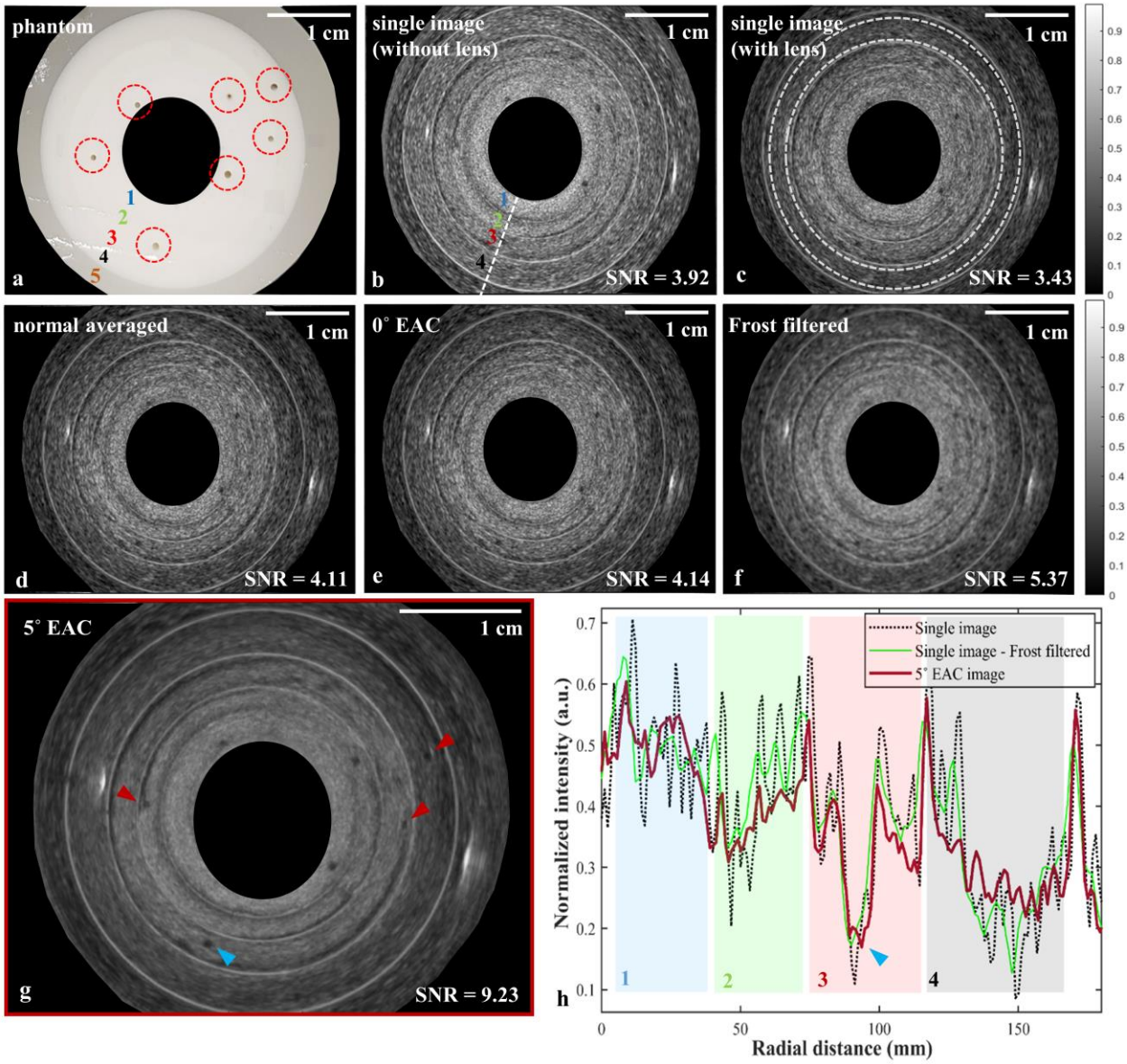

Figure 3. 2 Speckle reduction by REACT in a radial geometry compared to single images, normal averaging, and Frost filtering. **(a)** Phantom A: a five-layered cylindrical phantom (labelled with numbers

1, 2, 3, 4, and 5 from inside out respectively) containing seven holes (specified with circular regions). **(b-g)** Ultrasound images of Phantom A: **(b)** a single image recorded without an acoustic lens, **(c)** a single image recorded with a stationary acoustic lens, **(d)** an averaged image using 100 single images recorded with a stationary acoustic cylindrical lens **(e)** a compounded image using 100 single images recorded with a translating acoustic cylindrical lens providing 0˚ elevational deflection, **(f)** a single image recorded with an acoustic lens after Frost filtering, **(g)** a compounded image using 100 single images recorded with a translating acoustic cylindrical lens providing 5˚ elevational deflection. The red arrows indicate holes that are not visible in b-f. Region between two white circles in c show the ROI used to derive the SNR in **(b)-(g)**. **(h)** A-line intensity profiles for the single, Frost filtered, and 5˚ EAC images, which were recorded along the dashed line shown in b. The blue, green, red, and gray rectangles indicate phantom layers 1, 2, 3, and 4, respectively. Blue arrows in g and h point to the same hole, which lies on the dashed line in b.

Figure 3. 3 depicts single and compounded ultrasound images of a single-layered cylindrical phantom containing spherical water beads to mimic lymph nodes (Phantom B), which illustrate the effect of the elevational angular deflection on speckle reduction efficiency and image fidelity for the radial implementation of REACT. The compounded images were recorded using 0° (Figure 3. 3b), 2.5° (Figure 3. 3c), 5° (Figure 3. 3d), 15° (Figure 3. 3e), and 30° (Figure 3. 3f) elevational angular deflections. Compounding at 0° (Figure 3. 3b) results in minimal image improvement over the uncompounded image (Figure 3. 3a). Increasing the elevational compounding angle results in a decrease in speckle noise, but also a loss of image fidelity at high angles (15° and 30°) due to increasing elevational angular width and a concomitant increase in interference from structures in adjacent elevational planes (Figure 3. 3e-f), which manifest as a loss of definition of the water bead boundaries (blue arrow). Visual inspection of the ultrasound images in Figure 3. 3a–f reveals that 5° EAC yields the optimum balance between speckle noise reduction and image fidelity. The edges of the holes and fine structures around them are preserved and are clearest in 5° EAC (highlighted by the red arrow in Figure 3. 3d)

To quantify the effect of the elevational angular deflection on the speckle reduction efficiency and image fidelity in REACT, SNR and CNR were calculated using two regions within and outside of a water sphere (Figure 3. 3a, white dashed circles) and plotted as a function of the number of compounded images (Figure 3. 3g, h). As expected, SNR increases with the number of compounded images for all cases, with the rate of SNR improvement increasing with the elevation deflection angle. At the upper end, the SNR for 30° EAC is 3.1 x greater than 0° EAC, after 100

images were compounded. This improvement results from the higher variation in the speckle pattern of the captured images within the higher elevational angular deflections. In contrast, CNR increases with an increasing number of compounded images only for the 0°, 2.5°, and 5° cases. CNR predominantly decreases with compounding for the 15° and 30° cases. Therefore, while higher elevational angular deflection results in a decrease in speckle noise (higher SNR), too great an angular deflection can cause severe degradation of image fidelity (lower CNR).

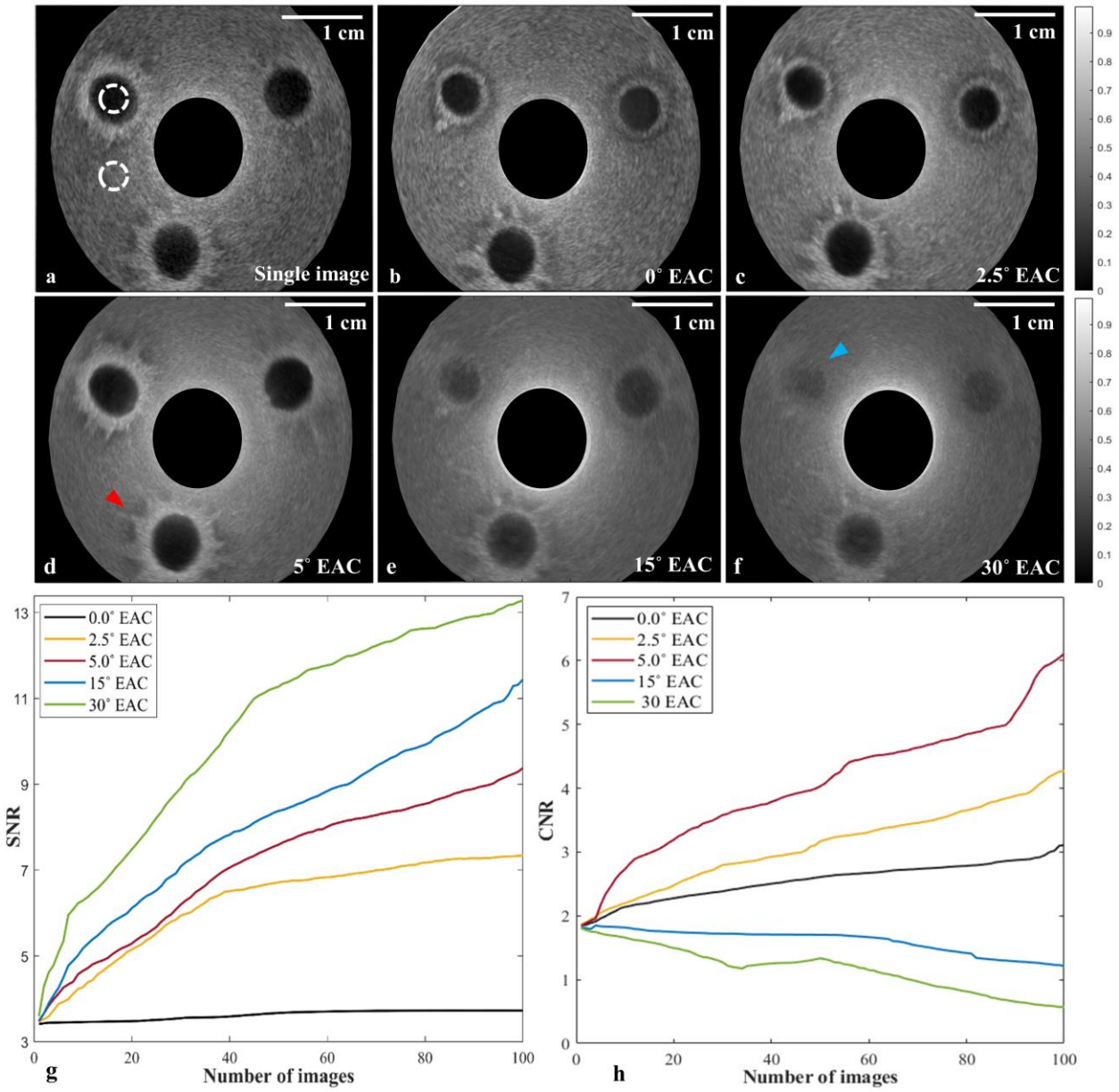

Figure 3. 3 The effect of elevational angular deflection on speckle reduction efficiency and image fidelity in REACT. **(a)** A single ultrasound image of a single-layered cylindrical phantom (Phantom

B) containing spherical water beads to mimic lymph nodes. The white dotted circles indicate the ROIs used to derive the SNR and CNR. **(b-f)** Compounded images of Phantom B using five different cylindrical acoustic lenses with the following angular deflections: **(b)** 0˚, **(c)** 2.5˚, **(d)** 5˚, **(e)** 15˚, **(f)** 30˚. The red arrow in d depicts fine structures, which are best resolved by 5˚ EAC. The blue arrow in f indicates a water bead that is barely visible due to loss of image fidelity at 30˚ EAC. **(g-h)** The change in SNR and CNR for each deflection angle with increasing number of compounded images.

3.4 Discussion

The accurate diagnosis and therapeutic utility of EUS for gastrointestinal disorders is limited by the presence of speckle noise [8, 9], which hinders the identification of gastrointestinal tract layer boundaries with low acoustic impedance differences [8]. To minimize speckle artifacts, compounding methods are preferable to image processing techniques because they yield both high quality images and reveal fine structures obscured by speckle noise, which are otherwise irretrievable using the aforementioned techniques [15, 16]. EAC is a preferred spatial compounding technique with both high despeckling efficiency and good temporal resolution, which makes it favorable for real time imaging18. However, tight anatomical constrains of hollow organs prevent implementation of EAC in EUS using 2D or tilting 1D transducer arrays. Here, we demonstrated a novel deployment of spatial compounding in radial EUS by implementing REACT in a radial geometry, which can lead to image quality improvements in clinical EUS and enable more accurate diagnoses of GI lesions.

Visual and quantitative inspection of the ultrasound images from a cylindrical layered phantom (Figure 3. 2) illustrates that spatial compounding in radial EUS can provide more efficient speckle reduction with retrieved fine structures, which are not recoverable with commonly used image post-processing techniques such as Frost filtering. As expected, the wider the elevational angle employed, the greater the speckle suppression in the compounded image, which translates into higher SNRs (Figure 3. g). Compounded images acquired with elevational angular deflections of 0°, 2.5°, 5°, 15°, and 30° had SNRs that were 0.27 ×, 1.19 × , 1.68 ×, 2.32 ×, and 2.91 × greater than their respective single images. The SNR enhancement is in agreement with previously reported findings using a linear configuration of REACT [18]. As expected, the similar SNRs obtained for

normal averaging (Figure 3. 2d) and 0° EAC (Figure 3. 2e) confirmed that the uncorrelated speckle patterns are produced by effectively changing the elevational angular deflection using an acoustic refractive lens. Moreover, SNR in REACT has an increasing trend by increasing the number of images, yet at a greater rate for the 30° EAC case (Figure 3. 3g), owing to the widest elevational angular width and therefore providing images with less correlated speckle patterns.

Although higher elevational angular deflection results in higher despeckling efficiency, a trade-off between speckle reduction and image distortion determines the optimal compounding angle for the imaging target of interest [18]. In agreement with our previous study [18], we found that out of plane signals can also degrades the quality of the elevational compounded image for radial EUS. This is relevant in particular when imaging small organs such as lymph nodes adjacent to the GI tract. We demonstrate an increase in SNR with wider elevational angular deflection in phantom containing lymph node like structures; however, angular deflection above 5° results in overall degradation of CNR (Figure 3. 3). This drop in CNR is due to the interference of the signals out of the imaging plane and represents a loss of image contrast, which can affect accurate diagnosis. Our experiments suggest that 5° EAC provides an optimal trade-off for high despeckling efficiency with minimal image fidelity loss for lymph nodes-like structures (Figure 3. 3).

This study demonstrates REACT as a first potential compact and low-cost solution to impart current radial echo-endoscopes with spatial compounding. The optimum elevational angular deflection for imaging lymph nodes was also investigated to achieve the best combination of despeckling efficiency and high image fidelity, required for accurate identification of pathological lymph nodes in the GI tract. However, further studies are needed to extract the optimum elevational angular deflections for other targets of interest in EUS. The lens material has an effect on SNR as can be seen by individual images captured with (Figure 3. 2c) and without (Figure 3. 2b) the acoustic lens. This is caused by the acoustic attenuation and reflection and could be diminished by either utilizing lower attenuating materials to manufacture the lens compared to PMMA (e.g., TPX) or diffractive lenses with lower effective thicknesses. To enable real-time despeckling in radial EUS using REACT, the translation of the lens should be automated to allow frame rates as high as the acquisition speed of the US imaging system. Future work will aim to translate REACT

into clinical settings by miniaturizing and integrating the acoustic lens to the existing radial echo-endoscopes.

In summary, we demonstrate that REACT is ideally suited for radial EUS and can uniquely impart spatial compounding to radial ultrasound endoscopy for the first time, enabling observation of fine structures hidden by speckle noise. This low-cost and simple spatial compounding method can be of great benefit in clinics to improve image quality and contrast in current radial echo-endoscopes to heighten the accuracy in visualization and identification of pathological lymph nodes in staging of gastrointestinal tract cancers.

Data Availability

The datasets generated during and/or analysed during the current study are available from the corresponding author on reasonable request.

References

[1] Friedberg, S. R. & Lachter, J. Endoscopic ultrasound: Current roles and future directions, World J. Gastrointest. Endosc. 9, 499-505 (2017).

[2] Mekky, M. A. & Abbas, W. A. Endoscopic ultrasound in gastroenterology: from diagnosis to therapeutic implications, world J. Gastroenterol. 20, 7801-7807 (2014).

[3] Kandel, p., Wallace, M. B. Recent advancement in EUS-guided fine needle sampling. J Gastroenterol. 54, 377-387(2019).

[4] Iglesias-Garcia, J., Larino-Noia, J. & Dominguez-Munos J. E. Contrast harmonic endoscopic ultrasound: Instrumentation, echoprocessors, and echoendoscopes. Endosc. Ultrasound 6, 37-42 (2016).

[5] Kalaitzakis, E., Vilmann, P. & Bhutani, M. Therapeutic endoscopic ultrasound. Springer Cham. (2020).

[6] Jenssen, Ch., Alvarez-Sanchez, M. V., Napoleon, B. & Faiss, S. Diagnostic endoscopic ultrasonography: Assessment of safety and prevention of complications. world J Gastroenterol 18, 4659-4676 (2012).

[7] Gaschen L., Kircher P., Lang J., Endoscopic ultrasound instrumentation, applications in humans, and potential veterinary application. Vet. Radiol. Ultrasound 44, 665-680 (2003).

[8] Li, J. J. et al. Superficial esophageal lesions detected by endoscopic ultrasound enhanced with submucosal edema. World J. Gastroenterol. 19, 9034-9042 (2013).

[9] Murad, F. M. et al. Echoendoscopes. Gastrointest. Endosc. 82, 189-202 (2015).

[10] Rimbas, M. & Larghi, A. Equipment and accessories for therapeutic endoscopic ultrasound. in Therapeutic endoscopic ultrasound, Springer Cham., 1-31 (2020).

[11] Lee, Y. S. et al. Comparison of endoscopic ultrasonography, computed tomography, and magnetic resonance imaging for pancreas cystic lesions. Medicine 94, (2015).

[12] Lu, X. et al. The diagnostic value of EUS in pancreatic cystic neoplasm compared with CT and MRI. Endosc. Ultrasound 4, 324- 329 (2015).

[13] Dewitt, J., Devereaux, B. M., Lehman, G. A., Sherman, S. & Imperiale, Th. F. Comparison of endoscopic ultrasound and computed tomography for the preoperative evaluation of pancreatic cancer: A systematic review. Clin. Gastroenterol hepatol. 4, 717-725 (2006).

[14] Mikhailovich, O. V. & Tannenbaum, A. Despeckling of medical ultrasound images. IEEE Trans. Ultrason. Ferroelectr, Freq. Control. 53, 64-78 (2006).

[15] Nwogu, I. & Chaudhary, V. Enhancing regional lymph nodes from endoscopic ultrasound images. Proc. SPIE 6914, medical imaging (2008).

[16] Li, P. C. & O'Donnell, M. Elevational spatial compounding. Ultrason. Imaging 16, 176-189 (1994).

[17] Perperidis, A., McDicken, N., MacGillivary, T. & Anderson, T. Elevational spatial compounding for enhancing image quality in echocardiography. Ultrasound. 24, 74-85 (2016).

[18] Afshari, P., Zakian, Ch., Ntziachristos, V. Novel implementation of elevational angular compounding using acoustic refraction principles. Sci. Rep. 10, 18173 (2020).

[19] Xia, W., Piras, D., van Hespen, J. C. G., Steenbergen, W. & Manohar, S. A new acoustic lens material for large area detectors in photoacoustic breast tomography. Photoacoustics 1, 9–18 (2013).

[20] Bloomfield, P. E., Lo, W. J. & Lewin, P. A. Experimental study of the acoustical properties of polymers utilized to construct PVDF ultrasonic transducers and the acousto-electric properties of PVDF and P(VDF/TrFE) films. IEEE Trans. Ultrason. Ferroelectr. Freq. Control. 47, 1397–1405 (2000).

[21] Hohenwarter, D. & Jelinek, F. Snell's law of refraction and sound rays for a moving medium. J. Acoust. Soc. Am. 105, 1387–1388 (1999).

[22] Finn, S., Glavin, M. & Jones, E. Speckle Reduction in Echocardiography: Trends and Perceptions. In Echocardiography—New Techniques, G. Bajraktari, 41–68 (InTech, 2012).

[23] Märkl, B. et al. The clinical significance of lymph node size in colon cancer. Mod. Pathol. 25, 1413-1422 (2012).

[24] Wilhjelm, J. E., Jensen, M. S., Jespersen, S. K., Sahl, B. & Falk, E. Visual and quantitative evaluation of selected image combination schemes in ultrasound spatial compound scanning. IEEE Trans. Med. Imaging 23, 181–190 (2004).

[25] Lopes, A., Touzi, R., and Nezry, E. Adaptive speckle filters and scene heterogeneity. IEEE Trans. Geosci. Remote Sens. 28, 992-1000 (1990)

[26] Jaybhay, J. & Shastri, R. A study of speckle noise reduction flters. Signal Image Process. Int. J. (SIPIJ) 6, 71–80 (2015).

[27] Bafaraj, A. S. Performance analysis of best speckle filter for noise reduction in ultrasound medical images. Int. J. Appl. Eng. Res. 14, 1340–1351 (2019).

Acknowledgements

This project has received funding from the European Union's Horizon 2020 research and innovation program under grant agreement 732720 (ESOTRAC) as well as from European Union's Horizon 2020 research and innovation program under the Marie-Sklodowska-Curie grant agreement No 721766 (FBI). The authors also thank Dr. Robert J. Wilson for proofreading the manuscript.

Author contributions

P.A. and C.Z. designed the study. J.B. provides information about the existing echo endoscopes and their application in monitoring of the GI tract, besides providing the access to the endoscopic imaging facility. P.A. produced phantoms and carried out the experiments. P.A. collected and analysed the data and prepared all figures in the manuscript. P.A. and C.Z. interpreted the data and wrote the manuscript. V.N. reviewed and approved the final manuscript.

Additional Information

Competing interests

The authors declare no competing interests.

Supplementary Information

To validate our theoretical design calculations for the desired refraction of each manufactured lens (Snell's law), we characterized the elevational angular view of the 30˚ EAC lens using a metal target (see our previous work [18]) and a needle hydrophone sensor for confirmation. A metal target (hex key, ~2 mm diameter) was attached to a XYZ micrometer stage, positioned vertically in front of the transducer, and monitored in real time on the US image. The target was moved to a position towards the edge of the ring transducer, such that it was barely visible in the image. The relative distance between the transducer and the target was measured and the inherent elevational angle of the transducer calculated using simple trigonometry, yielding $\theta_i = 29.4^\circ$. The manufactured acoustic lens was subsequently inserted between the transducer and the target. The lens was translated until the target reappeared in the image due to acoustic refraction. The target was then moved vertically outwards until it just disappeared from the image. This process was iterated until the target no longer became visible after repositioning the acoustic refraction lens. The new relative distance between the transducer and the target were measured and utilized to calculate the extended elevational angle of $\theta_E = 59.1^\circ$ and subsequently the lens's effective maximum elevational angular deflection of $\theta_E - \theta_i = 29.7^\circ$ (Figure 3. 1a-c in supplementary). A similar iterative measurement process was performed to find the outer most position where a needle hydrophone could detect, through the 30° EAC lens, the pulses emitted by the transducer. This point corresponds to the maximum possible deflection of the lens, and the subtended angle was calculated by simple trigonometry using the relative distance between the needle and the edge of the transducer, yielding, for this lens, an extended elevational angle $\theta_E = 59.3^\circ$ (Figure 3. 1d in supplementary). The subtraction of the inherent and extended elevational angle yielded to the

effective maximum elevational angular deflection of 29.9˚. Additionally, we recorded the maximum voltage sensed by the needle hydrophone as the lens was translated through its full length to confirm the refractive capability of the lens (Figure 3. 1e in supplementary).

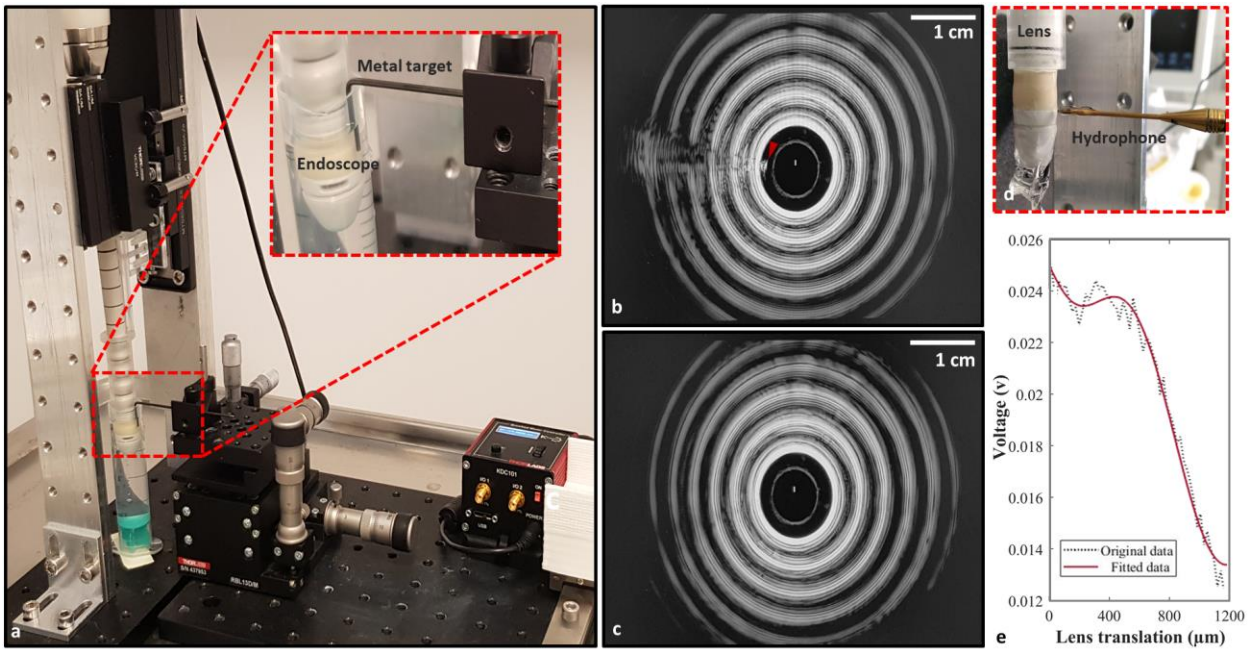

Supplementary Figure 3. 1 Elevational angular characterization of the manufactured lenses based on hydrophone measurements and the proposed sliding metal target method. **(a)** Photograph of the characterization set-up used for both approaches. The picture inset shows a detailed view of the sliding metal target in front of the top edge of the radial endoscope transducer, inside the water tank. **(b), (c)** Ultrasound images showing the absence and presence of the metal target in the transducer field of view, respectively. The red arrow points to the tip of metal target. **(d)** Detailed picture of the hydrophone placed on the lower edge of the radial endoscope transducer, coupled with ultrasonic gel. **(e)** Hydrophone maximum voltage at each position of the translating 30° EAC lens.

Supplementary Figure 3. 2a, b display the variation in pixel intensity for images compounded using 0° and 5° EAC lens, which was mapped to explore the speckle pattern decorrelation between individual recorded images (Figure 3. 2e, g). As predicted, images taken inside the 5° elevational angular deflection have stronger speckle pattern decorrelation, resulting in greater speckle reduction, as seen in Figure 3. 2g. To investigate the effect of step size on image decorrelation of the speckle pattern when translating the 5˚ and 0˚ EAC lens, we performed a correlation coefficient analysis of the captured images. Decorrelation from consecutive image pairs (e.g., 1 vs. 2, 2 vs. 3,

etc.; supplementary Figure 3. 2c) was used to determine which region of the lens afforded the most effective decorrelation. A correlation coefficient calculation was also performed between an arbitrary image (here, image number 2) and each of the 100 acquired images to confirm that the center of the lens was in the optimum position to capture images with maximum decorrelation (e.g., 2 vs. 1, 2 vs. 2, 2 vs. 3, etc.; supplementary Figure 3. 2d, respectively). We observed that a similar despeckling power could be achieved by compounding fewer images at unequal step sizes compared to 100 images with equal step sizes through linear translation of the lens. The optimized step size would be achieved by linearly translating the lens to positions that provide equidistant acoustic beam deflections.

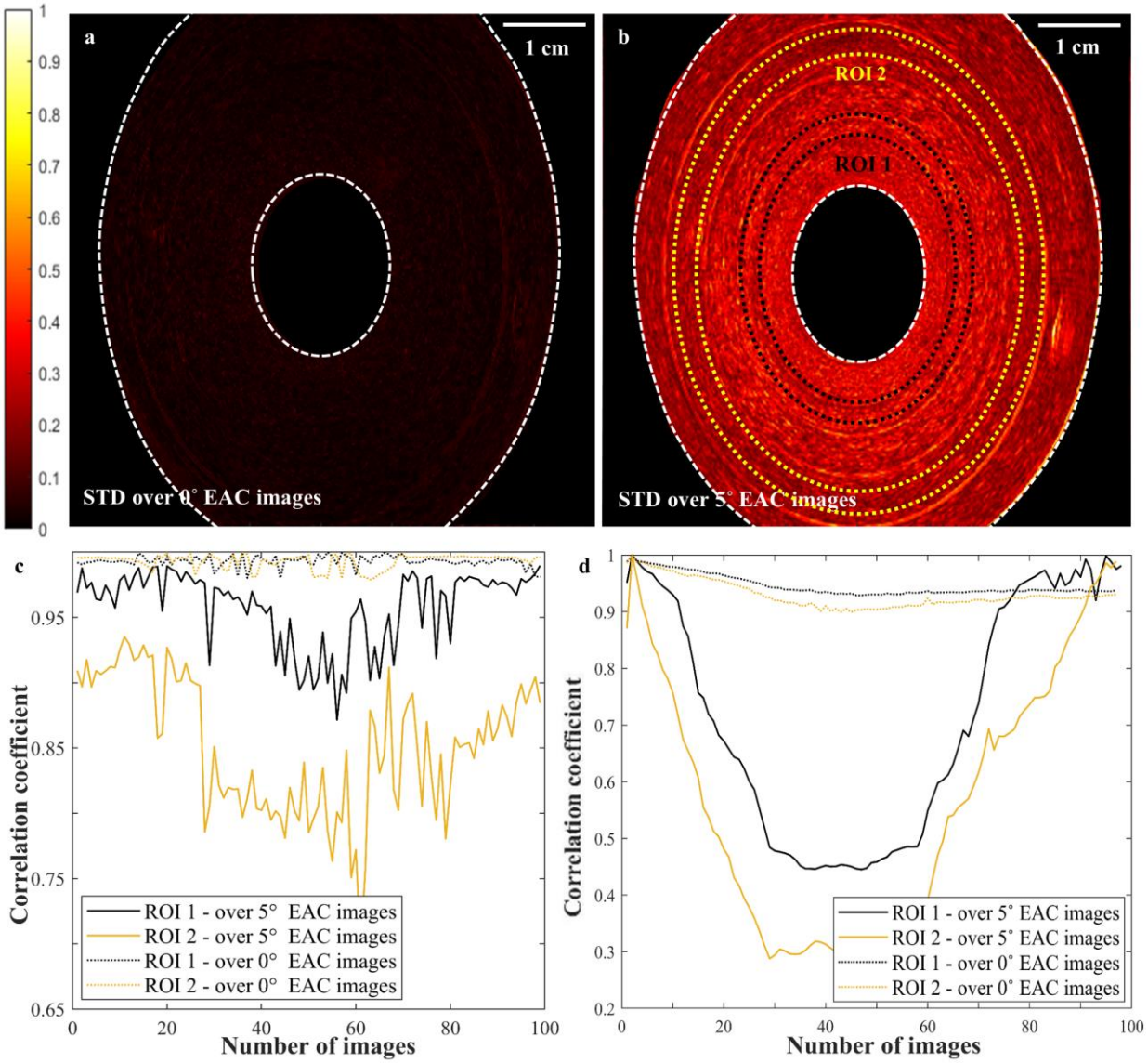

Supplementary Figure 3. 2 Elevational angular deflection results in speckle pattern decorrelation. Intensity of STD maps at pixel-level along all captured images with **(a)** 0° and **(b)** 5° EAC lenses, respectively; white dashed lines delineate the phantom inner and outer surface contours. Regions enclosed by the black (ROI 1) and yellow (ROI 2) circular rings used to derive the correlation coefficient shown in panel c and d. Correlation coefficient between **(c)** consecutive image pairs (e.g., 1 vs 2, 2 vs 3, etc.) and **(d)** an arbitrary selected image (here, image number 2) and each of the 100 captured images (e.g. 2 vs 1, 2 vs 2, 2 vs 3, etc.), resulting from the translation of the 5° and 0° EAC lens at equal step sizes in front of the transducer.

Chapter 4

4 Conclusion and Future work

4.1 Conclusion

The presence of speckle noise, an inherent property to coherent imaging techniques, significantly compromises diagnostic accuracy of US imaging. While speckle noise can provide valuable insights into assessment of dynamic aspects, it simultaneously degrades the clarity and contrast of static structures. This effect notably has a significant impact on the interpretation of structures and, consequently, diagnostic procedures. Among the various methods proposed to mitigate this issue, compounding techniques stand out as a preferred solution. This is due the fact that they rely on averaging the information of the sequential images from the same field of view containing correlated features and uncorrelated speckle noise pattern. This enables them to retrieve the data hidden beneath speckle noise, the feature which is not available in image processing approaches as they rely solely on information in a single image. However, the necessity of obtaining several images in compounding approaches poses a challenge to acquisition speeds, hindering real-time monitoring crucial for studying dynamic aspects like

cardiac function and morphology. Additionally, the collection of signals from adjacent fields of view to achieve uncorrelated speckle pattern results in a reduction of lateral resolution. This requirement often leads to an increased size and complexity of the imaging setup, posing challenges and limitations for seamless integration and therefore their implementation for clinical practice. These practical limitations highlight the need for a solution that could balance the speckle reduction with the preservation of temporal and spatial resolution.

The primary objective of this thesis is to tackle and overcome the challenges associated with compounding methods, aiming to enhance the feasibility of these techniques for widespread adoption in clinical settings. To this end, the introduction contributes to the theoretical understanding of compounding techniques, emphasizing their superiority over traditional image processing techniques for speckle reduction and highlighting Elevational Angular Compounding (EAC) as a preferred compounding technique due to its ability to simultaneously reduce speckle noise while maintaining in-plane spatial and temporal resolution. EAC involves adjusting the elevational imaging plane with small angular steps to acquire partially correlated image contents and uncorrelated speckle patterns. For this purpose, EAC relies on either cost-effective one-dimensional (1D) arrays with bulky mechanical stages for elevational steering or more expensive and larger two-dimensional (2D) arrays that electronically control the beam. 1D arrays are affordable but necessitate cumbersome mechanical stages for elevational steering, rendering them less feasible for clinical applications. Conversely, 2D arrays electronically control the beam without displacing the detector; however, they come with a higher cost and larger physical footprint. This limitation impedes the practical application of elevational angular compounding in clinical contexts.

In response to these challenges, a novel implementation of elevational angular compounding using a refractive element, the Refraction-Based Elevational Angular Compounding Technique (REACT), has been introduced. REACT utilizes a translating cylindrical acoustic lens to steer ultrasound beams along the elevational direction. This approach overcomes the drawbacks of previous EAC implementations, demonstrating superior speckle reduction without the need for bulky mechanical adjustments or expensive 2D arrays. Further quantitative analyses, including Signal-to-Noise Ratios (SNR), Contrast-to-Noise Ratios (CNR) and an exploration of the impact of

elevational angular deflection on despeckling efficiency and image fidelity, provided valuable insights into the efficacy of REACT to suppress speckle noise in US imaging.

The application of REACT has been further extended into radial Endoscopic Ultrasonography (EUS), marking the first spatial compounding method in radial endoscopy. This adaptation enables real-time speckle noise reduction in a compact and cost-effective manner, addressing the challenges posed by spatial constraints in hollow organs. By adopting an annular-shaped acoustic cylindrical lens for elevational angular steering, REACT also demonstrated promising results in speckle noise reduction in radial geometry, particularly in layered cylindrical phantoms. The impact of elevational angular deflection on image accuracy was additionally examined in a phantom containing structures resembling lymph nodes, aiming to identify the optimal elevational angular width that achieves efficient speckle reduction without compromising image fidelity.

In conclusion, the study herein presents a novel implementation of elevational angular compounding by introducing acoustic refraction to existing 1D transducer arrays for providing elevational angular steering, named REACT. The proposed approach brings a practical and cost-effective solution for adoption of spatial compounding methods in clinical settings. REACT holds tremendous potential for enhancing image quality and contrast in US imaging and therefore heighten monitoring accuracy. REACT also offers a feasible and affordable approach to impart the existing radial echo-endoscopes for the first time with spatial compounding method. This advancement has the potential to facilitate precise visualization and identification of pathological lymph nodes, particularly in the staging of gastrointestinal tract cancers.

Many aspects of this work can be improved in the future, including both algorithmic optimization and hardware improvement.

4.2 Recommendations for the future work

This research with proposing REACT as a novel approach for the implementation of the elevational angular compounding has made significant achievements in addressing the challenges associated with implementation of compounding methods in clinical application. However, there are important avenues for future exploration and translation of REACT into clinical settings. Future work should focus on miniaturizing, automating, and integrating it into existing US transducers, ensuring seamless applicability in real-world clinical setting. The following steps will pave the way for future advancement in the promising direction.

Algorithmic Optimization: Further studies should focus on developing optimization algorithms to determine the most effective elevational angular width for various imaging targets. While our study here optimized for lymph nodes, extending this optimization framework to other anatomical structures will broaden the utility of REACT. This will ensure the highest despeckling efficiency without significant loss of image fidelity. Besides, the adaptability of REACT in clinical settings, especially in dynamic applications like cardiac imaging, could be further improved by exploring real-time optimization algorithms.

Hardware Improvement: Improvements in hardware is critical for translating research findings into practical clinical applications. The automation of lens translation is essential for achieving real-time speckle reduction using REACT. Future efforts should be directed towards miniaturizing and automating acoustic lens translation to enable real-time despeckling, providing a seamless integration into existing ultrasound imaging systems. Additionally, alternative materials with lower acoustic impedance and attenuation for the acoustic lens should be investigated to decrease signal loss and improve signal-to-noise ratios (SNR). In this regard, investigating diffractive lenses with reduced effective thicknesses may also improve REACT's overall efficacy.

Clinical Translation: The transition from experimental validation to clinical applicability is crucial for the successful adoption of any imaging technique. Future studies should emphasize comprehensive clinical validation of REACT, including evaluations on a diverse range of

anatomical structures and clinical settings. This will ensure that REACT proves not only effective in reducing speckle noise but also safe, reliable, and suitable for widespread clinical use.

Lastly, we expect that the implementation of acoustic refraction concept would be a great of benefits in improving US visualization and disease diagnosis in clinical settings by enabling the use of the existing 1D transducer arrays with elevational angular steering. The future advancements and adaptations of the proposed method could bring the real-time speckle reduction using a spatial compounding, enabling high despeckling efficiency without compromising spatial and temporal resolution, as is typical of these methods. This study, together with the proposed improvement, has the potential to bring the use of spatial compounding without spatial and time resolution compensation to real-time US imaging, as well as applications that were previously unavailable as radial EUS.

Acknowledgments

How can man adequately acknowledge people who contributed to four years of intensive, deep, and application-focused research? The very research that led me to meet fantastic people at prestigious universities and companies through conferences, workshops, scientific gatherings, and collaborations. This unique and comprehensive opportunity which enabled me to immerse myself in the multi-layered subject of biomedical imaging and was not only a fantastic finding for me, but also an outstanding learning experience in every aspect.

Still, it is custom to attempt to acknowledge people who have been supportive, and I would like to thank two people in particular: **Prof. Vasilis Ntziachristos**, who supervised and supported my thesis. The person whose far-sighted perspective to both research and science inspired me to think outside the box and work creatively on number of interesting projects simultaneously. Moreover, his trust in my abilities led me receiving the prestigious Marie Skodowska-Curie research scholarship and being a member of the Future of Biomedical Imaging group (FBI) to further develop my dissemination and soft skills, in addition to developing my own ideas and approaches, which helped me win awards and establish honorable collaboration and network. Thank you, Vasilis!

Dr. Christian Zakian, who supervised my projects for four years and kept supporting and encouraging me in my challenges even when I was burned out or going through a hard time in my life. I am grateful for his patience both while introducing me to the right way of doing research and translating them into a scientific paper. His door was always open for hour-long discussions of drafting and developing new research ideas. This thesis would not have been possible without his encouragement, insightful guidance, analytical talks, and emotional support. Thank you Christian!

After that, I owe a great debt to the CBI/IBMI pack: Sarah Glasl, Uwe Klemm and Pia Anzenhofer for keeping order in the labs and assisting me with experimental setups. Andreas Hillmair and Susanne Stern for their availability, support, and chats in all difficult circumstances. Thomas Gerlach, for his hands-on mechanical engineering expertise, and patience despite our repeated requests for micron-level modifications to his already manufactured components.

I'd also like to thank the Future of Biomedical Imaging group, especially Zak Ali and Antonia Longo, for their emotional and scientific support during our PhD journey.

Fortunately, the lack of strict formalities for acknowledgement chapter allows me also to express my heartfelt appreciation to my loved ones: My dear parents and my adored brother. People who were always there for me along my academic path with constant emotional support, encouragement, and advice. Your faith in my abilities has been a constant source of motivation and inspiration to keep pushing forward, especially in the face of life difficulties. This thesis is a monument to the love and strength you have bestowed upon me, and I dedicate it to each one of you with all my heart and respect. Thank you for being my rock on this challenging but rewarding journey.

Thank you.

List of Figures

List of Tables

Original of the Papers with the Publisher Letters of Approval

scientific reports

Check for updates

OPEN

Improving ultrasound images with elevational angular compounding based on acoustic refraction

Parastoo Afshari[1,2], Christian Zakian[1,2] & Vasilis Ntziachristos[1,2]✉

Ultrasound imaging is affected by coherent noise or speckle, which reduces contrast and overall image quality and degrades the diagnostic precision of the collected images. Elevational angular compounding (EAC) is an attractive means of addressing this limitation, since it reduces speckle noise while operating in real-time. However, current EAC implementations rely on mechanically rotating a one-dimensional (1D) transducer array or electronically beam steering of two-dimensional (2D) arrays to provide different elevational imaging angles, which increases the size and cost of the systems. Here we present a novel EAC implementation based on a 1D array, which does not necessitate mechanically rotating the transducer. The proposed refraction-based elevational angular compounding technique (REACT) instead utilizes a translating cylindrical acoustic lens that steers the ultrasound beam along the elevational direction. Applying REACT to investigate phantoms and excised tissue samples demonstrated superior suppression of ultrasound speckle noise compared to previous EAC methods, with up to a two-fold improvement in signal- and contrast-to-noise ratios. The effects of elevational angular width on speckle reduction was further investigated to determine the appropriate conditions for applying EAC. This study introduces acoustic refractive elements as potential low cost solutions to noise reduction, which could be integrated into current medical ultrasound devices.

Speckle noise is an inherent property of ultrasound (US) imaging that results from constructive and destructive interference of backscattered acoustic waves caused by heterogeneities in tissue[1–4]. While speckle can be exploited to obtain dynamic information (e.g. on blood flow)[5], it can also degrade both the resolution and contrast of static structures and blur the boundaries of layered tissues, which can hinder the interpretation of tissue morphology and fine structure and adversely affect diagnostic procedures[6–10]. Image post-processing or compounding methods are commonly used to reduce speckle in US imaging[11–20]. Post-processing is based on image filter algorithms that use information extracted from the images[11–13], which limits realistic enhancement of structures obscured by speckle noise. Compounding methods average sequential images from the same field of view (FOV) with varied spatial or frequency content[7–10], enhancing correlated features while removing uncorrelated speckle noise, which can reveal structures obscured by speckle in individual images. Frequency compounding methods either vary the emitted frequency or decompose the spectrum of the echo signal to obtain images with uncorrelated speckle patterns, while spatial compounding methods acquire images at different US beam orientations[14–20]. However, both compounding methods typically result in a loss of spatial or temporal resolution, as capturing multiple images reduces acquisition speeds and collecting signals from adjacent fields of view reduces the lateral resolution[18].

Elevational angular compounding (EAC) is a type of spatial compounding that can simultaneously offer high speckle noise reduction and good temporal resolution, making it desirable for medical applications[19]. EAC obtains partially correlated images by steering the elevational imaging plane with small angular steps[19,20]. EAC methods typically employ either one-dimensional (1D) arrays that can only control the US beam in the azimuthal direction (i.e. parallel to the imaging plane) or two-dimensional (2D) arrays that can control the US beam in both the azimuthal and elevational directions (the latter being perpendicular to the imaging plane)[21–23]. US systems with 1D arrays are simple and inexpensive. However, implementing EAC in such systems necessitates bulky mechanical stages to physically move or rotate the 1D array in order to steer the beam in the elevational direction[19], which is impractical in clinical applications. In contrast, US systems integrating 2D arrays can electronically steer the beam along the elevational direction without changing the detector's position[21–23].However,

[1]Chair of Biological Imaging, Technical University of Munich, 81675 Munich, Germany. [2]Institute of Biological and Medical Imaging, Helmholtz Zentrum München, 85764 Neuherberg, Germany. ✉email: v.ntziachristos@tum.de

EAC has only been preliminarily validated in systems integrating 2D detector arrays on simulated data and, although this implementation was reported in patents[24,25], it has not thus far been experimentally validated. Furthermore, the use of 2D array detectors increases the size and cost of the US system. Thus, there is a need for a means of incorporating EAC into US systems that are both economical and have a small form factor.

In this work, we aimed to develop a method of implementing EAC, which could be integrated into simple and low cost US system without sacrificing the image enhancement capabilities. We hypothesized that an acoustic refractive lens could steer a US beam from a 1D transducer array, imparting it with the elevational steering ability of a stationary 2D array while retaining the advantages in size, cost, and simplicity of a 1D array. Furthermore, linear micro-translation of a refractive element should impart precision control of elevational angular steering in a 1D transducer array while minimizing motion artefacts compared to rotating the entire transducer. We describe herein this refraction-based EAC technique (REACT) and assess its qualitative and quantitative enhancements of US images in experiments on phantoms and tissues ex vivo. Moreover, we examine the effect of experimental parameters that can cause image deformation due to compounding different elevational angular views.

Methods

Image acquisition. The implementation scheme of REACT using an acoustic refractive element is shown in Fig. 1a,c. In short, linear translation of the acoustic cylindrical lens (ACL) across the stationary 1D transducer array steers the acoustic beam along the elevation direction and can be adjusted by changing the ACL's position and radius of curvature (Fig. 1b). A linear transducer array with 128 unfocused elements and a central frequency of 7.5 MHz (12L5V, Terason, USA) connected to a portable acquisition console (Terason 2000+, USA) was employed for US imaging. A motorized translation stage (MTS50-Z8, Thorlabs) was used to shift the ACL at predetermined linear steps (δ) in front of the 1D array transducer to obtain different elevational angular views by virtue of acoustic refraction. Each step has an approximate error of 0.7% of the step size. Because the lens translation was not automated, the acquisition was limited to an average of 20 frames per minute. However, implementing REACT with automated lens translation would allow for frame rates that are only limited by the acquisition speed of the US imaging system. Moreover, to provide two different effective elevational angular widths (Δ) needed for image fidelity exploration, samples were imaged at two different imaging depths (d). Figure 1d depicts the elevational steering angle of the acoustic beam at different positions of the ACL.

Refractive element fabrication. Customized ACLs designed to cover the full sensor area were manufactured from Polymethyl methacrylate (PMMA), which has a sound speed of 2750 m/s and low acoustic attenuation of 1.4 dB/cm/MHz[26,27]. The lenses were fabricated from 2.5 mm ± 4 μm thick PMMA blocks. Figure 1b shows a schematic of the three manufactured lenses, ACL1, ACL2, and ACL3, with infinite (flat), 88 mm, and 24 mm curvature radii, respectively. The acoustic beam was steered in the elevational direction by refraction caused by the difference in acoustic impedance (Z) between the PMMA lens ($Z = 3.23 \times 10^6$ kg/m^{2}s) and water (the imaging medium, $Z = 1.49 \times 10^6$ kg/m^{2}s)[26,27]. The distance between the transducer and ACL was held to < 1 mm (while avoiding contact) to minimize the effect of multiple reflection artefacts on the image due to the impedance mismatch between the PMMA and water. Each ACL can produce a characteristic maximum elevational angular deflection, which is 0° for ACL1, 2.5° for ACL2, and 5° for ACL3. Given the radius of curvature, the usable scanning length (w) is geometrically constrained and the translation step is defined to acquire a fixed number of images (N = 100). ACL1 and ACL2 were scanned with steps of $\delta_1 = \delta_2 = 150$ μm, whereas ACL3 was scanned in steps of $\delta_3 = 100$ μm. The total deflection angle was theoretically calculated using Snell's law as $c_1 \sin\theta_2 = c_2 \sin\theta_1$ (where c_1 and c_2 are the longitudinal wave velocities, and θ_1 and θ_2 are incidence and exit angles in materials 1 and 2, respectively)[28,29] and confirmed experimentally as follows.

Effective field of view and elevation angle characterisation. The transducer's inherent elevational angular FOV (θ_i), without ACLs, was first determined by measuring the distance between two opposing needle tips, which were inserted into opposite sides of an agar phantom until they just appeared on each side of the image. By recording their imaging depth, an inherent elevation angular FOV of 29.5° was calculated for the employed linear transducer. Similarly, the extended elevational angular FOVs (θ_E) when employing ACL2 and ACL3 were calculated as 32° and 34.5°, respectively. The effective compounding angles of 0° (ACL1, serving as a non-angular compounding reference), 2.5° (ACL2), and 5° (ACL3) were computed by subtracting the inherent transducer angular elevation FOV from the extended ones obtained for each ACL.

Imaging samples. Custom acoustic phantoms (50 mm × 20 mm × 15 mm) comprising 2% agar and 4% TiO_2 in 100 ml water were manufactured to assess speckle reduction efficiency and image fidelity. Phantom A embedded three 7 mm-diameter cylindrical holes and was used to evaluate REACT's speckle reduction efficiency. Phantom B contained three different holes in the shape of a cylinder (no diameter gradient), frustum (intermediate diameter gradient), and cone (high diameter gradient) and was used to explore the effect of elevational angular width and the target's cross-sectional variation on EAC image fidelity. An excised chicken heart and swine kidney were utilized as biological phantoms to further explore the importance of the cross-sectional appearance of the sample on image fidelity for a given elevational angular width using REACT. The chicken heart was chosen due to its conical shape to represent a sample with high cross-sectional variation. The swine kidney, which is larger than a chicken heart, was selected because of its low cross-sectional variation. For comparability, US images of the biological phantoms were captured and despeckled under the same imaging condition utilizing ACL3. The phantoms were stabilized during imaging by pinning them to polystyrene foam. No live specimens were used in the experiments.

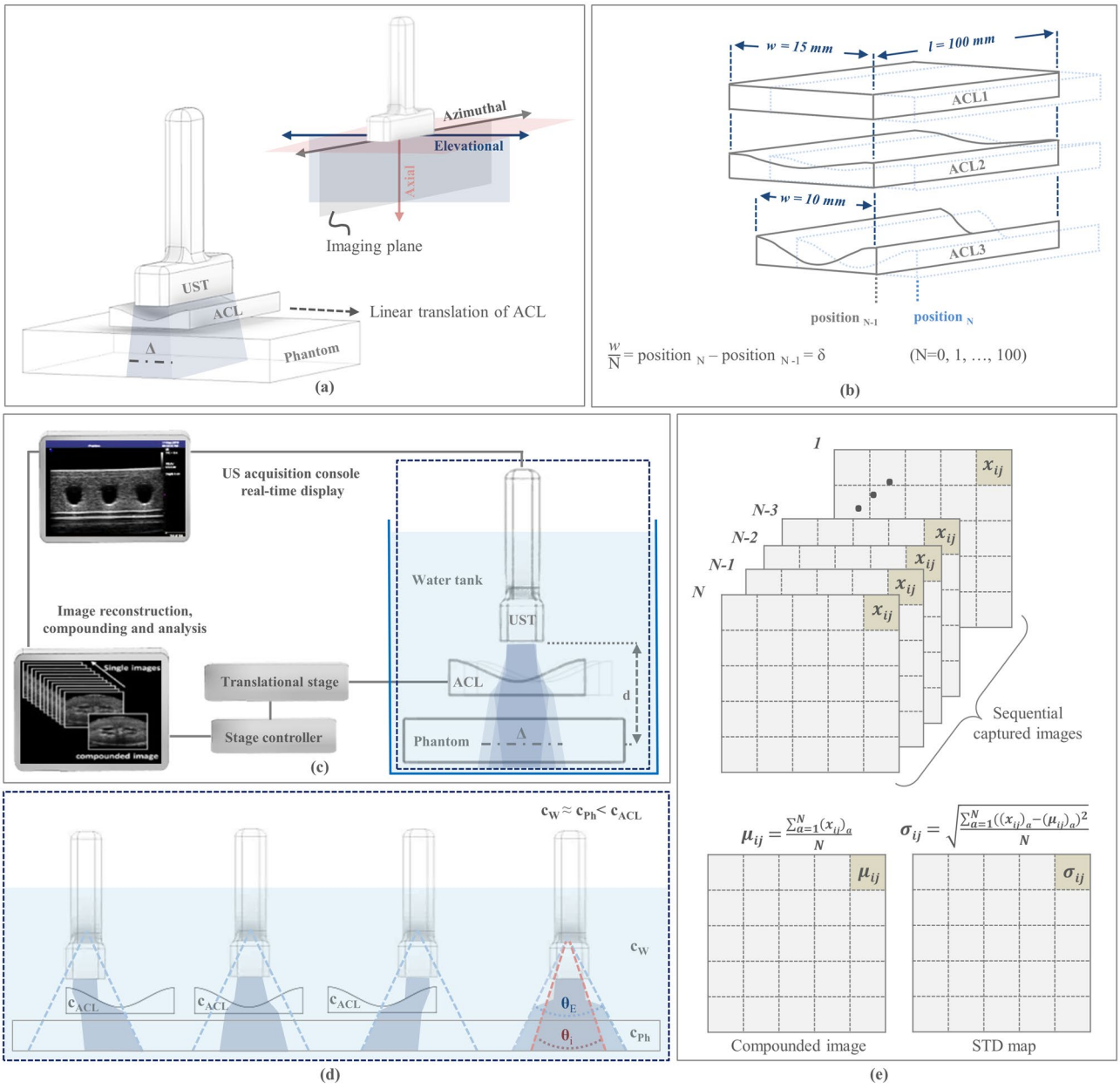

Figure 1. REACT elevational angular steering concept and implementation. (**a**) Linear translation of the ACL along the elevational direction in front of the stationary 1D transducer controls the elevational angular FOV. UST, ultrasound transducer, ACL, acoustic cylindrical lens, Δ, elevational angular width. (**b**) Renderings of ACL1, ACL2, and ACL3, which produce 0°, 2.5° and 5° angular deflections, respectively. The width and length of the ACLs are indicated by *w* and *l*, respectively. The ACLs are moved in consistent step sizes (δ), which are equal to the width of the ACL (w) divided by number of images (N) needed for compounding. (**c**) REACT imaging acquisition configuration. d, imaging depth. (**d**) Elevational angular steering in different positions of the ACL. Sound waves propagate through the water, phantom, and ACLs at speeds of c_w, c_{Ph}, and c_{ACL}, respectively, where $c_w \approx c_{Ph} < c_{ACL}$. Imaging at different positions of the ACL extends the elevational angular FOV (θ_E) of the transducer compared to its inherent elevational angular FOV (θ_i). (**e**) Matrix operators used to compute the compounded image and standard deviation (STD) decorrelation map at the pixel level using the sequentially captured images.

Analysis method. Sequential images were captured in different positions of the ACL and compounded using a mean compound operator[30] (Fig. 1e). The intensity and standard deviation (STD) were mapped at the pixel-level to investigate the efficiency of REACT to generate correlated structures and uncorrelated speckle patterns across acquired images (Fig. 1e). Single and compounded images were compared for each elevational angular deflection case to assess the despeckling efficiency. Rectangular regions of interest (ROIs = 28 × 140 pixels) within solid and empty (holes) regions in the phantom were selected to derive the intensity average and standard deviation to compute SNR and CNR. These indices were used as quantitative indicators of image

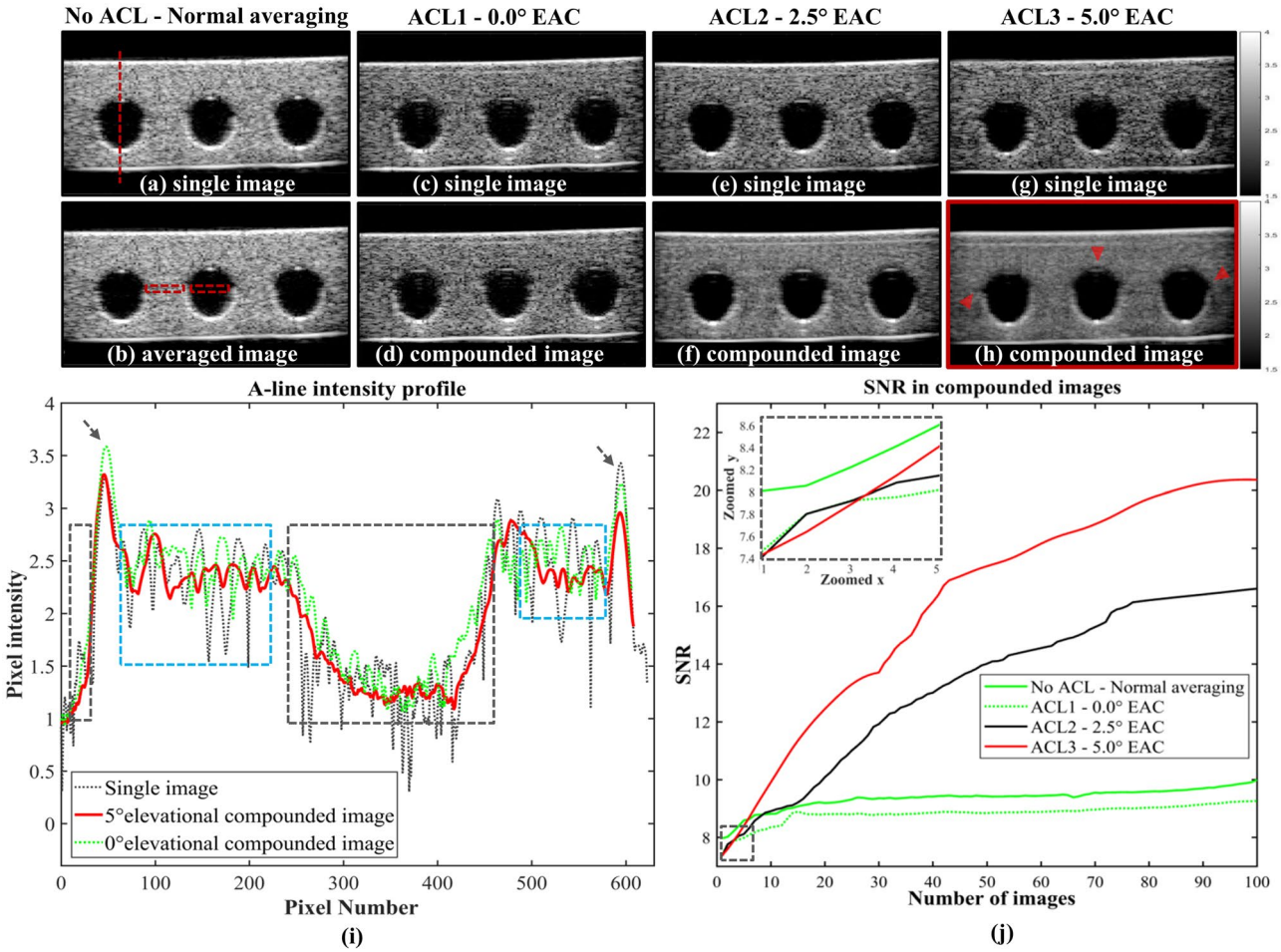

Figure 2. Speckle reduction achieved with REACT. (**a**)–(**h**) Single and compounded US images of a phantom with embedded cylindrical holes (phantom A) using three different ACLs. Images captured through no ACL in (**a**) and (**b**), ACL1 (0° deflection angle) in (**c**) and (**d**), ACL2 (2.5° deflection angle) in (**e**) and (**f**), and ACL3 (5° deflection angle) in (**g**) and (**h**). Arrows in (**h**) show despeckled features and preserved edges obtained with the 5° elevational compounding. (**i**) A-line intensity profiles along the vertical dashed line in (**a**) applied through the single and compounded images with 0° and 5° elevation angle deflection; arrows indicate the phantom's surfaces. Gray rectangles indicate water-filled regions above the top surface and inside the hole, blue rectangles indicate the regions inside the solid phantom. (**j**) Effect of increasing the number of images on SNR for the cases of normal averaging, using no ACL, and compounding, using ACL1, ACL2, and ACL3. Rectangular ROIs in (**b**) show regions used for deriving the SNR and CNR in (j) and Table 1.

improvement. The speckle and electrical noise suppression was also evaluated by inspecting the A-line intensity profiles of the single and compounded images.

Results

Figure 2 shows the speckle reduction efficiency achieved using REACT. Figure 2a–h depict uncompounded (single), averaged and compounded US images of a phantom with cylindrical holes (phantom A) at direct view and elevational angular deflections of 0°, 2.5°, and 5°.Visual inspection of the US image pairs in Fig. 2a–h reveals noticeable speckle noise reduction with wider elevational angular deflection, with the greatest despeckling effect observed for the 5° case. Despite this wide deflection angle (5°), the edges of the holes in the phantom are preserved upon compounding, as highlighted by the arrows in Fig. 2h. Figure 2i shows the A-line intensity profiles obtained for a single image (Fig. 2c) compared to profiles of the images that were compounded at elevational deflections of 0° (Fig. 2d) and 5° (Fig. 2h). Inspecting the A-line intensity profile of the single image across the solid phantom sections (blue rectangles in Fig. 2i) shows high intensity variations related to the granular nature of speckle noise. These variations are strongly suppressed by REACT at an elevational angular deflection of 5°. In contrast, compounding with a 0° elevational angular deflection, which acts as a comparative reference to normal averaging, only moderately suppresses the intensity variations. The noise reduction upon compounding at 0° is primarily due to electrical noise averaging, which is apparent in the A-line intensity profile variation across the water-filled regions (gray rectangles in Fig. 2i), where no scatterers are expected to produce speckle. Still, even in the absence of speckle, compounding at a 5° elevational angle results in greater noise reduction than at 0°, demonstrating that REACT reduces both speckle noise and overall US electrical noise more efficiently than

ACL Type	Phantom ($SNR_{compounded}/SNR_{single} - 1$)	Phantom and Hole ($CNR_{compounded}/CNR_{single} - 1$)
No ACL (normal averaging)	0.24	0.27
ACL1 (0.0° deflection angle)	0.23	0.28
ACL2 (2.5° deflection angle)	1.22	1.84
ACL3 (5.0° deflection angle)	1.72	2.18

Table 1. SNR and CNR improvement using REACT. SNR: signal to noise ratio = μ/σ, CNR: contrast to noise ratio = $|\mu_{Hole} - \mu_{Phantom}|/\sigma_{Hole}$.

normal averaging. To quantify this observation, Fig. 2j shows the effect of increasing the number of images used for averaging and compounding on the SNR, as calculated within the ROI (red rectangle) in the solid region of the phantom in Fig. 2b. As expected, SNR increases for all cases, yet at a greater rate for the 5° EAC case, owing to a reduction in both speckle and electrical noise. Note that, for all EAC cases (with the ACL), initial SNR is lower compared to the normal averaging case (without the ACL), as seen in the inset of Fig. 2j. This is due to the signal loss caused by the acoustic attenuation and reflection. However, owing to the high despeckling efficiency of REACT, the final SNR in the 5° EAC case is two times higher than for normal averaging (Fig. 2j).

Table 1 shows SNR and CNR improvements obtained using REACT. Quantitative indices extracted from the two ROIs (28×140 pixels) specified in Fig. 2b were used to compare the despeckling efficiency of normal averaging and REACT at different elevational angular deflections. The higher SNR and CNR in the wider elevational angular acquisition are consistent with the observations in Fig. 2.

Figure 3 demonstrates the effect of elevational angular width (Δ) and the target's cross-sectional variation on image fidelity after elevational angular compounding. The schematic in Fig. 3a illustrates the configuration of phantom B, which contains three holes with shapes approximating a cylinder, frustum, and cone. These holes have different diameter gradients along the entire angular imaging width, enabling the investigation of the correlation between Δ and image fidelity. Phantom B was imaged using ACL3 at two different imaging depth ($d_1 = 1.5$ cm and $d_2 = 5.5$ cm), i.e. two effective Δ values. A single image and two compounded images using 5° elevational angular deflection are shown in Fig. 3b–d. As expected, image fidelity upon compounding suffered most for the conical hole (Fig. 3c,d, cone), which has the highest diameter gradient along elevational direction, even for the shallow imaging depth (d_1, smaller Δ). The cone with an intermediate diameter gradient (Fig. 3c,d, frustum) displays acceptable image fidelity for the smaller Δ at d_1, but is more impacted at d_2. However, the cylindrical hole (no diameter gradient, labelled cylinder) shows image fidelity for both Δ cases, without blurry edges. The impacts of these findings were further explored using a biological phantom of an excised chicken heart (Fig. 3e). Figures 3f,g show the single (Fig. 3f) and compounded (Fig. 3g) images obtained from the organ with the ACL3 at d_2. Visual examination of these US images reveal edge blurring and structure distortion in the compounded image (arrows in Fig. 3g) due to the high diameter gradient of the organ in the elevational direction, similar to the cone case in Phantom B (as depicted by the blue dotted triangle in Fig. 3e).

Figure 4 demonstrates speckle reduction upon applying REACT to image a swine kidney (Fig. 4a), which has a cylindrical shape and thus a low diameter gradient. Figure 4b,c show single and compounded US images of the swine kidney, with the latter produced using ACL3 at a depth of $d_2 = 5.5$ cm. Visual inspection of the US images in Fig. 4 reveals marked speckle noise reduction using REACT without blurriness or structure distortion, despite the use of the same imaging conditions as for the chicken heart (Fig. 3g). The difference in image fidelity between the two organs is attributable to the lower variation of the swine kidney's cross-sectional appearance (low diameter gradient) across the angular imaging width compared to that of the chicken heart. Figure 4e,f display the variation in pixel intensity for images compounded at elevational angles of 0° and 5°, which was mapped to investigate the speckle pattern decorrelation between individual captured images (Fig. 4d). As expected, higher speckle pattern decorrelation is obtained for images captured within the 5° elevational angle, which therefore resulted in higher speckle reduction as demonstrated in Fig. 4c.

Figure 4g shows A-line intensity profiles from a single image of the swine kidney (corresponding to the red dotted line in Fig. 4c) compared to images compounded at elevational angle of 0° and 5°. As in the case of phantom A (Fig. 2g), the high variation of the A-line intensity profile of the single image across solid tissue sections (blue rectangles in Fig. 4g) is strongly suppressed upon compounding at a 5° elevational angle, but much less so at 0°. It can be seen that electrical noise is largely suppressed using compounding at both 0° and 5° elevational angles, observable in the A-line intensity profile across the hypoechoic regions where minimal speckle source is expected (gray rectangles in Fig. 4g). It is noteworthy that using REACT with 5° elevational compounding shows better efficiency not only in speckle reduction but also in US electrical noise suppression, similar to the results in Fig. 2g. To quantify this observation, Fig. 4h,i show the effect of increasing the number of images used for compounding on SNR, standard deviation (STD), and CNR for 0° and 5° EAC, calculated within the specified ROIs in Fig. 4b. In both cases, SNR and CNR trend upward while STD trends downward, yet with greater rates for the 5° case due to reduction in both speckle and electrical noise.

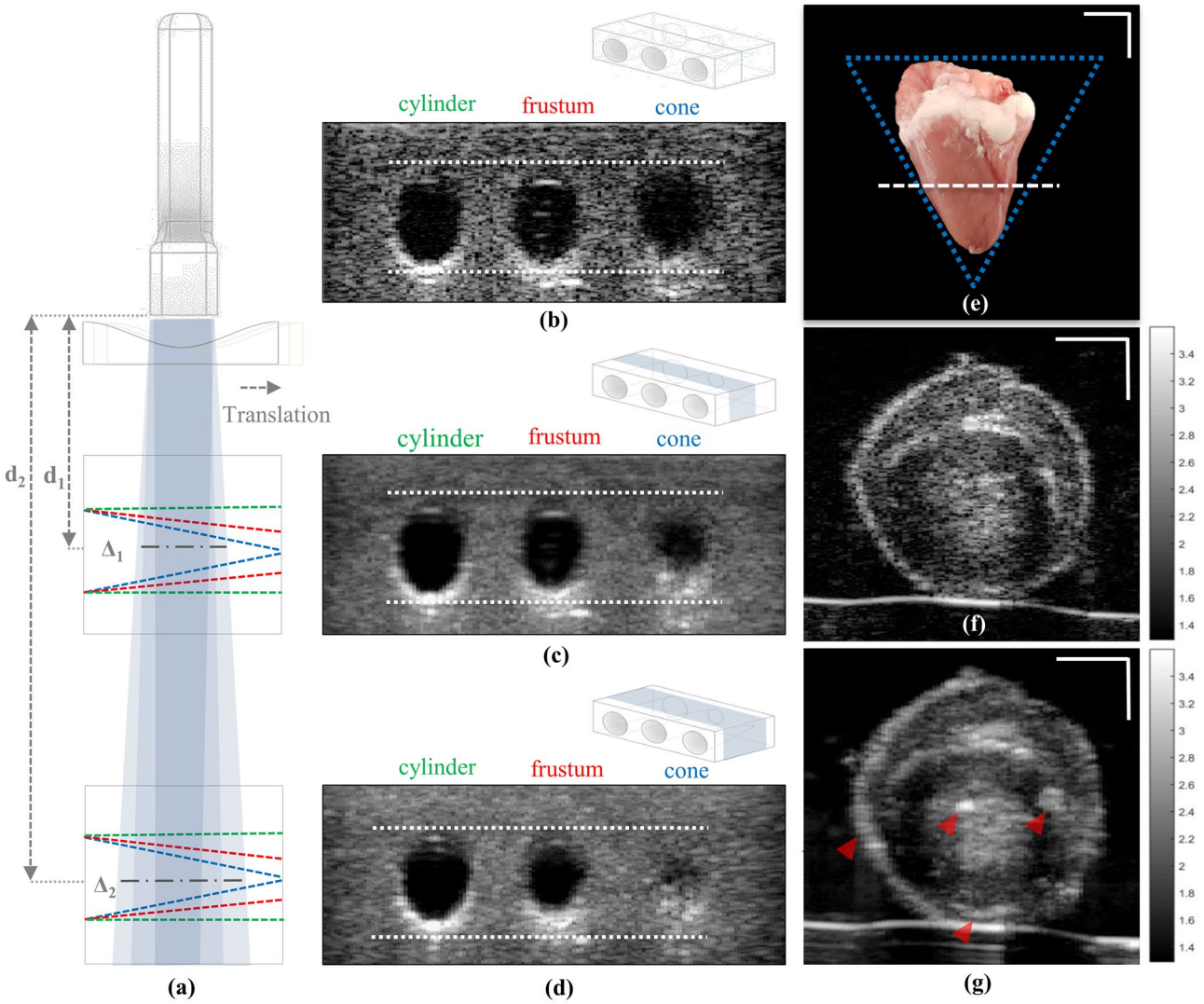

Figure 3. Elevational angular width affects elevational angular compounded image fidelity. (**a**) Schematic of the imaging acquisition configuration depicting the elevation angular width ($\Delta_1 \simeq 1.3$ mm and $\Delta_2 \simeq 4.8$ mm) at different phantom distance positions ($d_1 = 1.5$ cm and $d_2 = 5.5$ cm). Green, red, and blue dashed lines show the cross-section of the cylinder, frustum, and conical hole shapes in the phantom, respectively (phantom B). (**b**) Single US image of the phantom at depth d_2. White dashed lines show the holes' boundaries. (**c**), (**d**) 5° elevational compounded images at depths d_1 and d_2, respectively. (**e**) Excised chicken heart; white dashed line shows the image cross section location in (**f**) and (**g**). Blue dashed lines indicate the conical shape of the chicken heart. (**f**), (**g**) Single and 5° elevational compounded US images of chicken heart at depth d_2. Red arrows highlight the effect of compounding and loss of fidelity compared to the single image in (**f**). Scale bars: 1 mm in e, 0.5 mm in (**f**) and (**g**).

Discussion

Speckle noise in US imaging adversely affects its diagnostic accuracy. Among proposed despeckling methods, compounding techniques are preferable because they can improve image quality and reveal real structures obscured by speckle noise, which are otherwise irretrievable using image processing techniques. This functionality requires the acquisition of multiple images with uncorrelated speckle patterns, which often comes at the cost of increased size and complexity of the imaging setup, limiting its applicability for clinical translation. Here, we have demonstrated a new refraction-based elevational angular compounding technique (REACT), which efficiently de-speckles US images using an acoustic refractive element. This method enables EAC in a US system comprising a low-cost 1D detector array without moving or tilting the entire transducer head, eliminating the need for bulky mechanical stages or costly 2D arrays and easing implementation in current US imaging systems equipped with 1D arrays.

In contrast to previous EAC implementations, REACT uses a fixed 1D transducer array with a translating acoustic cylindrical lens. Visual and quantitative inspection of US images depicted in Fig. 2 and Fig. 4 illustrates the capability of REACT to reduce speckle noise. Compounded images acquired with elevational angular deflections of 0°, 2.5°, and 5° improved the CNR by 0.28×, 1.84×, and 2.18× and SNR by 0.23×, 1.22×, and

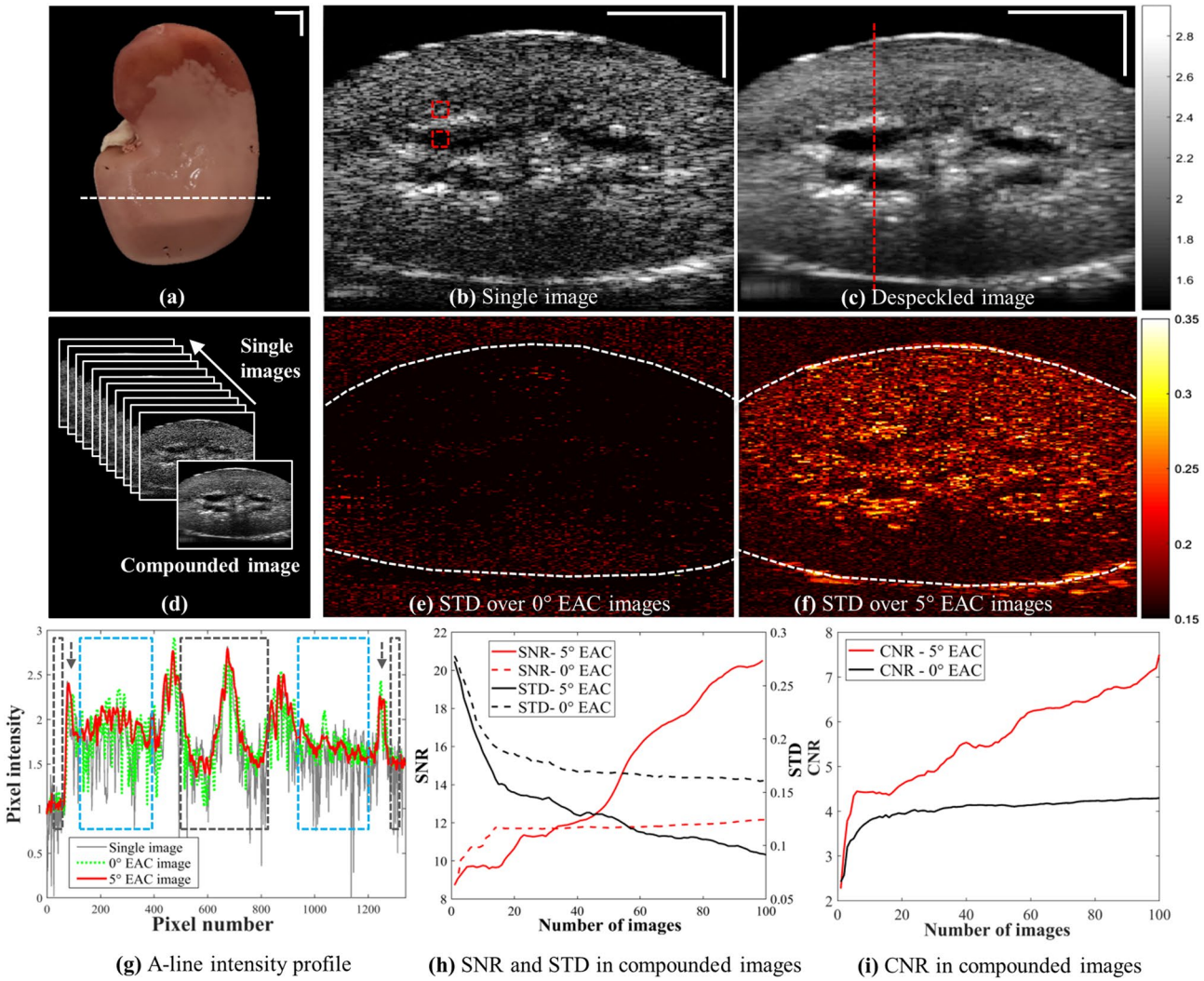

(g) A-line intensity profile **(h)** SNR and STD in compounded images **(i)** CNR in compounded images

Figure 4. REACT demonstrates efficient US speckle reduction in a swine kidney. (**a**) Excised swine kidney; white dashed line shows the image cross-section location in (**b**,**c**). (**b**), (**c**) Single and compounded US images of a swine kidney at a depth of 5.5 cm using ACL3. Rectangular ROIs in (**b**) show regions used for deriving the SNR, STD and CNR indices plotted in (**h**) and (**i**). (**d**) Representation of the compounding of a series of images by REACT. (**e**), (**f**) Intensity of STD maps at pixel-level along all captured images, using ACL1 and ACL3, respectively; dashed lines delineate the tissue surface contour. (**g**) A-line intensity profiles along the vertical dashed line in (**c**) applied through the single and elevational compounded images within 0° and 5° elevation angle deflection. Arrows demonstrate the tissue's surfaces. Grey rectangles indicate hypoechoic regions above the top surface and inside the holes. Blue rectangles indicate regions within the tissue. Scale bars: 1 mm. (**h**) Effect of increasing the number of images used for compounding on SNR and STD within tissue and inside the hole for the cases of 0° and 5° EAC. (**i**) Effect of increasing the number of images used for compounding on CNR for the cases of 0° and 5° EAC.

1.72 × compared to single images, respectively. Note that CNR and SNR improvement in the 0° elevational compounded image is due to electrical noise suppression, whereas the corresponding improvement for the 2.5° and 5° cases is due to the both electrical and speckle noise reduction achieved by averaging uncorrelated speckle image patterns from different elevational angular views. As expected, the wider the elevational angular acquisition, the greater the speckle suppression in the compounded image[13,14]. While the widest angle employed in our study was 5°, the selection of the optimal compounding angle should take into account the trade-off between speckle reduction efficiency and image distortion (discussed below). Our results in Table 1 suggest that REACT offers at least twice the enhancement in SNR and CNR compared to previous reported implementations of EAC[14]. This superior enhancement could be attributed to a reduction in motion artefacts because of the fixed transducer. Note that imaging through the PMMA refractive lenses caused a 7.5% signal loss due to acoustic attenuation and reflection (inset in Fig. 2j). REACT's SNR could be further improved by minimizing this signal loss using materials with lower acoustic impedance and attenuation compared to PMMA (e.g. TPX[27]) and utilizing diffraction lenses with lower effective thicknesses[31].

Although EAC is recognized as an efficient way to suppress speckle noise in US images, it suffers from anatomic structure deformation and edge blurriness in compounded images captured within wide elevational angular views[13,14]. Our results demonstrate that image deformation can also occur in EAC with narrow elevational angles, particularly from deeper imaging positions, due to the associated increase in elevational angular width (Δ). Image fidelity in EAC, or in other words, accurate representation of structural features from the despeckled plane, is affected by interference from structures in adjacent elevational planes. We explored the trade-off between imaging depth and elevational angular width when employing EAC methods on targets with shapes that have no (cylinder), low (frustum), and high (cone) diameter gradient along the elevational direction (Fig. 3). We found that higher image fidelity is obtained with targets that preserve their cross-sectional appearance along the elevational angular width (cylinder), while image fidelity increasingly suffers for targets with intermediate and high diameter gradients (frustum and cone). The effect of cross-sectional variation on image fidelity was further validated by imaging an *ex vivo* chicken heart and swine kidney with REACT, which demonstrated the importance of accounting for the morphology of the sample for a given elevational angular width in EAC. The spatial resolution along elevational direction is the main limiting factor in all EAC implementation and depends on the total elevational beam width. Hence, out of plane signals can degrade compounding quality, particularly when imaging small organs. This was confirmed in our experiments, where the high variation of the cross-sectional appearance of the chicken heart resulted in distortions in the compounded image (Fig. 3f,g), whereas the low variation in the cross-sectional appearance of the excised swine kidney led to speckle reduction with no loss in image fidelity (Fig. 4b,c). Despeckling of smaller organs using EAC could be performed by reducing the angular compounding width at the cost of a lower despeckling efficiency. We found through experiment that 5° EAC afforded high despeckling efficiency with minimal image fidelity loss in large organs, such as the kidney. However, determination of the optimal elevational angle width for different organs or applications is required to ensure the highest despeckling efficiency without significant loss of image fidelity. Future studies will be conducted on optimization algorithms using quantitative image analysis to investigate the optimal compounding angle for specific targets. REACT could be attractive in targets with lower expected elevational variations such as peripheral vascular, muscle, or bone imaging.

In summary, we utilized acoustic refraction to introduce elevational angular steering into existing 1D transducer arrays and demonstrated its application in a novel implementation of EAC called REACT. Such a low-cost and simple compounding de-speckling method can be of great benefit in clinics to improve current US visualization and interpretation during disease diagnosis. Further work aims at miniaturising ACL embodiments and allowing real-time despeckling by automating the position of the lens and synchronizing frames to evaluate REACT in a clinical context.

Data availability

The datasets generated during and/or analysed during the current study are available from the corresponding author on reasonable request.

Received: 11 August 2020; Accepted: 12 October 2020
Published online: 23 October 2020

References

1. Rumack, C. M., Wilson, S. R. & Charboneau, J. W. *Diagnostic Ultrasound, 1–28* (Elsevier Mosby, London, 2005).
2. Szabo, T. L. Diagnostic *Ultrasound Imaging: Inside Out*, 1–37 (Academic press, 2013).
3. Goodman, J. W. Some fundamental properties of speckle. *J. Opt. Soc. Am.* **66**, 1145–1150 (1976).
4. Burckhardt, Ch. B. Speckle in ultrasound B-mode scans. *IEEE Trans. Sonics Ultrason.* **25**, 1–6 (1978).
5. Nyrnes, S. A., Fadnes, S., Wigen, M. S., Mertens, L. & Lovstakken, L. Blood speckle-tracking based on high-frame rate ultrasound imaging in pediatric cardiology. *J. Am. Soc. Echocardiogr.* **33**, 493–503 (2020).
6. Tay, P. C., Garson, Ch. D., Acton, S. T. & Hossack, J. A. Ultrasound despeckling for contrast enhancement. *IEEE Trans. Image Process.* **19**, 1847–1860 (2010).
7. Zhang, J. & Cheng, Y. *Despeckling Methods for Medical Ultrasound Images* (Springer, Singapore, 2020).
8. Park, J., Kang, J. B., Chang, J. H. & Yoo, Y. Speckle reduction techniques in medical ultrasound imaging. *Biomed. Eng. Lett.* **4**, 32–40 (2014).
9. Narayanan, S. K. & Wahidabanu, R. S. D. A view on despeckling in ultrasound imaging. *Int. J. Signal Process. Image Process. Pattern Recognit.* **2**, 85–98 (2009).
10. Michailovich, O. V. & Tannenbaum, A. Despeckling of medical ultrasound images. *IEEE Trans. Ultrason. Ferroelectr. Freq. Control.* **53**, 64–78 (2006).
11. Joel, T. & Sivakumar, R. An extensive review on despeckling of medical ultrasound images using various transformation techniques. *Appl. Acoust.* **138**, 18–27 (2018).
12. Loupas, T., McDicken, W. N. & Allan, P. L. An adaptive weighted median filter for speckle suppression in medical ultrasonic images. *IEEE Trans. Circuits Syst.* **36**, 129–135 (1989).
13. Karaman, M. A., Kutay, M. A. & Bozdagi, G. An adaptive speckle suppression filter for medical ultrasonic imaging. *IEEE Trans. Med. Imag.* **14**, 283–292 (1995).
14. Shattuck, D. P. & von Ramm, O. T. Compound scanning with a phased array. *Ultrason. Imaging* **4**, 93–107 (1982).
15. Magnin, P. A., von Ramm, O. T. & Thurstone, F. L. Frequency compounding for speckle contrast reduction in phased array images. *Ultrason. Imaging* **4**, 267–281 (1982).
16. Trahey, G. E., Allison, J. W., Smith, S. W. & von Ramm, O. T. A quantitative approach to speckle reduction via frequency compounding. *Ultrason. Imaging* **8**, 151–164 (1986).
17. Trahey, G. E., Smith, S. W. & von Ramm, O. T. Speckle pattern correlation with lateral aperture translation: experimental results and implications for spatial compounding. *IEEE Trans. Ultrason. Ferroelectr. Freq. Control* **33**, 257–264 (1986).
18. Chang, J. H., Kim, H. H., Lee, J. & Shung, K. K. Frequency compounded imaging with a high-frequency dual element transducer. *Ultrasonics* **50**, 453–457 (2010).
19. Perperidis, A., McDicken, N., MacGillivary, T. & Anderson, T. Elevational spatial compounding for enhancing image quality in echocardiography. *Ultrasound* **24**, 74–85 (2016).

20. Li, P. C. & O'Donnell, M. Elevational spatial compounding. *Ultrason. Imaging* **16**, 176–189 (1994).
21. Hooi, F. M., Thomenius, K. E., Fisher, R. & Carson, P. L. Hybrid beamforming and steering with reconfigurable arrays. *IEEE Trans. Ultrason. Ferroelectr. Freq. Control.* **57**, 1311–1319 (2010).
22. Shung, K. K. The principle of multidimensional arrays. *Eur. J. Echocardiogr.* **3**, 149–153 (2002).
23. Wildes, D. G. *et al.* Elevation performance of 125D and 15D Transducer arrays. *IEEE Trans. Ultrason. Ferroelectr. Freq. Control.* **44**, 1027–1037 (1997).
24. Haugen, G. U., Kristoffersen, K. & Sornes A. R. Method and apparatus for performing ultrasound elevation compounding. U.S. Patent 9 204 862. (2015).
25. Adams, D. P. & Thiele, K. E. Ultrasound imaging system and method for spatial compounding. U.S. Patent 6 464 638. (2002).
26. Xia, W., Piras, D., van Hespen, J. C. G., Steenbergen, W. & Manohar, S. A new acoustic lens material for large area detectors in photoacoustic breast tomography. *Photoacoustics* **1**, 9–18 (2013).
27. Bloomfield, P. E., Lo, W. J. & Lewin, P. A. Experimental study of the acoustical properties of polymers utilized to construct PVDF ultrasonic transducers and the acousto-electric properties of PVDF and P(VDF/TrFE) films. *IEEE Trans. Ultrason. Ferroelectr. Freq. Control.* **47**, 1397–1405 (2000).
28. Hohenwarter, D. & Jelinek, F. Snell's law of refraction and sound rays for a moving medium. *J. Acoust. Soc. Am.* **105**, 1387–1388 (1999).
29. Finn, S., Glavin, M. & Jones, E. Speckle Reduction in Echocardiography: Trends and Perceptions. In *Echocardiography—New Techniques*, G. Bajraktari, 41–68 (InTech, 2012).
30. Wilhjelm, J. E., Jensen, M. S., Jespersen, S. K., Sahl, B. & Falk, E. Visual and quantitative evaluation of selected image combination schemes in ultrasound spatial compound scanning. *IEEE Trans. Med. Imaging* **23**, 181–190 (2004).
31. Chen, J., Xiao, J., Lisevych, D., Shakouri, A. & Fan, Zh. Deep-subwavelength control of acoustic waves in an ultra-compact metasurface lens. *Nat. Commun.* **9**, 4920 (2018).

Acknowledgements

This project has received funding from the European Union's Horizon 2020 research and innovation program under grant agreement 732720 (ESOTRAC) as well as from European Union's Horizon 2020 research and innovation program under the Marie-Sklodowska-Curie grant agreement No 721766 (FBI). The authors also thank Dr. Robert J. Wilson for proofreading the manuscript.

Author contributions

P.A. and C.Z. designed the study. P.A. produced phantoms, prepared ex vivo samples and carried out the experiments. P.A. collected and analysed the data and prepared all figures in the manuscript. P.A. and C.Z. interpreted the data and wrote the manuscript. V.N. reviewed and approved the final manuscript.

Funding

Open Access funding enabled and organized by Projekt DEAL.

Competing interests

The authors declare no competing interests.

Additional information

Correspondence and requests for materials should be addressed to V.N.

Reprints and permissions information is available at www.nature.com/reprints.

Publisher's note Springer Nature remains neutral with regard to jurisdictional claims in published maps and institutional affiliations.

Improving ultrasound images with elevational angular compounding based on acoustic refraction

Author: Parastoo Afshari et al
Publication: Scientific Reports
Publisher: Springer Nature
Date: Oct 23, 2020

Creative Commons

scientific reports

Check for updates

OPEN

Speckle reduction in ultrasound endoscopy using refraction based elevational angular compounding

Parastoo Afshari[1,2], Christian Zakian[1,2], Jeannine Bachmann[3] & Vasilis Ntziachristos[1,2]✉

Endoscopic ultrasonography (EUS) is a safe, real-time diagnostic and therapeutic tool. Speckle noise, inherent to ultrasonography, degrades the diagnostic precision of EUS. Elevational angular compounding (EAC) can provide real-time speckle noise reduction; however, EAC has never been applied to EUS because current implementations require costly and bulky arrays and are incompatible with the tight spatial constraints of hollow organs. Here we develop a radial implementation of a refraction-based elevational angular compounding technique (REACT) for EUS and demonstrate for the first time spatial compounding in a radial endoscopy. The proposed implementation was investigated in cylindrical phantoms and demonstrated superior suppression of ultrasound speckle noise and up to a two-fold improvement in signal- and contrast- ratios, compared to standard image processing techniques and averaging. The effect of elevational angular deflection on image fidelity was further investigated in a phantom with lymph node-like structures to determine the optimum elevational angular width for high speckle reduction efficiency while maintaining image fidelity. This study introduces REACT as a potential compact and low-cost solution to impart current radial echo-endoscopes with spatial compounding, which could enable accurate identification and precise sizing of lymph nodes in staging of gastrointestinal tract cancers.

Endoscopic ultrasonography (EUS) is a real-time, minimally invasive diagnostic imaging modality with therapeutic applications in the gastrointestinal (GI) tract region[1–7], as well as neighboring organs within 4–5 cm of the GI tract, such as the pancreas, liver, and lymph nodes[8–10]. Because of the high spatial resolution and the proximity to the organs, EUS is superior to spiral computed tomography (CT) and magnetic resonance imaging (MRI) for detecting small lesions[11–13]. Thus, EUS is an ideal modality to detect lymph node tumor metastasis, which is crucial for staging of GI tract cancers[8–13].

Despite these advantages, EUS suffers from poor contrast in the mucosal layers of the GI tract wall[8,9] due to speckle noise, which is inherent in coherent imaging and arises from the interference of the backscattered waves from tissue microstructures. Speckle noise hinders the identification of tissue-layer boundaries within the GI tract where differences in acoustic impedance are low[10]. Therefore, speckle degrades image quality and contrast, which impedes accurate identification of pathological tissues.

Post-processing techniques to remove speckle from ultrasound images often fail to reveal structures that were obscured by speckle in the original image[14,15]. In contrast, compounding methods can overcome missing information in individual frames by acquiring and averaging a sequence of images containing both correlated features and uncorrelated speckle patterns, with spatial compounding being preferred due to its higher speckle reduction efficiency[14]. To our knowledge, spatial compounding in linear EUS has only been implemented using azimuthal angular compounding[4,10]. Azimuthal angular compounding suffers from limited spatial overlap of images acquired from multiple transmission angles and reduced frame rates due to additional pre-processing for image alignment. Despite its use in linear ultrasound endoscopy, azimuthal compounding is not applicable for radial EUS, as the radial geometry captures the image over a full 360-degree angle in the azimuthal plane, which negates the option of acquiring multiple decorrelated speckle patterns. In contrast, elevational angular compounding (EAC), which relies on capturing partially correlated images by steering the imaging plane with small angular steps in the elevational direction (perpendicular to the imaging plane)[16], is ideal for radial EUS because its geometry is suitable for capturing sequential frames in a radial configuration. In addition, EAC allows imaging of the same region of interest in all sequential frames, therefore eliminating the need for spatial

[1]Chair of Biological Imaging, Technical University of Munich, 81675 Munich, Germany. [2]Institute of Biological and Medical Imaging, Helmholtz Zentrum München (GmbH), 85764 Neuherberg, Germany. [3]Department of Surgery, Klinikum Rechts der Isar, Technical University of Munich, 81675 Munich, Germany. ✉email: bioimaging.translatum@tum.de

alignment, which is desirable for real time imaging[16–18]. However, no EAC implementations for EUS have yet been introduced, likely due to spatial and cost constraints. Previous implementations of EAC for traditional ultrasound imaging used either a two dimensional (2D) array[16] or a mechanical rotating one dimensional (1D) array[17] to provide the elevational angular imaging; however, 2D arrays are costly and images from mechanically rotating 1D arrays are susceptible to motion artefacts. Moreover, the need for multiple piezoelectric elements in 2D arrays and mechanical stage in rotating 1D arrays make these implementations of EAC bulky and cumbersome, which increases the risk of damage to the GI tract during examination. These factors prevent the translation of EAC to clinical EUS applications.

Our group recently introduced a refraction-based elevational angular compounding technique (REACT), wherein a customized refractive element imparts a fixed linear array with elevational angular steering capabilities[18]. REACT demonstrated more efficient ultrasound despeckling compared to the previous EAC implementations, primarily because the fixed transducer array minimized motion artefacts. However, the refractive element of the REACT prototype was designed for linear arrays, and was therefore not suitable for use in radial ultrasound endoscopy[18].

In this work, we developed a radial implementation of REACT by using an engraved acoustic cylindrical refractive lens on an annular PMMA substrate to steer ultrasound waves along the elevational angle in cylindrical coordinates. This development represents the first application of spatial compounding in radial EUS. Our radial implementation of REACT achieves elevational angular steering using a stationary 1D-array transducer, making it more compact to avoid potential damage to the GI tract during examination. By integrating radial REACT into a commercially available radial ultrasound endoscope, we image cylindrical layered phantom and demonstrate a two-fold improvement in contrast- and signal-to-noise ratios over uncompounded US images. Moreover, we characterize the optimal elevation angle of deflection for the lymph node- like structures to yield both high speckle reduction efficiency and image fidelity.

Methods

Image acquisition. The implementation scheme of REACT in EUS is shown in Fig. 1a. The employed ultrasound imaging system (HI VISION Avius, Hitachi) utilized a convex radial 360-degree transducer array with central frequency of 7.5 MHz (EUP-R54AW-19, Hitachi). Filters in the software of the EUS system were deactivated prior to capturing images to minimize the amount of pre-processing performed. We acquired all images under the same testing conditions to ensure the validity of the despeckling efficiency comparison between the different refractive lenses. An annular-shaped acoustic cylindrical lens (see below) was attached to a linear translation stage to provide the fixed radial transducer with the elevational angular steering capability. A motorized linear translation stage (MTS50-Z8, Thorlabs) was used to shift the acoustic lens at predetermined linear steps, δ, along the longitudinal axis of the fixed transducer to obtain different elevational angular views by virtue of acoustic refraction (Fig. 1b). Each longitudinal step has an approximate error of 0.7% of the step size. Compounded images were attained by capturing (N = 100) sequential images from the same region of interest, yet at different elevational angular views with a rate of 20 frames per minute. The elevational angular field-of-view (FOV) of the transducer were adjusted by changing the acoustic lens's position and radius of curvature.

Refractive element fabrication. Figure 1c shows a schematic of the annular-shaped acoustic cylindrical lens. Customized acoustic cylindrical lenses were manufactured from Polymethyl methacrylate (PMMA), which has a speed of sound of 2750 m/s and a low acoustic attenuation of 1.4 dB/cm/MHz compared to other materials used for acoustic lens fabrication[19,20]. Solid PMMA rods with a diameter of 15 mm ± 4 µm were used as substrate for the acoustic lenses. A 13 mm hole was drilled through the center of the rods to allow a hollow passage for the convex radial 360-degree transducer array. The inner surface of each PMMA tube was later further machined to afford the different curvatures of the refractive acoustic lenses. The acoustic beam refracts in the elevational direction due to the acoustic impedance (Z) difference between the PMMA lens ($Z = 3.23 \times 10^6$ kg/m^{2}s) and water (the imaging medium, $Z = 1.49 \times 10^6$ kg/m^{2}s)[19,20]. The distance between the transducer and cylindrical acoustic lenses was held to <1 mm (while avoiding contact) to minimize the effect of multiple reflection artefacts on the image due to the impedance mismatch between the PMMA and water. Depending on the curvature and position in front of the transducer, each cylindrical acoustic lens can provide an extended elevational angle that corresponds to the union set of all angular deflections attained by translating the full length of the lens, *l*, in front of the transducer (Fig. 1c). The specific maximum elevational angular deflection for each lens is achieved when the lens is positioned at the edge of the transducer and all other deflections occur as the lens is translated towards the middle of the transducer. The five manufactured acoustic lenses used in this study provide maximum elevational angular deflections of 0°, 2.5°, 5°, 15°, and 30°. Here, the 0° lens serves as a control case for the refraction-based despeckling principle by yielding the same imaging plane in all relative positions in front of the transducer. To acquire the same number of images for compounding using different lenses, the translation step (δ) for each acoustic lens was selected by dividing the length of each lens (*l*) by the number of acquired images (N = 100; δ: 200 µm, 200 µm, 150 µm, 50 µm, 24 µm, for the 0°, 2.5°, 5°, 15°, and 30° acoustic lenses, respectively). The effective deflection angle was calculated using Snell's law as $c_1 \sin Ø_2 = c_2 \sin Ø_1$ (where c_1 and c_2 are the longitudinal wave velocities, and $Ø_1$ and $Ø_2$ are incidence and exit angles in materials 1 and 2, respectively)[21,22] and confirmed experimentally in a similar manner to that reported in our previous study[18]. ("See supplementary Fig. 1—Elevational angular characterization of the manufactured lenses using hydrophone and metal target").

Imaging samples. Two custom tube-shaped phantoms were manufactured to assess speckle reduction efficiency and image fidelity. They comprised 2% agar and different concentrations of TiO_2 (0.25–4%) and had outer diameters of 80 mm and inner diameters of 20 mm. Phantom A consisted of five agar layers with TiO_2

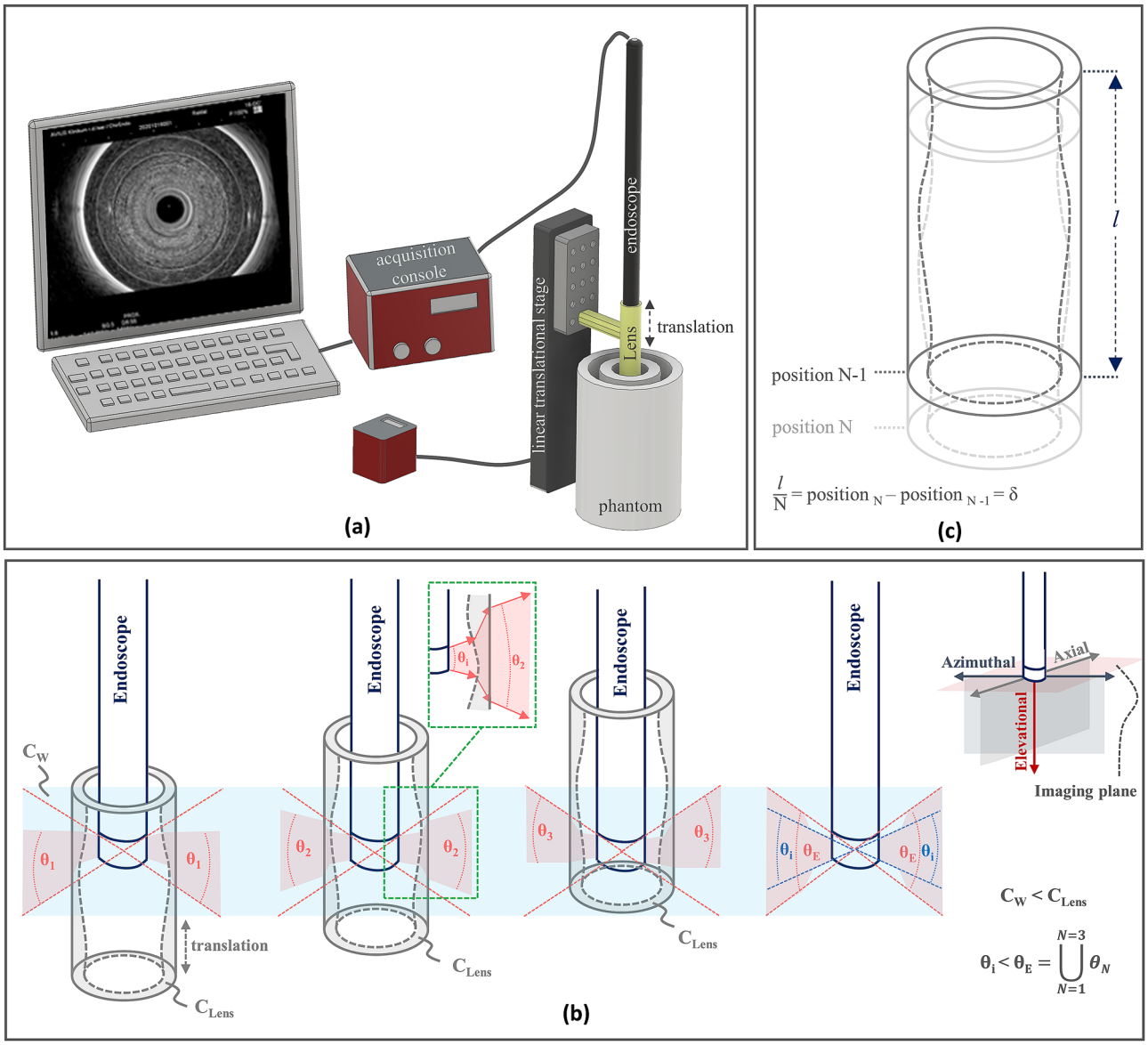

Figure 1. REACT implementation in EUS. **(a)** REACT imaging acquisition configuration using radial transducer array. Linear translation of the annular-shaped acoustic cylindrical lens along the elevational direction in front of the stationary radial transducer array controls the elevational angular FOV. **(b)** Elevational angular steering in different positions of the acoustic cylindrical lens. Sound waves propagate through the water and lens substrate at speeds of c_w and c_{Lens}, respectively, where $c_w < c_{Lens}$. Example of an incidence angle and refracted angle through the lens shown in the inset. The total elevational angular FOV of the transducer (θ_E: union set of refracted elevational angular views from all positions of the acoustic lens) compared to its inherent elevational angular FOV (θ_i) is extended. **(c)** Schematic of annular-shaped acoustic cylindrical lens. The annular-shaped acoustic cylindrical lens is moved in consistent step sizes (δ), which are equal to the length of the acoustic lens (l) divided by the number of recorded images (N) for compounding.

concentrations of 0.25%, 0.5%, 1%, 2%, and 4%, from the outer to the innermost layer, respectively. The phantom contained rod-shaped holes with a 1 mm-diameter to test REACT's ability to reveal fine structures obscured by speckle noise. Phantom B consisted of a single agar layer with 4% TiO_2 concentration with embedded spherical water beads with diameters ranging between 10 and 12 mm to mimic lymph nodes-like structures in the GI tract[23]. Phantom B was used to determine the optimum elevational angular width needed for imaging lymph nodes to achieve both high speckle reduction efficiency and image fidelity.

Analysis method. To attain each compounded image, 100 sequential images were captured in different positions of the annular-shaped acoustic cylindrical lens and compounded using a mean compound operator[24]. To perform image post-processing for despeckling of the US images, MATLAB was used to perform Frost filtering, which is a commonly used speckle noise filtering technique based on an adaptive filter reported in the

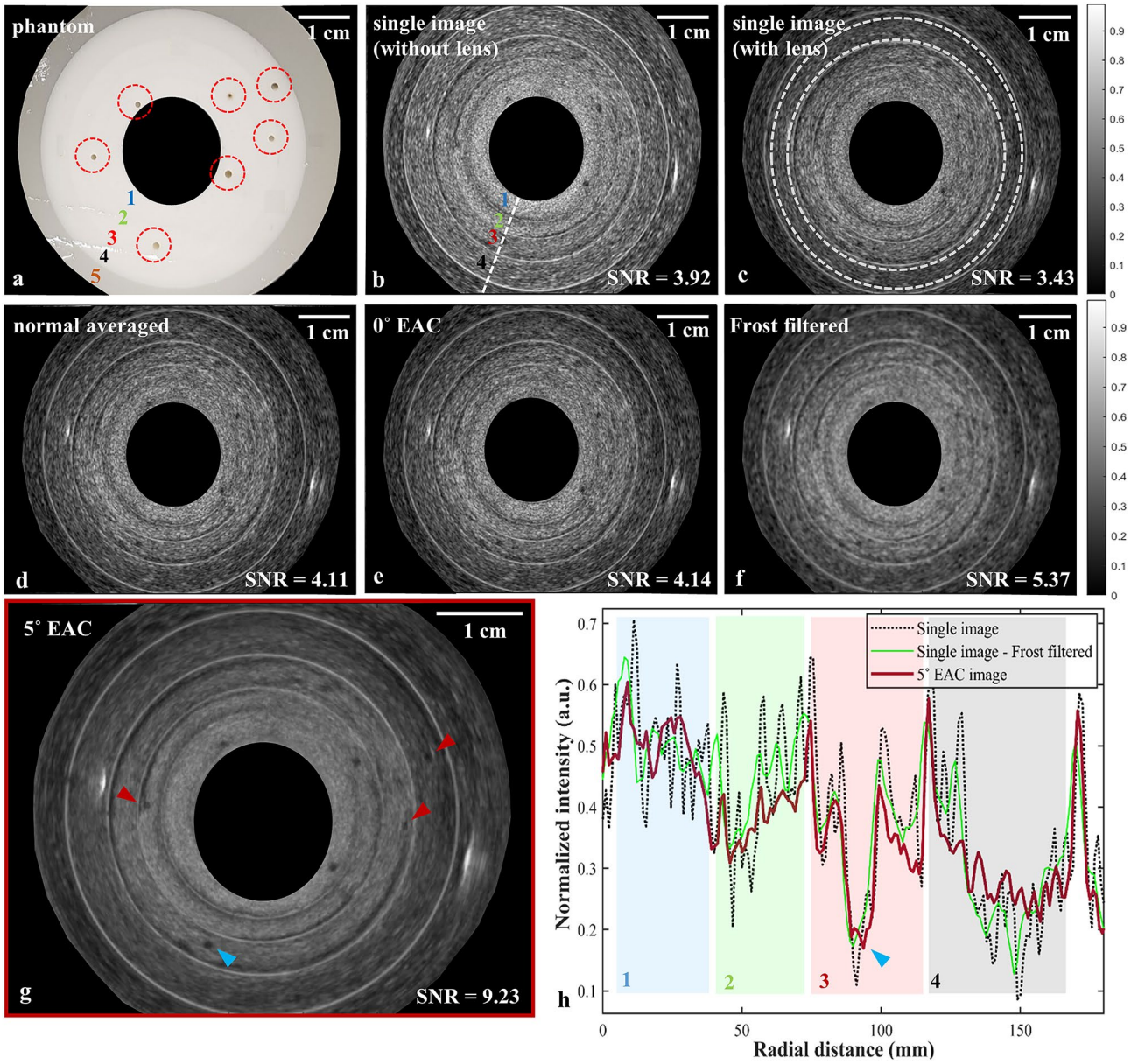

Figure 2. Speckle reduction by REACT in a radial geometry compared to single images, averaging, and Frost filtering. **(a)** Phantom A: a five-layered cylindrical phantom (labelled with numbers 1, 2, 3, 4, and 5 from inside out respectively) containing seven holes (specified with circular regions). **(b–g)** US images of Phantom A: **(b)** a single image recorded without an acoustic lens, **(c)** a single image recorded with a stationary acoustic lens, **(d)** an averaged image using 100 single images recorded with a stationary acoustic cylindrical lens **(e)** a compounded image using 100 single images recorded with a translating acoustic cylindrical lens providing 0° elevational deflection, **(f)** a single image recorded with an acoustic lens after Frost filtering, **(g)** a compounded image using 100 single images recorded with a translating acoustic cylindrical lens providing 5° elevational deflection. The red arrows indicate holes that are not visible in b-f. Region between two white circles in c show the ROI used to derive the SNR in **(b)–(g)**. **(h)** A-line intensity profiles for the single, Frost filtered, and 5° EAC images, which were recorded along the dashed line shown in b. The blue, green, red, and gray rectangles indicate phantom layers 1, 2, 3, and 4, respectively. Blue arrows in g and h point to the same hole, which lies on the dashed line in **(b)**.

literature[25–27]. Processed and compounded images were compared to their respect single images to assess the despeckling efficiency. Circular regions of interests (ROI = 13,500 pixels in Fig. 2c, ROIs = 1950 pixels in Fig. 3a) within a water sphere and solid regions in the phantom were selected to derive the average (μ) and standard deviation (σ) of the pixel intensities in order to compute signal-to-noise ratio (SNR : $\mu_{Phantom}/\sigma_{Phantom}$) and contrast-to-noise ratio (CNR : $|\mu_{water} - \mu_{Phantom}|/\sigma_{water}$). These indices were used as quantitative indicators of image improvement to evaluate the despeckling efficiency and preserving the image fidelity. The despeckling efficiency was also evaluated by inspecting the A-line intensity profiles of the single, processed, and compounded images.

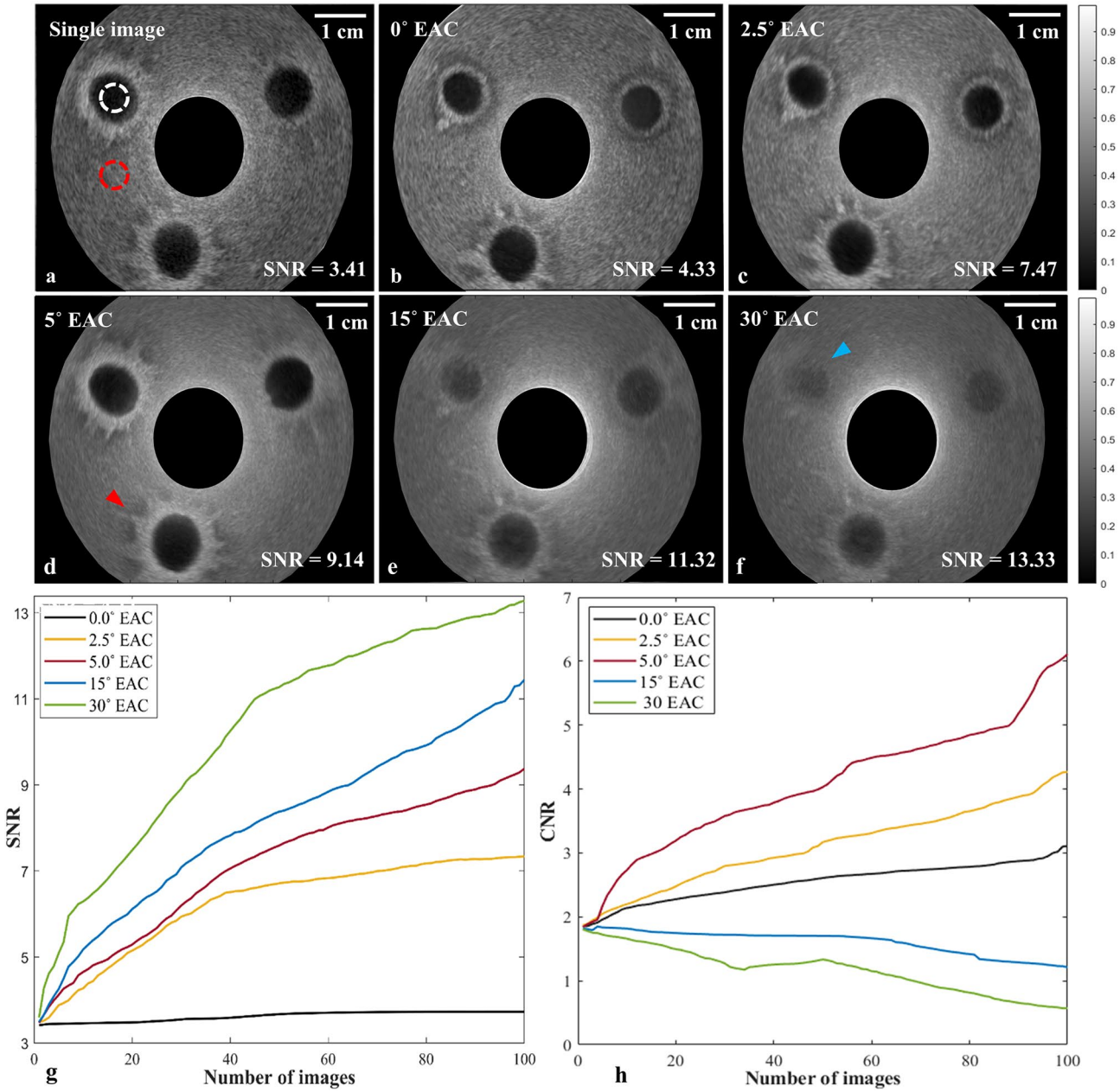

Figure 3. The effect of elevational angular deflection on speckle reduction efficiency and image fidelity in REACT. **(a)** A single US image of a single-layered cylindrical phantom (Phantom B) containing spherical water beads to mimic lymph nodes. The white dotted circles indicate the ROIs used to derive the SNR and CNR. **(b–f)** Compounded images of Phantom B using five different cylindrical acoustic lenses with the following angular deflections: **(b)** 0°, **(c)** 2.5°, **(d)** 5°, **(e)** 15°, **(f)** 30°. The red arrow in d depicts fine structures, which are best resolved by 5° EAC. The blue arrow in f indicates a water bead that is barely visible due to loss of image fidelity at 30° EAC. **(g,h)** The change in SNR and CNR for each deflection angle with increasing number of compounded images.

Results

In order to evaluate the speckle reduction efficiency of REACT in a radial geometry and verify its advantage over image post-processing, ultrasound images of a five-layered cylindrical phantom containing seven 1 mm-diameter holes (Phantom A, Fig. 2a) using a radial ultrasound endoscope were recorded and analysed. Figure 2b–g show single images recorded without (Fig. 2b) and with (Fig. 2c) an acoustic lens, an averaged image of 100 single images recorded with a stationary acoustic lens (Fig. 2d), a processed image by Frost filtering (Fig. 2f), and compounded images of 100 single images using a translating acoustic lenses providing 0° (as a control, Fig. 2e) and 5° elevational angular deflections (Fig. 2g). Visual inspection of the ultrasound images in Fig. 2b–g reveals noticeable speckle noise reduction with 5° EAC compared to the single images. Furthermore, the boundaries

of the layers and edges of the holes in the phantom are clearer upon 5° EAC compared to averaging and Frost filtering, as highlighted by the red arrows in Fig. 2g.

To quantify the speckle reduction performance, we calculated SNR values (Fig. 2b-g, lower right corner) for each image (See "Methods", Analysis method subsection). To access a higher number of pixels within the same radius for the SNR calculation, a ring-shaped region within the outer layers of the phantom was selected (enclosed by the dashed white circles in Fig. 2c). The single image recorded with the acoustic lens (Fig. 2c) exhibits a slightly lower SNR than recorded without a lens (Fig. 2b) due to the acoustic attenuation and reflection induced by the cylindrical lens substrate. As expected, images are decorrelated by the REACT method as confirmed by the STD maps (see Supplementary Fig. 2). Compounding of 100 images recorded using both a stationary (Fig. 2d) and translating acoustic lens with a 0° elevational angular deflection (Fig. 2e) improved the SNR by 1.20 times compared to the single image ($SNR_{single} = 3.43$, $SNR_{0° EAC, stationary (averaged)} = 4.11$, $SNR_{0° EAC, translating} = 4.14$). The identical SNR measured for the 0° deflection lens both when stationary and translating reflects its non-refractive nature, which leads to all corresponding images being in the same imaging plane (unchanged speckle pattern). However, due to the refractive capability of the 5° elevational angular deflection lens, the SNR obtained with this lens (Fig. 2g, $SNR_{5°EAC} = 9.23$) was 2.69 times greater than the SNR of the single image (Fig. 2c) and 1.71 times greater the SNR of the Frost filtered image (Fig. 2f, $SNR_{Frost\ filtered} = 5.37$). The speckle pattern decorrelation is related to the elevational angular deflection obtained with the movement of the refractive lens. However, the linear translation of the lens results in non-uniform angular deflection across the field-of-view, as confirmed by the speckle pattern decorrelation obtained with the 5° EAC lens (see Supplementary Fig. 2). An optimal number of compounding images would be obtained by linearly translating the lens to positions that deflect the acoustic beam to equidistant angular steps.

Figure 2h shows the A-line intensity profiles (dashed line in Fig. 2b) for a single image recorded with lens (dotted black line), Frost filtered image (solid green line), and the compounded image using 5° EAC (solid red line). The blue, green, red, and gray rectangles in Fig. 2h indicate layers 1–4 of Phantom A, respectively. Inspecting the A-line intensity profile of the single image shows high intensity variations due to presence of scatterers producing speckle noise. Frost filtering affords a slight dampening of the high intensity variations (solid green line), yet it follows the noise pattern of the main signal since it operates only on the available data in a single image. In contrast, these variations are strongly suppressed by 5° EAC (solid red line), regardless of the noise pattern of the original signal. The higher speckle noise suppression in 5° EAC is due to compounding of different speckle patterns acquired at different elevational angular views. The high speckle reduction afforded by REACT is exemplified by a hole that is only reveal upon 5° EAC (blue arrow in Fig. 2g,h).

Figure 3 depicts single and compounded ultrasound images of a single-layered cylindrical phantom containing spherical water beads to mimic lymph nodes (Phantom B), which illustrate the effect of the elevational angular deflection on speckle reduction efficiency and image fidelity for the radial implementation of REACT. The compounded images were recorded using 0° (Fig. 3b), 2.5° (Fig. 3c), 5° (Fig. 3d), 15° (Fig. 3e), and 30° (Fig. 3f) elevational angular deflections. Compounding at 0° (Fig. 3b) results in minimal image improvement over the uncompounded image (Fig. 3a). Increasing the elevational compounding angle results in a decrease in speckle noise, but also a loss of image fidelity at high angles (15° and 30°) due to increasing elevational angular width and a concomitant increase in interference from structures in adjacent elevational planes (Fig. 3e,f), which manifest as a loss of definition of the water bead boundaries (blue arrow). Visual inspection of the ultrasound images in Fig. 3a–f reveals that 5° EAC yields the optimum balance between speckle noise reduction and image fidelity. The edges of the holes and fine structures around them are preserved and are clearest in 5° EAC (highlighted by the red arrow in Fig. 3d).

To quantify the effect of the elevational angular deflection on the speckle reduction efficiency and image fidelity in REACT, SNR was calculated using a region within the solid phantom (Fig. 3a, red dashed circle) and CNR was calculated using regions within and outside the solid region (Fig. 3a, white and red dashed circles); SNR and CNR were then plotted as a function of the number of compounded images (Fig. 3g,h). As expected, SNR increases with the number of compounded images for all cases, with the rate of SNR improvement increasing with the elevation deflection angle. At the upper end, the SNR for 30° EAC is 3.1 times greater than 0° EAC, after 100 images were compounded ($SNR_{0°EAC} = 4.33$, $SNR_{30°EAC} = 13.33$). This improvement results from the higher variation in the speckle pattern of the captured images within the higher elevational angular deflections. In contrast, CNR increases with an increasing number of compounded images only for the 0°, 2.5°, and 5° cases. CNR predominantly decreases with compounding for the 15° and 30° cases. Therefore, while higher elevational angular deflection results in a decrease in speckle noise (higher SNR), too great an angular deflection can cause severe degradation of image fidelity (lower CNR).

Discussion

The accurate diagnosis and therapeutic utility of EUS for gastrointestinal disorders is limited by the presence of speckle noise[8,9], which hinders the identification of gastrointestinal tract layer boundaries with low acoustic impedance differences[8]. To minimize speckle artefacts, compounding methods are preferable to image processing techniques because they yield both high quality images and reveal fine structures obscured by speckle noise, which are otherwise irretrievable using the aforementioned techniques[15,16]. EAC is a preferred spatial compounding technique with both high despeckling efficiency and good temporal resolution, which makes it favorable for real time imaging[18]. However, tight anatomical constraints of hollow organs prevent implementation of EAC in EUS using 2D or tilting 1D transducer arrays. Here, we demonstrated a novel deployment of spatial compounding in radial EUS by implementing REACT in a radial geometry, which can lead to image quality improvements in clinical EUS and enable more accurate diagnoses of GI lesions.

Visual and quantitative inspection of the ultrasound images from a cylindrical layered phantom (Fig. 2) illustrates that spatial compounding in radial EUS can provide more efficient speckle reduction with retrieved fine structures, which are not recoverable with commonly used image post-processing techniques such as Frost filtering. As expected, the wider the elevational angle employed, the greater the speckle suppression in the compounded image, which translates to higher SNRs (Fig. 3g). Compounded images acquired within elevational angular deflections of 0°, 2.5°, 5°, 15°, and 30° yielded SNR improvements of 1.27, 2.19, 2.68, 3.32, and 3.91-fold, respectively, compared to the single image ($SNR_{single} = 3.41$, $SNR_{0° EAC} = 4.33$, $SNR_{2.5° EAC} = 7.47$, $SNR_{5° EAC} = 9.14$, $SNR_{15° EAC} = 11.32$, $SNR_{30° EAC} = 13.33$). The SNR enhancement is in agreement with previously reported findings using a linear configuration of REACT[18]. As expected, the similar SNRs obtained for averaging (Fig. 2d) and 0° EAC (Fig. 2e) confirmed that the uncorrelated speckle patterns are produced by effectively changing the elevational angular deflection using an acoustic refractive lens. Moreover, SNR in REACT has an increasing trend by increasing the number of images, yet at a greater rate for the 30° EAC case (Fig. 3g), owing to the widest elevational angular width and therefore providing images with less correlated speckle patterns.

Although higher elevational angular deflection results in higher despeckling efficiency, a trade-off between speckle reduction and image distortion determines the optimal compounding angle for the imaging target of interest[18]. In agreement with our previous study[18], we found that out-of-plane signals can also degrade the quality of the elevational compounded image for radial EUS. This is relevant in particular when imaging small organs such as lymph nodes adjacent to the GI tract. We demonstrate an increase in SNR with wider elevational angular deflection in a phantom containing lymph node like structures; however, angular deflection above 5° results in overall degradation of CNR (Fig. 3). This drop in CNR is due to the out-of-plane artefacts and represents a loss of image contrast and resolution, which can affect accurate diagnosis. Our experiments suggest that 5° EAC provides an optimal trade-off for high despeckling efficiency with minimal image fidelity loss for lymph node-like structures (Fig. 3).

This study demonstrates REACT as a first potential compact and low-cost solution to impart current radial echo-endoscopes with spatial compounding. The optimum elevational angular deflection for imaging lymph nodes was also investigated to achieve the best combination of despeckling efficiency and high image fidelity, required for accurate identification of pathological lymph nodes in the GI tract. However, the optimum extended elevational angular deflection that can provide high despeckling efficiency while preserving image fidelity in EUS depends on the size and depth of the organ imaged within the body. Hence, further studies are required to define the best organ-specific angular deflections. The lens material has an effect on SNR as can be seen by individual images captured with (Fig. 2c) and without (Fig. 2b) the acoustic lens. This is caused by the acoustic attenuation and reflection and could be diminished by either utilizing lower attenuating materials to manufacture the lens compared to PMMA (e.g. TPX) or diffractive lenses with lower effective thicknesses. To enable real-time despeckling in radial EUS using REACT, the translation of the lens should be automated to allow frame rates as high as the acquisition speed of the US imaging system. Future work will aim to translate REACT into clinical settings by miniaturizing and integrating the acoustic lens to the existing radial echo-endoscopes.

In summary, we demonstrate that REACT is ideally suited for radial EUS and can uniquely impart spatial compounding to radial ultrasound endoscopy for the first time, enabling observation of fine structures hidden by speckle noise. This low-cost and simple spatial compounding method can be of great benefit in clinics to improve image quality and contrast in current radial echo-endoscopes to heighten the accuracy in visualization and identification of pathological lymph nodes in staging of gastrointestinal tract cancers.

Data availability

The datasets generated during and/or analysed during the current study are available from the corresponding author on reasonable request.

Received: 2 March 2021; Accepted: 30 August 2021
Published online: 15 September 2021

References

1. Friedberg, S. R. & Lachter, J. Endoscopic ultrasound: Current roles and future directions. *World J. Gastrointest. Endosc.* **9**, 499–505 (2017).
2. Mekky, M. A. & Abbas, W. A. Endoscopic ultrasound in gastroenterology: From diagnosis to therapeutic implications, world. *J. Gastroenterol.* **20**, 7801–7807 (2014).
3. Kandel, P. & Wallace, M. B. Recent advancement in EUS-guided fine needle sampling. *J. Gastroenterol.* **54**, 377–387 (2019).
4. Iglesias-Garcia, J., Larino-Noia, J. & Dominguez-Munos, J. E. Contrast harmonic endoscopic ultrasound: Instrumentation, echoprocessors, and echoendoscopes. *Endosc. Ultrasound* **6**, 37–42 (2016).
5. Kalaitzakis, E., Vilmann, P. & Bhutani, M. *Therapeutic Endoscopic Ultrasound*. (Springer, 2020).
6. Jenssen, Ch., Alvarez-Sanchez, M. V., Napoleon, B. & Faiss, S. Diagnostic endoscopic ultrasonography: Assessment of safety and prevention of complications. *World J. Gastroenterol.* **18**, 4659–4676 (2012).
7. Gaschen, L., Kircher, P. & Lang, J. Endoscopic ultrasound instrumentation, applications in humans, and potential veterinary application. *Vet. Radiol. Ultrasound* **44**, 665–680 (2003).
8. Li, J. J. *et al.* Superficial esophageal lesions detected by endoscopic ultrasound enhanced with submucosal edema. *World J. Gastroenterol.* **19**, 9034–9042 (2013).
9. Murad, F. M. *et al.* Echoendoscopes. *Gastrointest. Endosc.* **82**, 189–202 (2015).
10. Rimbas, M. & Larghi, A. Equipment and accessories for therapeutic endoscopic ultrasound. in *Therapeutic Endoscopic Ultrasound*. 1–31 (Springer, 2020).
11. Lee, Y. S. *et al.* Comparison of endoscopic ultrasonography, computed tomography, and magnetic resonance imaging for pancreas cystic lesions. *Medicine* **94**, 13 (2015).
12. Lu, X. *et al.* The diagnostic value of EUS in pancreatic cystic neoplasm compared with CT and MRI. *Endosc. Ultrasound* **4**, 324–329 (2015).

13. Dewitt, J., Devereaux, B. M., Lehman, G. A., Sherman, S. & Imperiale, Th. F. Comparison of endoscopic ultrasound and computed tomography for the preoperative evaluation of pancreatic cancer: A systematic review. *Clin. Gastroenterol. Hepatol.* **4**, 717–725 (2006).
14. Michailovich, O. V. & Tannenbaum, A. Despeckling of medical ultrasound images. *IEEE Trans. Ultrason. Ferroelectr. Freq. Control.* **53**, 64–78 (2006).
15. Nwogu, I. & Chaudhary, V. Enhancing regional lymph nodes from endoscopic ultrasound images. In *Proceedings of the SPIE 6914 Medical Imaging* (2008).
16. Li, P. C. & O'Donnell, M. Elevational spatial compounding. *Ultrason. Imaging* **16**, 176–189 (1994).
17. Perperidis, A., McDicken, N., MacGillivary, T. & Anderson, T. Elevational spatial compounding for enhancing image quality in echocardiography. *Ultrasound* **24**, 74–85 (2016).
18. Afshari, P., Zakian, Ch. & Ntziachristos, V. Novel implementation of elevational angular compounding using acoustic refraction principles. *Sci. Rep.* **10**, 18173 (2020).
19. Xia, W., Piras, D., van Hespen, J. C. G., Steenbergen, W. & Manohar, S. A new acoustic lens material for large area detectors in photoacoustic breast tomography. *Photoacoustics* **1**, 9–18 (2013).
20. Bloomfield, P. E., Lo, W. J. & Lewin, P. A. Experimental study of the acoustical properties of polymers utilized to construct PVDF ultrasonic transducers and the acousto-electric properties of PVDF and P(VDF/TrFE) films. *IEEE Trans. Ultrason. Ferroelectr. Freq. Control.* **47**, 1397–1405 (2000).
21. Hohenwarter, D. & Jelinek, F. Snell's law of refraction and sound rays for a moving medium. *J. Acoust. Soc. Am.* **105**, 1387–1388 (1999).
22. Finn, S., Glavin, M. & Jones, E. Speckle reduction in echocardiography: Trends and perceptions. in *Echocardiography—New Techniques* (Bajraktari, G. ed.) 41–68 (InTech, 2012).
23. Märkl, B. *et al.* The clinical significance of lymph node size in colon cancer. *Mod. Pathol.* **25**, 1413–1422 (2012).
24. Wilhjelm, J. E., Jensen, M. S., Jespersen, S. K., Sahl, B. & Falk, E. Visual and quantitative evaluation of selected image combination schemes in ultrasound spatial compound scanning. *IEEE Trans. Med. Imaging* **23**, 181–190 (2004).
25. Lopes, A., Touzi, R. & Nezry, E. Adaptive speckle filters and scene heterogeneity. *IEEE Trans. Geosci. Remote Sens.* **28**, 992–1000 (1990).
26. Jaybhay, J. & Shastri, R. A study of speckle noise reduction filters. *Signal Image Process. Int. J. (SIPIJ)* **6**, 71–80 (2015).
27. Bafaraj, A. S. Performance analysis of best speckle filter for noise reduction in ultrasound medical images. *Int. J. Appl. Eng. Res.* **14**, 1340–1351 (2019).

Acknowledgements

This project has received funding from the European Union's Horizon 2020 research and innovation program under grant agreement 732720 (ESOTRAC) as well as from European Union's Horizon 2020 research and innovation program under the Marie-Sklodowska-Curie grant agreement No 721766 (FBI). The authors also thank Dr. Robert J. Wilson for proofreading the manuscript.

Author contributions

P.A. and C.Z. designed the study. J.B. provided expert clinical advice and insightful discussions on validation of REACT in echo-endoscopy. P.A. produced phantoms and carried out the experiments. P.A. collected and analysed the data and prepared all figures in the manuscript. P.A. and C.Z. interpreted the data and wrote the manuscript. V.N. reviewed and approved the final manuscript.

Funding

Open Access funding enabled and organized by Projekt DEAL.

Competing interests

The authors declare no competing interests.

Additional information

Supplementary Information The online version contains supplementary material available at https://doi.org/10.1038/s41598-021-97717-2.

Correspondence and requests for materials should be addressed to V.N.

Reprints and permissions information is available at www.nature.com/reprints.

Publisher's note Springer Nature remains neutral with regard to jurisdictional claims in published maps and institutional affiliations.

Speckle reduction in ultrasound endoscopy using refraction based elevational angular compounding

Author: Parastoo Afshari et al
Publication: Scientific Reports
Publisher: Springer Nature
Date: Sep 15, 2021

Creative Commons